# Theoretical Studies on Fragmentation of Nuclei at Intermediate Energies

*By*

**Prabrisa Das**

**Enrolment No: PHYS04201304006**

*Variable Energy Cyclotron Centre, Kolkata*

***A thesis submitted to***

***The Board of Studies in Physical Sciences***

***In partial fulfillment of requirements***

***For the Degree of***

**DOCTOR OF PHILOSOPHY**

***of***

**HOMI BHABHA NATIONAL INSTITUTE**

**September, 2019**

# Homi Bhabha National Institute[1]

## Recommendations of the Viva Voce Committee

As members of the Viva Voce Committee, we certify that we have read the dissertation prepared by **PRABRISA DAS** entitled **Theoretical Studies on Fragmentation of Nuclei at Intermediate Energies** and recommend that it may be accepted as fulfilling the thesis requirement for the award of Degree of Doctor of Philosophy.

| | | | |
|---|---|---|---|
| Chairman - | **Prof. Jan-e-Alam** | Jan e Alam | **Date:** 30.8.2019 |
| Guide / Convener - | **Prof. Gargi Chaudhuri** | Gargi Chaudhuri | **Date:** 30·8·2019 |
| Examiner - | **Prof. Rajeev Puri** | | **Date:** 30·8·2019 |
| Member 1 - | **Prof. Debades Bandyopadhyay** | Debades Bandyopadhyay | **Date:** 30.8.2019 |
| Member 2 - | **Prof. D. N. Basu** | DN Basu | **Date:** 30/08/2019 |

Final approval and acceptance of this thesis is contingent upon the candidate's submission of the final copies of the thesis to HBNI.

I/We hereby certify that I/we have read this thesis prepared under my/our direction and recommend that it may be accepted as fulfilling the thesis requirement.

**Date:** 30·8·2019

**Place:** KOLKATA

Gargi Chaudhuri
**Guide**

---

[1] This page is to be included only for final submission after successful completion of viva voce.

# STATEMENT BY AUTHOR

This dissertation has been submitted in partial fulfilment of requirements for an advanced degree at Homi Bhabha National Institute (HBNI) and is deposited in the Library to be made available to borrowers under rules of the HBNI.

Brief quotation from this dissertation are allowable without special permission, provided that accurate acknowledgement of source is made. Requests for permission for extended quotation from or reproduction of this manuscript in whole or in part may be granted by the Competent Authority of HBNI when in his or her judgement the proposed use of the material is in the interests of scholarship. In all other instances, however, permission must be obtained from the author.

Prabrisa Das
Prabrisa Das

# DECLARATION

I, hereby declare that the investigation presented in the thesis has been carried out by me. The work is original and has not been submitted earlier as a whole or in part for a degree/diploma at this or any other Institution/University.

Prabrisa Das

Prabrisa Das

# List of Publications

**Journals :**

1. *P. Das*, S. Mallik, G. Chaudhuri; First-order derivative of cluster as a new signature of phase transition in heavy ion collisions at intermediate energies; Phys. Lett. B **783**, (2018) 364.
2. S. Mallik, G. Chaudhuri, *P. Das* and S. Das Gupta, Multiplicity derivative: A new signature of first-order phase transition in intermediate-energy heavy-ion collisions; Phys. Rev. C **95**, 061601(R)(2017).
3. *P. Das*, S. Mallik and G. Chaudhuri, Statistical ensembles and fragmentation of finite nuclei; Phys. Rev. C **96**, 034609 (2017).
4. *P. Das*, S. Mallik, and G. Chaudhuri; Effect of hyperons on phase coexistence in strange matter; Phys. Rev. C **95**, 014603 (2017).

**Conferences:**

1. *P. Das*, S. Mallik, G. Chaudhuri, S. Das Gupta, Multiplicity Derivative: A New Signature of Phase Transition in Nuclear Multifragmentation; DAE Symp. Nucl. Phys. **62** (2017) 402-403.
2. *P. Das*, S. Mallik, G. Chaudhuri, Nuclear Multi-fragmentation: Canonical-Grand Canonical Ensemble Transformation; DAE Symp. Nucl. Phys. **62** (2017) 582-583.
3. G. Chaudhuri, *P. Das*, S. Mallik, Statistical Ensemble and Fragmentation of Finite Nuclei; DAE Symp. Nucl. Phys. **61** (2016) 51-52.
4. *P. Das*, S. Mallik, G. Chaudhuri, Effect of Hyperons on Nuclear Phase Transition; DAE Symp. Nucl. Phys. **61** (2016) 400-401.

5. *P. Das*, G. Chaudhuri, S. Mallik, Hyper-nuclear Liquid-Gas Phase Transition; DAE Symp. Nucl. Phys. **60** (2015) 362-363.

Prabrisa Das

Prabrisa Das

*Dedicated*

*to*

*My Ludicrous Destiny*

# ACKNOWLEDGMENTS

I thank my guide, Dr. Gargi Chaudhuri and collaborators for their support. I would like to thank my family, teachers, friends, my cats and dogs, and all those who have inspired me, helped me to live a healthy life and accomplish this thesis.

I want to thank my "jethu", who was always very concerned about my thesis, but to whom I failed to convey the news of its completion before his demise.

Prabrisa Das

Prabrisa Das

# Contents

**List of Publications** **i**

**Synopsis** **xi**

**List of Figures** **1**

**List of Tables** **9**

**1 Introduction** **13**

1.1 Experimental Facilities . . . . . . . . . . . . . . . . . . . . . . . . . . . 15

1.2 Theoretical Models . . . . . . . . . . . . . . . . . . . . . . . . . . . . . 16

1.2.1 Statistical Approach . . . . . . . . . . . . . . . . . . . . . . . . . 16

1.2.2 Dynamical Approach . . . . . . . . . . . . . . . . . . . . . . . . 17

1.3 Physical Picture in the Statistical Approach . . . . . . . . . . . . . . . 19

1.4 Characteristics of Fragmentation . . . . . . . . . . . . . . . . . . . . . 21

1.4.1 Mass Distribution . . . . . . . . . . . . . . . . . . . . . . . . . . 21

1.4.2 Intermediate Mass Fragment (IMF) Production . . . . . . . . . . . . . 22

1.4.3 Phase Transition . . . . . . . . . . . . . . . . . . . . . . . . . . . . . . 23

1.5 Organisation of Present Work . . . . . . . . . . . . . . . . . . . . . . . . . . . 24

**2 Statistical Physics: Overview 31**

2.1 Phase Space Representation and Definition of Equilibrium . . . . . . . . . . . . 32

2.2 Theory of Statistical Ensemble . . . . . . . . . . . . . . . . . . . . . . . . . . 35

2.2.1 Isolated System: Microcanonical Ensemble . . . . . . . . . . . . . . . . . . 36

2.2.2 Closed System: Canonical Ensemble . . . . . . . . . . . . . . . . . . . . . 37

2.2.3 Open System: Grand Canonical Ensemble . . . . . . . . . . . . . . . . . . 39

2.2.4 Equivalence of Ensembles . . . . . . . . . . . . . . . . . . . . . . . . . . . 41

2.3 Phase Transition . . . . . . . . . . . . . . . . . . . . . . . . . . . . . . . . . 43

**3 Statistical Models of Fragmentation of Nuclei 49**

3.1 Micro-Canonical Model . . . . . . . . . . . . . . . . . . . . . . . . . . . . . . 50

3.2 Canonical Model . . . . . . . . . . . . . . . . . . . . . . . . . . . . . . . . . 51

3.2.1 One Component Canonical Thermodynamical Model . . . . . . . . . . . 51

3.2.2 Two Component CTM . . . . . . . . . . . . . . . . . . . . . . . . . . . . 59

3.3 Two Component Grand-Canonical Thermodynamical Model . . . . . . . . . . . 63

**4 Ensemble Transformation 67**

4.1 Theoretical Formalism . . . . . . . . . . . . . . . . . . . . . . . . . . . . . . 69

4.2 Results . . . . . . . . . . . . . . . . . . . . . . . . . . . . . . . . . . . . . . 75

4.2.1 Multiplicity . . . . . . . . . . . . . . . . . . . . . . . . . . . . 77

4.2.2 Largest Cluster . . . . . . . . . . . . . . . . . . . . . . . . . . 78

4.2.3 Isoscaling Parameters . . . . . . . . . . . . . . . . . . . . . . . 79

4.2.4 Table . . . . . . . . . . . . . . . . . . . . . . . . . . . . . . . 81

**5 Proposition of New Observables to Study Nuclear Phase Transistion 85**

5.1 Existing Signatures of Nuclear Phase Transition . . . . . . . . . . . . . . . . . 86

5.1.1 Signatures of Nuclear Phase Transition Obtained in Theoretical Models . 87

5.1.2 Experimental Signatures of Nuclear Phase Transition . . . . . . . . . . . 91

5.2 Search for Alternatives . . . . . . . . . . . . . . . . . . . . . . . . . . . . 95

5.3 Observables Proposed . . . . . . . . . . . . . . . . . . . . . . . . . . . . . 96

5.3.1 Multiplicity . . . . . . . . . . . . . . . . . . . . . . . . . . . . 96

5.3.2 Largest Cluster . . . . . . . . . . . . . . . . . . . . . . . . . . 103

**6 Phase Transition in Hypernuclei 111**

6.1 Three-component Canonical Thermodynamical Model . . . . . . . . . . . . . 114

6.2 Results and Discussions . . . . . . . . . . . . . . . . . . . . . . . . . . . . 116

6.2.1 Free Energy, Entropy, Specific Heat . . . . . . . . . . . . . . . . . . 116

6.2.2 Caloric Curve . . . . . . . . . . . . . . . . . . . . . . . . . . . . 118

6.2.3 P Vs V : Isotherms . . . . . . . . . . . . . . . . . . . . . . . . . 119

6.2.4 Largest Cluster and Bimodality . . . . . . . . . . . . . . . . . . . . 120

6.2.5 Effect of coulomb interaction . . . . . . . . . . . . . . . . . . . . . . . . . . 123

**7 Summary and outlook 127**

**Appendix: 133**

**A Wigner - Seitz Approximation 135**

**B Secondary decay scheme 139**

**C Second Largest Cluster 143**

# Homi Bhabha National Institute

## SYNOPSIS OF Ph.D. THESIS

1. **Name of the Student:** Prabrisa Das
2. **Name of the Constituent Institution:** Variable Energy Cyclotron Centre
3. **Enrolment No.:** PHYS04201304006
4. **Title of the Thesis:** Theoretical Studies on Fragmentation of Nuclei at Intermediate Energies
5. **Board of Studies:** Physical Sciences

## SYNOPSIS

## Introduction

Fragmentation of nuclei, also called ”multi-fragmentation”, is a phenomenon of prompt decay of highly excited nuclear system to several fragments of different sizes. In heavy ion collisions at intermediate energy, such an unstable excited intermediate nuclear system can be formed due to collision of the projectile with the target, which then breaks-up instantaneously to several fragments [[1]-[4]]. To understand the respective decay-mechanism and to explain the experimental data, various theoretical models have been developed. There are, mainly, two distinct ways of approach, e.g., a) Dynamical approach simulating time evolution of the system, b) Statistical approach assuming the system attains statistical equilibrium at some point.

The present study, using the statistical approach, can be classified into two sections:

i) Canonical-grand canonical ensemble transformation in connection with multi-fragmentation,

ii) Nuclear liquid-gas phase transition. The nuclear fragmentation is frequently described as liquid-gas phase transition, where depending upon the excitation energy fragments can be in liquid phase or in gaseous phase. a) The first part of the study introduces new observables that show signatures of phase transition, which are easily accessible in experiment. b) The second part is on the effect of hyperon on nuclear phase transition.

## Canonical-Grand Canonical Ensemble Transformation in Connection with Multi-fragmentation

In order to describe a situation from statistical point of view, one needs to take a collection of a very large number of identically prepared system including all the micro-states, which is called the ensemble. For a thermodynamic system this ensemble is defined by the constraints, which the system is restricted to follow, and depending upon this one can consider any of the three basic thermodynamic ensembles i.e.; micro-canonical, canonical or grand canonical ensemble.

For an isolated system having fixed volume V, total number of particles N and total energy E, the ensemble to be considered is the micro-canonical ensemble. If the system is a closed system but in thermal contact with the surroundings, it has a definite volume V and total particles N but its total energy E can vary; now if the system is in statistical equilibrium, its temperature T can be defined and that will take a constant value, then the system can be defined by (T, N, V) and corresponding ensemble is the canonical ensemble. A more general situation is an open system in thermal contact with the surroundings, which will have a fixed volume but not the total energy or the particle number; such a system in equilibrium is defined by (T, $\mu$, V) where the average of E or N has a definite value and are restricted by fixed T and $\mu$ (chemical potential) respectively and the ensemble, in this case, one has to consider is the grand canonical ensemble [5]. Therefore, for the statistical description of the fragmentation of nuclei, as the fragmenting system in laboratory is practically an isolated system neither in contact with heat reservoir nor with the particle reservoir, micro-canonical ensemble is the appropriate one.

In principle three ensembles converge for a macroscopic system at equilibrium in the thermodynamic limit, so that one can be replaced by others [5] but for finite system they do not. So for multi-fragmentation of finite nuclei, calculations considering different ensembles give different results. Moreover these three ensembles have different levels of computational difficulties. Calculations in grand canonical ensemble is the most easy as there is no restriction on E or N. Canonical calculation is more easy than micro-canonical one; as in latter, there are two restrictions both on E and N though it is physically appropriate for the fragmentation of nuclei. For this extreme computational difficulty in case of micro-canonical ensemble one generally use canonical or grand canonical description of fragmentation [[1],[2],[6],[7]] and results successfully describe the experimental data [[8]-[12]]. Among these two, grand canonical calculation is easier than canonical though latter is more appropriate. Now, if one can develop a mathematical relation between the average values of any observable in three ensembles then one would get the value of the average in other two ensembles when it is calculated in one ensemble. Thus the difficulties related to the above mentioned restricted sum can be avoided. For a single component ideal nuclear system such a relation between canonical and grand canonical averages of any observable has already been developed [13] within some approximation. Here we have tried to develop such a relation for realistic two component system to extrapolate canonical results from grand canonical calculations. Then we have checked its validity using exact canonical and grand canonical ensemble calculation since both the calculations can be done analytically in thermodynamic models of multi-fragmentation. We have studied mass distribution, largest cluster and other observables and the results are in good agreement except in regions which are beyond the domain of validity.

# Nuclear Liquid-Gas Phase Transition

Liquid-Gas phase transition for ordinary water or any other substance is a very common phenomenon. It is also well known that Van Der Waals equation of state and the Lennard-Jones type interaction potential between molecules can successfully model such transition. This similarity between inter-molecular interaction and nucleon-nucleon short range attractive interaction with a hard core leads to expect the occurrence of such phase transition in nuclear matter.

Liquid-gas phase transition in nuclear system has been studied over past few decades, both in theoretical modeling as well as in experiment of nuclear multi-fragmentation, that establish the existence of finite size counterpart of such transition from which one can extrapolate the case of infinite nuclear matter [[14]-[18]]. In the phase transition study one generally examine different thermodynamic variables like pressure, free energy and its temperature derivatives which are related to entropy and specific heat, caloric curve. Theoretical models of nuclear multi-fragmentation show signals of 1st order phase transition from these studies [[5],[19]-[21]]. Caloric Curves obtained from multi-fragmentation experiments give the signals of phase transition. Apart from this no direct experimental measurement is possible for other thermodynamic variables such as free-energy or specific heat in this case. Moreover in caloric curve the measurement of temperature is not unambiguous.

In this situation we have tried to find some other observables which can give the message of 1st order phase transition and can be measured experimentally as well. We propose that the total multiplicity of fragments produced in fragmentation of nuclei can be used to serve this purpose. Total multiplicity ie., the total number of fragments produced in fragmentation, is a very basic observable of multi-fragmentation and is measured in most of the multi-fragmentation experiments. We have shown using Canonical Thermodynamical Model of nuclear multi-fragmentation that, derivative of the total multiplicity with respect to temperature shows a clear peak at transition temperature exactly like specific heat; thus multiplicity gives signature of phase transition very successfully and predicts the same value of transition temperature as it is from specific heat. We have also shown that these signals can be obtained from experimental measurement as they persist after the secondary decay of the primary fragments. This implies the cold fragments, that are detected by the detector, carry the signature of phase transition.

Another important observable is the size of the largest fragment produced in fragmentation of nuclei, which is considered as a order parameter of nuclear phase transition. Probability distribution of the size of the largest cluster shows double peaked distribution near phase transition region, at transition point height of those are exactly the same. This is known in the literature as bimodality of the distribution and is taken as a signature of 1st order phase transition for finite system [[22]-[25]]. In recent days, bimodal behavior has been observed in multi-fragmentation experiment of INDRA and ALADIN collaboration [[26],[27]]. But there may be some uncertainties both theoretically and experimentally to identify the two peaks of equal height, thereby the transition point, since the sharpness of the distribution becomes fade due to finite size effect [28]. So we have done the similar study (as multiplicity), for this latter observable, on its temperature derivative to get a clear view. In this connection we also studied the normalized parameter $a_2 = \frac{\langle A_{max}\rangle - \langle A_{max_2}\rangle}{\langle A_{max}\rangle + \langle A_{max_2}\rangle}$ and its derivative with respect to temperature. $a_2$ is used as a measure of the bimodality [[29],[30]] where $\langle A_{max}\rangle$, $\langle A_{max_2}\rangle$ are the average size of the 1st and 2nd largest fragments produced in fragmentation respectively [23]. For one-component ideal system these give the same signatures as multiplicity. Sometimes, experimentally, it is more advantageous to measure the size of the largest fragments or the second largest cluster than total multiplicity.

## Nuclear phase transition in presence of $\Lambda$ hyperon

In peripheral collisions of relativistic heavy ions the $\Lambda$ hyperons can be produced in participating region, which may get attached with the spectator, forming a highly excited hyper-nuclear system. This strange nuclear system may go through the process of multi-fragmentation. Therefore we have studied how the hyperon can modify the situation.

Studies of fragmentation of normal nuclei have been extended to three component system containing lambda hyperons with ordinary neutrons and protons. It has also been observed that liquid-like heavy hyper-fragments and gas-like small hyper-fragments co-exist in some temperature range, that indicates liquid-gas type phase transition occurs in fragmentation of hyper-nuclear system also, which is already established in case of normal nuclear fragmentation [[31]-[34]].

Here we have extended that study of phase transition for hyper system, examined the behavior of different thermodynamic variables e.g. entropy, specific heat, pressure over some temperature interval and how their behavior get modified by the presence of hyperons. We have shown that in this case the signals of phase transition get enhanced with a shift in the transition temperature.

# Bibliography

[1] C.B. Das, S. Das Gupta, W.G. Lynch, A.Z. Mekjian, M.B. Tsang, Phys. Rep. 406 (2005) 1.

[2] J.P. Bondorf, A.S. Botvina, A.S. Iljinov, I.N. Mishustin, K. Sneppen, Phys. Rep. 257 (1995) 133.

[3] D.H. Gross, Phys. Rep. 279 (1997) 119.

[4] A. J. Cole, Statistical Models for Nuclear Decay: From Evapo-ration to Vaporization (Institute of Physics, London, 2000).

[5] F. Reif, Fundamentals of Statistical and Thermal Physics, McGrawHill, New York, 1965.

[6] J. Randrup, S.E. Koonin, Nucl. Phys. A 471 (1987) 355c.

[7] Al.H. Raduta, Ad.R. Raduta, Phys. Rev. C 55 (2002) 1344.

[8] A.S. Botvina, et al., Phys. Rev. C 65 (2002) 044610.

[9] G. Chaudhuri, S. Das Gupta, M. Mocko, Nucl. Phys. A 813 (2008) 293.

[10] G. Chaudhuri, S. Das Gupta, W.G. Lynch, M. Mocko, M.B. Tsang, Phys. Rev. C 75 (2007) 067601.

[11] H.W. Barz, et al., Phys. Lett. B 191 (1987) 232.

[12] R. Ogul, et al., J. Phys. G 36 (2009) 115106.

[13] G. Chaudhuri, F. Gulminelli, S. Mallik, Phys. Lett. B 724 (2013) 115.

[14] P.J. Siemens, Nature 305 (1983) 410.

[15] D.H.E. Gross, Prog. Part. Nucl. Phys. 30 (1993) 155. (1995) 133.

[16] S. Das Gupta, A.Z. Mekjian, M.B. Tsang, in: J.W. Negele, E. Vogt (Eds.), Advances in Nuclear Physics, vol. 26, Plenum Publishers, New York, 2001, p. 89.

[17] P. Chomaz, et al., Phys. Rep. 389 (2004) 263.

[18] B. Borderie, M.F. Rivet, Prog. Part. Nucl. Phys. 61 (2008) 551.

[19] J. Bondorf, et al., Nucl. Phys. A 433 (1985) 321.

[20] J. Pochodzalla, et al., Phys. Rev. Lett. 75 (1995) 1040.

[21] C.B. Das, S. Das Gupta, A.Z. Mekjian, Phys. Rev. C 68 (2003) 031601 (R).

[22] F. Gulminelli, Ph. Chomaz, Phys. Rev. C 71 (2005) 054607.

[23] G. Chaudhuri, S. Das Gupta, F. Gulminelli, Nucl. Phys. A 815 (2009) 89.

[24] S. Mallik, S. Das Gupta, G. Chaudhuri, Phys. Rev. C 93 (2016) 041603.

[25] E. Bonnet, et al., Phys. Rev. Lett. 103 (2009) 072701.

[26] M. Pichon, et at., Nuclear Physics A 779 (2006) 267.

[27] M. Bruno, et al., Nuclear Physics A 807 (2008) 48.

[28] S. Mallik, F. Gulminelli, G. Chaudhuri, Phys. Rev. C 92 (2015) 064605.

[29] A. Le Fevre, et al., Phys. Rev. Lett. 100 (2008) 042701.

[30] A. Le Fevre, et al., Phys. Rev. C 80 (2009) 044615.

[31] A.S. Botvina, J. Pochodzalla, Phys. Rev. C 76 (2007) 024909.

[32] S. Das Gupta, Nucl. Phys. A 822, 41 (2009).

[33] V. Topor Pop and S. Das Gupta, Phys. Rev. C 81, 054911 (2010).

[34] S. Mallik and G. Chaudhuri, Phys. Rev. C 91, 054603 (2015).

## Publications in Refereed Journal:

a. Published:

  i. Effect of Hyperons on Phase Coexistence in Strange Matter, P. Das, S. Mallik, and G. Chaudhuri, Phys. Rev. C 95, 014603 (2017).

  ii. Multiplicity Derivative: A new Signature of a First-Order Phase Transition in Intermediate-Energy Heavy-Ion Collisions; S. Mallik, G. Chaudhuri, P. Das, and S. Das Gupta, Phys. Rev. C 95, 061601(R) (2017).

  iii. Statistical Ensembles and Fragmentation of Finite Nuclei; P. Das, S. Mallik, and G. Chaudhuri, Phys. Rev. C 96, 034609 (2017).

  iv. First-Order Derivative of Cluster Size as a New Signature of Phase Transition in Heavy Ion Collisions at Intermediate Energies; P. Das , S. Mallik, G. Chaudhuri, Phys. Lett. B 783 (2018) 364.

b. Accepted: None.

c. Communicated: None.

## Other Publications:

a. Book/Book Chapter: None.

b. Conference/Symposium:

  i. Hyper-nuclear Liquid-Gas Phase Transition, P. Das, G. Chaudhuri, S. Mallik; DAE Symp. Nucl. Phys. 60 (2015) 362-363.

  ii. Effect of Hyperons on Nuclear Phase Transition, P. Das, S. Mallik, G. Chaudhuri; DAE Symp. Nucl. Phys. 61 (2016) 400-401.

  iii. Statistical Ensemble and Fragmentation of Finite Nuclei, G. Chaudhuri, P. Das, S. Mallik; DAE Symp. Nucl. Phys. 61 (2016) 51-52.

  iv. Multiplicity Derivative: A New Signature of Phase Transition in Nuclear Multifragmentation, P. Das, S. Mallik, G. Chaudhuri, S. Das Gupta; DAE Symp. Nucl. Phys. 62 (2017) 402-403.

  v. Nuclear Multi-fragmentation: Canonical-Grand Canonical Ensemble Transformation, P. Das, S. Mallik, G. Chaudhuri; DAE Symp. Nucl. Phys. 62 (2017) 582-583.

Signature of Student: Pralerise Das

Date: 31/08/2018.

**Doctoral Committee**:

| S. No. | Name | Designation | Signature | Date |
|---|---|---|---|---|
| 1. | Dr. Jan-e Alam | Chairman | Jane Alam | 31.8.2018 |
| 2. | Dr. Gargi Chaudhuri | Convener | Gargi Chaudhuri | 31.8.2018 |
| 3. | Dr. D. N. Basu | Member | DN Basu | 31/08/2018 |
| 4. | Dr. Debades Bandyopadhyay (SINP) | Member | Debades Bandyopadhyay | 31.8.2018 |

# List of Figures

1.1 An illustrative sketch of the events of nuclear multifragmentation. . . . . . . . . 14

1.2 Mass distribution of fragments produced in fragmentation of a system of charge $Z_0 = 50$ and mass $A_0 = 120$ at three different temperatures T=3.5 MeV (solid line), T=4.7 MeV (dashed line) and T=5.5 MeV (dotted line) evaluated using CTM. . . . . . . . . . . . . . . . . . . . . . . . . . . . . . . . . 21

1.3 Variation of IMF multiplicity with incident beam energy in the central collision of Kr+Au. [59] . . . . . . . . . . . . . . . . . . . . . . . . . . . . . 22

2.1 A typical P - T phase diagram of a ordinary substance . . . . . . . . . . . . . 44

2.2 P Vs. V Phase diagram . . . . . . . . . . . . . . . . . . . . . . . . . . . . 45

2.3 Variation of temperature (T) with energy (E) supplied to the system in case of an ordinary liquid. . . . . . . . . . . . . . . . . . . . . . . . . . . . . . . 46

4.1 Grand canonical (a) proton, and (b) neutron number distributions for fragmenting source $Z_0 = 28$, $N_0 = 30$ at three different temperatures, T =3.6 MeV (black solid line), 4.5 MeV (red dashed line), 10.0 MeV (blue dotted line). . . . . . . . 75

4.2 Variation of $\sigma_n^2$ with freeze-out temperature (T) for the fragmenting system of charge 28 and mass 58. [4] . . . . . . . . . . . . . . . . . . . . . . . . . . 76

4.3 Grand canonical proton and neutron number distributions for fragmenting source $Z_0 = 28$, $N_0 = 30$ at temperature T =8 MeV. [4] . . . . . . . . . . . . . . . . . . . 77

4.4 Mass distribution of the fragments produced from disassembly of a source of mass number 58 and proton number 28, calculated from canonical (black dotted line) and grand canonical (blue dashed line) models for two different temperatures, T =6MeV (left panel) and 8MeV (right panel). There solid lines represent the canonical result obtained from the grand canonical model by using Eq. 4.23.[4] . 78

4.5 Multiplicities of Z =7 (left panels) and Z =12 (right panels) isotopes produced from two fragmenting systems of the same atomic number 28, but different mass numbers 58 (upper panels) and 64 (lower panels), calculated from canonical (black dotted line) and grand canonical (blue dashed line) models. The freeze-out temperature for both the system is T = 8 MeV. The red triangles represent the canonical result obtained from the grand canonical model by using Eq. 4.23.[4] 79

4.6 Variation of average size of the largest cluster ($Z_{max}$) with temperature (T) for the fragmenting system of charge 28 and mass 58 calculated from canonical (black dotted line) and grand canonical (blue dashed line) models. There solid lines represent the canonical result obtained from the grand canonical model by using Eq. 4.23.[4] . . . . . . . . . . . . . . . . . . . . . . . . . . . . . 80

4.7 Ratios ($R_{21}$) of multiplicities of fragments (N,Z) where mass and charge of the fragmenting system for reaction 1 are 58 and 28 respectively and those for reaction 2 are 64 and 28. The freeze-out temperature for both the fragmenting systems is T =8MeV. The left panel shows the ratios as a function of neutron number N for fixed Z values, while the right panel displays the ratios as a function of proton number Z for fixed neutron numbers (N) calculated from canonical (black dotted line) and grand canonical (blue dashed line) models. The red triangles represent the canonical result obtained from the grand canonical model by using Eq. 4.23. [4] . . . . . . . . . . . . . . . . . . . . . . . . . . . 80

5.1 Equation of state of nuclear matter obtained from the Nuclear Mean Field theory considering Skyrme interaction with compressibility 201MeV.[1] . . . . . . . . . . 87

5.2 Comparition between EOS for a Van der Waals gas and a system interacting via Skyrme interaction.[2] . . . . . . . . . . . . . . . . . . . . . . . . . . . 88

5.3 Mass distribution of the fragments produced in fragmentation of a source of size $A_0 = 200$ at three temperatures, 3.5MeV (black solid line), 4.0MeV (red dashed line) and 5.0MeV (blue dotted line). . . . . . . . . . . . . . . . . . . . . . . . . 89

5.4 Variation of free-energy (F/A), entropy (S/A) and specific heat ($C_V/A$) with temperature T in the upper, middle and lower panel, respectively, for two fragmenting sources $A = 200$, $A = 500$. T, F, S, $C_V$ all are plotted in MeV. . . . . . 89

5.5 (a) Caloric curve and (b) the variation of normalised size of the average largest cluster $\langle A_{max} \rangle / A_0$ with temperature are plotted for two different fragmenting system of size $A_0 = 200$ and $A_0 = 500$ using CTM. . . . . . . . . . . . . . . . . . 90

5.6 Variation of IMF multiplicity with incident energy for the central collision of Kr+Au (left) [17], and with impact parameters for “Au+Au” projectile fragmentation reaction. (right)[18]. . . . . . . . . . . . . . . . . . . . . . . . . . . 92

5.7 Caloric curves measured in the experiments. [1] . . . . . . . . . . . . . . . . . 93

5.8 Variation of (a) excitation energy $E^*/A$ (MeV/A), (b) total multiplicity M, (c) average size of the largest cluster $Z_{max}$ with temperature T (MeV) for the fragments produced in the fragmentation of an ideal one-component system of size A=500. . . . . . . . . . . . . . . . . . . . . . . . . . . . . . . . . . . . . . . . 95

5.9 Variation of multiplicity M (left panels) and dM/dT (right panels) with temperature (bottom x axes) and excitation per nucleon (top x axes) from the CTM calculation for fragmenting systems having Z =82 and N =126 (top panels). Bottom panels represent the same but for a hypothetical system of one kind of particle with no Coulomb interaction but the same mass number (A =208). $E^* = E - E_0$, where $E_0$ is the ground-state energy of the dissociating system in the liquid drop model whose parameters are given in Ref. [21].[23] . . . . . . . . 97

5.10 Same as Fig. 5.9 but the fragmenting systems are Z =28 and N =30 (top panels) and A =58 (bottom panels). [23] . . . . . . . . . . . . . . . . . . . . . . . . 98

5.11 Variation of dM/dT (red solid lines) and $C_v$ (green dashed lines) with temperature from CTM for fragmenting systems having Z =82 and N =126 (left panel) and for hypothetical systems of one kind of particle with no Coulomb interaction of mass number A =208. To draw dM/dT and $C_v$ in the same scale, Cv is normalized by a factor of 1/50. [23] . . . . . . . . . . . . . . . . . . . . . . . . 99

5.12 Same as in Fig. 5.11, but the fragmenting systems are Z =28 and N =30 (left panel) and A =58 (right panel). [23] . . . . . . . . . . . . . . . . . . . . . . . . 100

5.13 Variation of entropy (blue dashed lines) and dM/dT (red solid lines) with temperature from CTM for fragmenting systems having Z =82and N =126 (top panel) and for hypothetical system of one kind of particle with no Coulomb interaction of mass number A =208 (bottom panel). To draw S and dM/dT in the same scale, S is normalized by a factor of 1/20 for Z =82 and N =126 system and 1/50 for hypothetical system of one kind of particle. [23] . . . . . . . . . . . 101

5.14 Variation of intermediate-massfragment(IMF) multiplicity $M_{IMF}$ (left panels) and first-order derivative of IMF multiplicity $dM_{IMF}/dT$ (right panels) with temperature from CTM calculation for fragmenting systems having Z =82 and N =126. Variation of $C_v$ with temperature (T) is shown by green dashed line in right panel. To draw d$M_{IMF}/dT$ and $C_v$ in the same scale, $C_v$ is normalized by a factor of 1/100. [23] . . . . . . . . . . . . . . . . . . . . . . . . . . . . . 102

5.15 Effect of secondary decay on M (left panel) and dM/dT (right panel) for fragmenting systems having Z =28 and N =30. Red solid lines show the results after the multifragmentation stage (calculated from CTM), whereas blue dashed lines represent the results after secondary decay of the excited fragments. [23] . . . . 103

5.16 Variation of (a) $\mathbf{a}_{max}$, (b) $\mathbf{a}_2$, (c) M, (d) S, (e) -$d\mathbf{a}_{max}/dT$, (f) -$d\mathbf{a}_2/dT$, (g) dM/dT and (h) $C_v$ with temperature for fragmenting system of mass A=200. [24]104

5.17 Variation of $d\mathbf{a}_{max}/dT$ with temperature (a) at constant freeze-out volume $V_f = 6V_0$ but for three fragmenting system of mass 50 (blue dotted line), 100 (red dashed line) and 200 (black solid line) and (b) for same fragmenting system of mass 200 but at three constant freeze-out volumes $V_f = 2V_0$ (magenta dotted line), $V_f = 6V_0$ (black solid line) anf $V_f = 8V_0$ (green dashed line). [24] . . . . . 105

5.18 Dependence of the peak position of -$d\mathbf{a}_{max}/dT$, -$d\mathbf{a}_2/dT$, dM/dT and $C_v$ on fragmenting system size (upper panel) and freeze-out volume (lower panel). [24] 106

6.1 Variation of Helmholtzs free energy per nucleon (upper panel), entropy per nucleon (middle panel), and specic heat per nucleon (bottom panel) with temperature for two fragmenting systems having the same $A_0 = 128$, $Z_0 = 50$ but different $H_0 = 8$ (black solid lines) and $H_0 = 0$ (red dashed lines).[21] . . . . . . 117

6.2 Variation of temperature (T) with excitation energy ($E$) for two fragmenting systems having the same $A_0 = 128$, $Z_0 = 50$ but different $H_0 = 8$ (black solid line) and $H_0 = 0$ (red dashed line).[21] . . . . . . . . . . . . . . . . . . . . . . . 118

6.3 Variation of pressure with volume for two fragmenting systems having the same $A_0 = 128$, $Z_0 = 50$ but different $H_0 = 8$ (solid lines) and $H_0 = 0$ (dashed lines) at four different temperatures T =5.0, 5.5, 6.0, and 6.5 MeV.[21] . . . . . . . . . 119

6.4 Largest cluster probability distribution for four different fragmenting systems having same $A_0 = 128$, $Z_0 = 50$ but different $H_0 = 8$ (black solid line), $H_0 = 4$ (blue dotted line), $H_0 = 2$ (green dash-dotted line), and $H_0 = 0$ (red dashed line). Calculations are done at constant temperature T =6.065 MeV.[21] . . . . 120

6.5 Variation of transition temperature ($T_p$) with the total strangeness content of the fragmenting system.[21] . . . . . . . . . . . . . . . . . . . . . . . . . . . . 121

6.6 Variation of average charge of the largest cluster ($Z_{max}$) with temperature (T) for two fragmenting systems having the same $A_0 = 128$, $Z_0 = 50$ but different $H_0 = 8$ (black solid line) and $H_0 = 0$ (red dashed line).[21] . . . . . . . . . . . . 122

6.7 Variation of average charge of the largest cluster ($Z_{max}$) (upper panel) and specic heat per nucleon (lower panel) with temperature (T) by switching on (blue dashed lines) and switching off (black solid lines) the Coulomb interaction. All the calculations are done for the fragmentation of a hypernucleus having $A_0 = 128$ baryons, $Z_0 = 50$ protons, and $H_0 = 8$ hyperons.[21] . . . . . . . . . . 123

A.1 Wignner-Seitz approximation . . . . . . . . . . . . . . . . . . . . . . . . . . 136

# List of Tables

4.1 The grand canonical result, as well as the approximation, Eq. 4.23, of the canonical result from the grand canonical ensemble are compared to the exact canonical calculation for different observables obtained from fragmentation of the source of mass number 58 and proton number 28 at freeze-out volume $V_f = 3V_0$ and two different temperatures T =6 and 8 MeV. . . . . . . . . . . . . . . . . . . . . . . 82

# Chapter 1

# Introduction

It has been a very long time since the curious human minds have been searching for the answers to the questions such as; what is everything made of and what laws govern them. In this quest, they do find that the level of fundamental constituent of matter depends on the amount of energy used to probe it. Higher the energy, deeper into the matter it is possible to probe, from atoms to the nucleus, nucleons to quarks [1]-[5]. Depending on the energy, dimensions and complexity of the system, different phenomenon is experienced. The behaviour of nuclei under extreme condition (of excess pressure, density, energy and temperature) is a fascinating field of research in recent days. Such a condition may occur spontaneously in nature, and can also be created artificially in a laboratory in the experiments of nuclear reaction with suitable bombarding energy. Heavy Ion Collisions (HIC) at very high energies, $\approx$ a few GeV/nucleon to TeV/n, produce the so-called 'Quark-Gluon-Plasma(QGP)' phase of matter [6], [7]. Our universe at the early stage, just after the big-bang, is believed to exist in such state, and according to some conjecture, the core of the neutron star may contain the matter in QGP phase. At comparatively low bombarding energies, $\approx$ a few tens of MeV/n to a few GeV/n, a very interesting phenomenon emerges in heavy ion collision, which is named as "Nuclear Multifragmentation". The phenomenon was observed to happen spontaneously, by the effect of cosmic rays. The present work is devoted to the nuclear multifragmentation phenomenon, and it is described in the next paragraph.

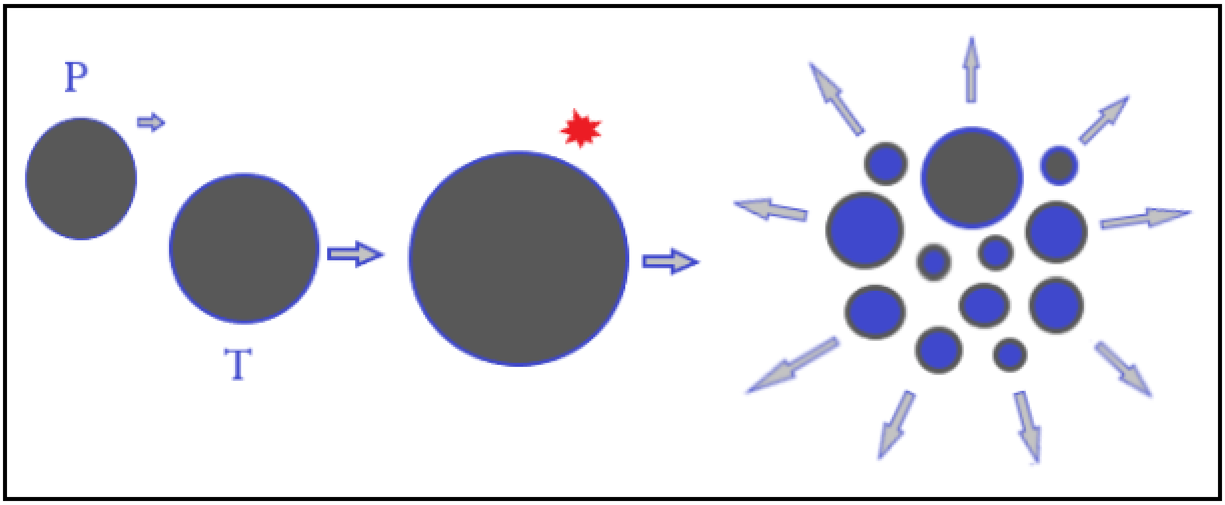

Figure 1.1: An illustrative sketch of the events of nuclear multifragmentation.

In the experiments of low energy nuclear collisions, depending upon the reaction energy, the following scenario may occur. For the reactions with beam energy below 10 MeV/n, the compound nucleus is formed due to the complete fusion of the target and the projectile nuclei. If the excitation energy ($\epsilon^*$) of this system is as low as, few MeV/n, the long-lived compound nucleus will decay through either evaporation by successive emission of particles or fission. The mechanism of these compound nuclear decay modes can be understood by the standard liquid-drop model. At a higher excitation energy ($\approx$ 2-3 MeV/n) emission of heavy nuclei ($Z \geq 2$) competes with the light particles ($Z \leq 2$) emission. When the excitation energy is comparable to the binding energy of the nucleus, $\epsilon^* \approx 5 - 8$ MeV/n, the long-lived compound nucleus no longer exists, and instead, the whole system decays through an explosion like process. The time scale for such processes is $\approx 10^{-21}$ sec. The phenomenon of instantaneous disintegration of a nucleus to multiple fragments of various mass is named as 'nuclear multifragmentation' [8] where the term 'multi' stands for 'more than two'.

## 1.1 Experimental Facilities

It is nearly a century ago when nuclear multifragmentation was first observed as a mysterious incident in the studies with the cosmic rays [9], [10]. Afterwards, during the 1950s, few records of such events were registered in the laboratory experiments with accelerators [11],[12]; though the reaction mechanism, then, was not comprehensible. A systematic study of fragmentation of nuclei was not initiated until the 1980s when multiple fragment emission was observed in a nuclear reaction of an emulsion target with the 250 MeV/n Carbon projectile in Bevalac experiments at the Lawrence Berkeley Laboratory (USA)[13]. At present, the experimental facilities for nuclear reactions at intermediate or high energies have been provided at the Grand Accelerateur National D'ions Lourds (GANIL, France), the Gesellschaft fur Schwerionenforschung mbH (GSI, Germany), the Superconducting Cyclotron at Laboratori Nazionali del Sud in INFN (Catania, Italy), Joint Institute for Nuclear Research (Dubna, Russia), Riken (Japan), National Superconducting Cyclotron Laboratory (NSCL) at Michigan State University (MSU, USA), Texas A and M Cyclotron (USA) etc. Experiments at these laboratories have enriched us with a lot of information regarding the fragmentation of the nucleus during a nuclear reaction.

## 1.2 Theoretical Models

The ample resource of experimental data on intermediate energy nuclear fragmentation lead to the theoretical investigations of this phenomenon. Several theoretical models have been developed to understand the mechanism of the process, and to give a satisfactory explanation of the data. According to the adopted reaction scenario, the existing theoretical studies can be categorised, primarily, into two different approaches: i. Statistical approach and ii. Dynamical approach, which will be introduced briefly in the following paragraphs.

### 1.2.1 Statistical Approach

The statistical model studies are based on the assumption that in the course of a reaction, fragments, produced in the decay of the parent nucleus, attain a statistical equilibrium state at some point. Then, the average quantities are calculated applying equilibrium statistical mechanics to the (thermally and chemically) equilibrated system of fragments. The dynamical evolution of a system, before the equilibrium is established, is not under the area of the studies using statistical approaches. The present dissertation is entirely based on the statistical model, so, a complete picture will be given latter. Here we are giving some historical remarks in the field of statistical fragmentation. The statistical study of multi-nucleon clusters was initiated by A. Mekijan [14] to describe the behaviour of a very hot nucleus. Later on, a grand canonical model developed by J. Randrup and S. Koonin [15] made an foremost contribution to the subject. Microcanonical calculations were developed by D. H. E Gross and his co-workers [16] and by Randrup and collaborators [17]. Statistical Multifragmentation Model (SMM) developed by Bondorf *et al.* [18] in Copenhagen is another important model in this area and is extensively used to compare experimental data. All these models need extensive numerical techniques. A comparatively simple model based on canonical ensemble is Canonical Thermodynamical

Model (CTM) [19] which can be implemented simply, without any complex numerical analysis. Statistical models perform satisfactorily well to reproduce experimental data, but they alone can not provide the complete information of the reaction at all the stages. Statistical models overlook the dynamical stage of the reaction. Parameters in the statistical models, e.g., temperature or the size of the fragmenting source are the inputs to the model, and can not be derived in this framework, and therefore, the dynamical stage of a reaction before equilibration needs to be explored.

### 1.2.2 Dynamical Approach

In the dynamical approach, the time evolution of the entire reaction process, collision, clusterisation, and evolution of the fragments is studied. The dynamical models can explain collective flow [20] , nuclear stopping [21], etc., and can provide the freeze-out conditions of statistical approaches. Different dynamical models have been developed to describe HICs depending upon the energy of the reaction, and how realistically the situations will be treated. Time-dependent Hartree-Fock theory has been used for low energy Heavy Ion Collisions where the nuclear mean fields are important in comparison to two body reaction dynamics. To describe intermediate energy HIC, where the two body dynamics becomes significant besides the mean field, there are mainly two types of microscopic dynamical models:

i. **Boltzmann-Uehling-Uhlenbeck (BUU) Models** [[22]-[26]]. In these semi-classical transport models, mean-fields and hard collisions both are incorporated. The entire many-body nuclear system of target and projectile of a nuclear reaction is approximated by a one-body phase space distribution function $f(\vec{r}, \vec{p}, t)$, time evolution of which is governed by the BUU equation,

$$\frac{\partial f}{\partial t} + \vec{v}.\nabla_r f - \nabla_r U.\nabla_p f = I_{coll} \tag{1.1}$$

Where U is the mean-field potential and the term in the right-hand side is the collision integral term that includes the Pauli blocking. For low energy collisions where the collision term in the R. H. S can be neglected; the equation gives the Vlasov equation. But at the intermediate energies, this collision term cannot be neglected, and the Eq. 1.1 needs to be solved. To solve the equation, different numerical realisations have been employed, which leads to different transport models, e.g., Boltzmann-Uehling-Uhlenbeck, Boltzmann-Langevin equation, Boltzmann-Nordheim-Vlasov, Landau-Vlasov. These transport models differ from one another by the separate mean field parametrization $U$ invoked or the execution of the test-particle method.

ii. **Quantum Molecular Dynamics (QMD) Models** ([27]-[30]). This is an n-body microscopic dynamical model which describes the formation of fragments in HIC in a more realistic way. Here every nucleon is represented by a coherent Gaussian wave packet of width $\sqrt{L}$, about the mean position $\vec{r_i}(t)$ and mean momentum $p_i\vec{(t)}$,

$$\phi_i(\vec{r}, \vec{p}t) = \frac{1}{(2\pi L)^{3/4}} e^{-(\vec{r}-r_i\vec{(t)})/4L}.e^{i\vec{p_i}(t).\vec{r}/h}. \qquad (1.2)$$

An initial n-body Wigner density is then constructed by these coherent states and time evolution of the system is achieved by incorporating a generalized variational principle.

Based on this common primary structure, various QMD realizations have been developed which differ in their detail descriptions, initialisation of the target and projectile. Such variants are BQMD [31], [32] which was designed to give proper binding of a nucleus for the study of low energy fragmentation, Isospin-QMD (IQMD) [[32]-[34]], which deals with the various nucleonic charge states, deltas, pions. To present a Lorentz-covariant description of heavy ion reaction, the relativistic formulation of QMD is relativistic quantum molecular dynamics (RQMD) [[35]-[37]]. An antisymmetrized version of molecular dynamics is fermionic molecular dynamics (FMD) which is a semi-quantal description that incorporates Fermi-Dirac statistics on the many-body state level [38]. Another version of antisymmetrized molecular dynamics including two-nucleon collisions is called AMD [39],[40].

Apart from the statistical and dynamical models, there are some other models like, lattice-gas model [41], [42], probabilistic models [[43]-[49]], e.g., minimum information principle, percolation model, which are used to describe the nuclear multifragmentation data. In addition, some hybrid models have been developed where different stages of a reaction are described by the different approaches [[50]-[57]].

In this thesis, we will be using statistical models only, so we introduce a general reaction scenario of a heavy ion collision at intermediate energy that has been adopted in almost all the statistical models.

## 1.3 Physical Picture in the Statistical Approach

In an intermediate energy nuclear reaction experiment, the entire process of the reaction can be, most generically, divided into three stages: i. Collision between projectile and target, and thereby the formation of an intermediate hot chunk of nuclear matter, ii. The expansion of this intermediate excited system and fragments production due to its break-up, iii. De-excitation of these excited primary fragments.

We begin by considering a situation in a heavy ion collision experiment where the projectile nucleus strikes a target nucleus. The nucleons from both of the nucleus begin to collide with each other. After multiple collisions, they lose their identity, and form, as a whole, an intermediate excited nuclear system which is called fragmenting system.

The target-projectile impact may cause an initial compression into this hot intermediate system depending upon the beam energy. This initial compression, along with an internal pressure due to the internal excitation energy in the system, results in an overall expansion. In the course of expansion, the density fluctuation occur, and the composites start to develop in the higher density portions. At this stage, nucleons interact with one another (at least with the nearest neighbour) and mass, charge, energy transfer, rearrangement continues to happen between different sections of the system. Very soon, the density decreases substantially so that the mean free path of these processes becomes greater than the dimension of the system. At this stage, nucleons on the surfaces of any two clusters are well separated, out of the range of nuclear force (typically 2-3 fm) so that strong interaction between any two clusters ceases. Here the break-up occurs, and fragments are emitted. At the time of the break-up, the average nucleon density decreases to 0.5 to 0.1 times the normal nuclear density ($\rho_0$ =0.16 n/$fm^3$). The entire process of the fragment production is very fast. A typical time is 50-100fm/c (order of $10^{-22}$ sec). Now the fragments interact with each other through Coulomb force only. At this point, the whole system containing all the fragments is assumed to be in thermal and chemical equilibrium. The chemical equilibrium is established in the sense that no further change will occur in fragment contents within a single break-up. Now the equilibrated system is said to attain a freeze-out condition. All the statistical model calculations start at this point, assuming the system is at freeze-out. Equilibrium temperature of the system at freeze-out is called the freeze-out temperature $T_f$, and the volume of the whole system containing all the fragments is named as freeze-out volume $V_f$.

After freeze-out, the fragments evolve under the influence of Coulomb force. These fragments are called ‘primary fragments’ or ‘pre-fragments’. They are, in general, excited, and therefore particle unstable, and they lose excitation by sequential binary decay. The final cold fragments after secondary decay are called ‘secondary fragments’, and the secondary fragments are detected in the experimental detectors.

The fragmenting nucleus can break-up in various ways satisfying mass and charge conservation. The number of such ways is connected to the partitions of the total charge ($Z_0$) and mass ($A_0$) of the fragmenting source. For example, if we consider only the partition of the total charge $Z_0$, the number of partitions can be estimated from the Hardy-Ramanujan asymptotic formula [58],

$$P(Z_0) \approx \frac{1}{4Z_0\sqrt{3}} \,.\, e^{\pi\sqrt{2Z_0/3}}. \tag{1.3}$$

For $Z_0 = 100$ one get $P(Z_0) \approx 2.10^8$. So, theoretically, the number of ways a nucleus can fragment is huge.

Each particular way, in which a nucleus can disintegrate, is called a channel or a partition. At an excitation energy $1-10$MeV/n, all these extremely large number of decay channels open up, and on this ground, the system is dealt with by using a statistical approach. In this approach, all the possible decay channels are sorted out, and their relative probabilities are estimated. These probabilities are used to calculate the final mean values of the observables. According to the statistical mechanics, the probability of a decay channel is proportional to its statistical weight, i.e., the number of microstates under this break-up channel. This statistical weight is estimated considering the constraints on total mass, charge, energy of the system. Further details can be seen in Chapter 3 where the thermodynamic models of nuclear multifragmentation [19] have been discussed. Before going into the subject of the present work, some important general features of nuclear fragmentation are worth mentioning, which will be given in the following section.

## 1.4 Characteristics of Fragmentation

### 1.4.1 Mass Distribution

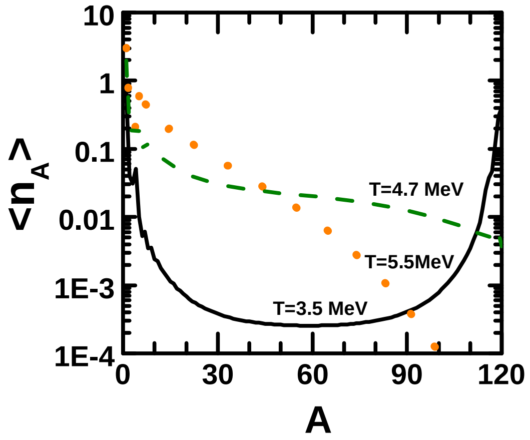

Figure 1.2: Mass distribution of fragments produced in fragmentation of a system of charge $Z_0 = 50$ and mass $A_0 = 120$ at three different temperatures T=3.5 MeV (solid line), T=4.7 MeV (dashed line) and T=5.5 MeV (dotted line) evaluated using CTM.

Mass distribution or multiplicity distribution means the variation of average fragment count with fragment mass. The mass distribution of the fragments produced in the fragmentation of a nucleus is crucial for the study of nuclear multifragmentation, and it is accessible in the experiments. It can clearly indicate the occurrence of fragmentation. A typical mass distribution of fragmentation is shown in Fig. 1.2 for three different freeze-out temperatures (T) for a fragmenting source $Z_0 = 50$, $A_0 = 120$. At low temperature T=3.5MeV, one get the so-called 'U'-shaped curve that indicates both heavy and low mass fragments are produced in the fragmentation. At T=4.7 MeV, the curve deviates from U-shape, and one can observe the notable presence of the intermediate fragments in between heavy and low mass limits. This is because, at this temperature (excitation), the fragmenting source produces multiple fragments. At a higher temperature, T=5.5 MeV, the curve becomes monotonically decreasing, which indicates the production of small fragments only. Mass distribution plots at different temperatures, thus, nicely indicate liquid or gaseous phase (explained latter) of the system after fragmentation.

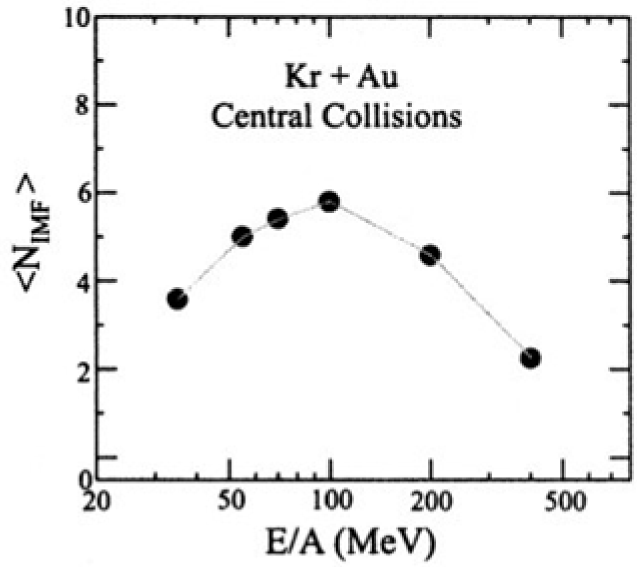

Figure 1.3: Variation of IMF multiplicity with incident beam energy in the central collision of Kr+Au. [59]

### 1.4.2 Intermediate Mass Fragment (IMF) Production

The fragments, having charge greater than 2 and in between 20 to 30 ($2 < Z < 20$ to 30) are termed as intermediate mass fragments (IMF). These are the fragments heavier than alpha but does not include fission like fragments. Production of IMF is a consequence of nuclear multifragmentation events. Therefore count of such fragments is a key observable for multifragmentation phenomenon. Variation of IMF number ($\langle N_{IMF} \rangle$) with different beam energy is shown in Fig. 1.3 [59].

### 1.4.3 Phase Transition

On several occasions, nuclear multifragmentation is described from the angle of the liquid-gas phase transition in excited nuclear matter. Heavy mass nuclei are considered as a nuclear liquid while nucleons and very light fragments are taken as nuclear gas. An early study of multifragmentation process by Gross *et al.* [60] in the framework of the statistical model gave first the possibility of a transition around 5 MeV temperature. Fragment mass distributions at low temperatures are generally of U-shape (Fig. 1.2) indicating the presence of both heavy mass and low mass fragments, and this is considered as liquid-gas coexistence. As temperature increases, peak height in the large mass region begins to fall; the shape deviates from 'U'. At sufficiently high temperature, it becomes exponential in nature since more light fragments are produced at a higher temperature. This can be interpreted as a passage over from co-existence zone to the gas phase. The temperature where the peak in the greater mass region just begins to decrease can be interpreted as transition temperature. The ordinary phase transitions are defined for a macroscopic system ($N \approx 10^{23}$) in the thermodynamic limit. The nuclear system at laboratory consists of at most a few hundreds of nucleons; therefore, the term 'phase transition' is not strictly valid in the finite nuclear system with long-range Coulomb interaction. But the real nuclear system (atomic nuclei) is recurrently extrapolated to an idealised system of nuclear matter. The nuclear matter is defined as an infinite sea (without surface) of neutrons and protons interacting only through nuclear force where the Coulomb force is assumed to be absent. Such a system gives liquid-gas type phase transition in many calculations. The fragmentation of a finite nucleus is considered as a parallel to the phase transition in infinite nuclear matter.

These are some of the very basic features of multifragmentation, which will be referred often throughout the thesis, while the major part of it is devoted to the last topic (phase transition). Now we present a formal outline of the thesis.

## 1.5 Organisation of Present Work

In the present thesis, built on the foundation of Statistical Models of multifragmentation, the focus has been on the following directions of fragmentation of the nucleus at intermediate energy: i. Grand canonical to canonical ensemble transformation, ii. Search for new observables showing signatures of phase transition, iii. Phase transition in the presence of hyperons within the nucleus. Since the three are based on three different themes, in each case, an introduction to the subject and motivation of the study have been presented at the starting of the respective chapters. Most of the work, here, has been done using the canonical thermodynamical model; at few places, grand canonical version of the thermodynamical model has been used. The thesis has been organised as follows.

In Chapter 2, we discuss the introductory concepts of statistical physics, statistical ensembles and ordinary phase transition in thermodynamic systems, briefly, since our latter works are the perquisites of these basics. In Chapter 3, the thermodynamical models of nuclear multifragmentation are discussed in detail. We derive all the important observables using canonical and grand canonical models. In Chapter 4, we develop a relation between canonical and the grand canonical average of any observable for a system consisting of two kinds of particles. The relation is applied to approximate the canonical average value of multifragmentation observables, and the performance of the derived relation is judged, using the thermodynamical models of fragmentation. In Chapter 5, we identify some fragmentation observables that show the signature of the first-order phase transition. We propose that those observables are suitable for experimental studies of phase transition. In Chapter 6, we study the phase transition in the hypernuclear system and try to find out the effect of hyperons in it. In Chapter 7, finally, we summarise all the results of this exploration, and indicate the provisions for further improvement.

# Bibliography

[1] J. J. Thomson, Phil. Mag. **44** (1897) 293.

[2] E. Rutherford, Phil. Mag. **21** (1911) 669.

[3] J. Chadwick, Proc. Roy. Soc. (London) A **136** (1932) 629.

[4] E. D. Bloom; et al. Phys. Rev. Lett. **23** (16) (1969) 930.

[5] M. Breidenbach; et al. Phys. Rev. Lett. **23** (16) (1969) 935.

[6] J. Adams et al. [STAR Collaboration], Nucl. Phys. A **757** (2005) 102 [nucl-ex/0501009].

[7] KAamodt et al. [ALICE Collaboration], Phys. Rev. Lett. **105** (2010) 252302 [arXiv:1011.3914 [nucl-ex]]; Phys. Rev. Lett. **105** (2010) 252301 [arXiv:1011.3916 [nucl-ex]]; Phys. Rev. Lett. **106** (2011) 032301 [arXiv:1012.1657 [nucl-ex]]; Phys. Rev. Lett. **107** (2011) 032301 [arXiv:1105.3865 [nucl-ex]].

[8] J.P. Bondorf, Journal de Physique **37** (1976) C5 - 195; J.P. Bondorf, Proceeding of the EPS topical conference on large amplitude collective nuclear motions, Keszthely, Hungary, June 1979

[9] I. I. Gurevich, et al., Dokl. AN SSSR. **18** (1938) 169.

[10] E. Schopper, Naturwissenschaftler. 1937. Bd.5. S.557.

[11] O. V. Lozhkin, N. A. Perfilov, Zh. Eksp. Teor. Fiz. **31** (1956) 913.

[12] N. A. Perfilov, O. V. Lozkin, V. P. Shamov, Sov. Phys. Usp. **38** (1960) 345.

[13] Jakobsson B. et al., Z. Phys. A. **307** (1982) 293.

[14] A.Z. Mekijan, Phys. Rev. C **l7** (1978) 1051.

[15] J. Randrup, S. E. Koonin, Nuclear Physics A **356** (1981) 223.

[16] D. H. E. Gross, Phys. Rep **279** (1997) 119.

[17] S. E. Koonin, J. Randrup, Nuclear Physics A **474** (1987) 173.

[18] J. P. Bondorf *et al.*, Phys. Rep. **257** (1995) 133.

[19] C. B. Das, S. Das Gupta, W. G. Lynch, A. Z. Mekjian and M. B. Tsang, Phys. Rep. **406**, 1 (2005).

[20] H.A. Gustafsson et. al., Phys. Rev. Lett. **52** (1984) 1590.

[21] W. Bauer, Phys. Rev. Lett. **61** (1988) 2534.

[22] G. F. Bertsch and S. Das Gupta, Phys. Rep **160** (1988) 189.

[23] B. A. Li, L. W. Chen, and C. M. Ko, Phys. Rep. **464** (2008) 113.

[24] S. Mallik, G. Chaudhuri and S. Das Gupta , Phys. Rev. C **91** (2015) 044614.

[25] S. Mallik, S. Das Gupta, and G. Chaudhuri, (Phys. Rev. C **93** (2016) 041063.

[26] S. Mallik, G. Chaudhuri and F. Gulminelli; Phys. Rev. C **97** (2018) 024606.

[27] J. Aichelin, Phys. Rep. **202** (1991) 233.

[28] J. Aichelin and H. Stocker, Phys. Lett. B **176** (1986) 14.

[29] G. E. Beauvais, D. H. Boal and J. C. K Wong, Phys. Rev. C **35** (1987) 545.

[30] J. Aichelin, A. Rosenhauer, G. Peilert, H. Stocker, and W. Greiner. Phys. Rev. Lett. **58** (1987) 1926.

[31] A. Bohnet et al. Phys. Rev. C **44** (1991) 2111.

[32] C. Hartnack et al., Eur. phys. J. A **1** (1998) 151.

[33] C. Hartnack, L. Zhuxia, L. Neise, G. Peilert, A. Rosenhauer, H. Sorge, J. Aichelin, H. Stocker, and W. Greiner. Nucl. Phys. A **495** (1989) 303.

[34] Ch. Hartnack. PhD thesis, GSI-Report 93-5 (1993).

[35] Heinz Sorge, Horst Stocker, and Walter Greiner; Annals of Physics **192** (1989) 266306.

[36] Tomoyuki Maruyama et al, Nucl. Phys. A **534** (1991) 720.

[37] Tomoyuki Maruyamaa et. al. ; Phys. Lett. B **358** (1995) 34.

[38] H. Feldmeier; Nucl. Phys. A **515** (1990) 147.

[39] A. Ono, H. Horiuchi, T. Maruyama, and A. Ohnishi; Phys. Rev. Lett. Vol. **68** Num. 19 (1992) 2898.

[40] A. Ono and H. Horiuchi, Prog. Part. Nucl. Phys **53** (2004) 501.

[41] J. Pan and S. Das Gupta, Phys. Lett B **344** (1995) 29.

[42] S. Das Gupta, S. Mallik and G. Chaudhuri; Phys. Rev. C **97** (2018) 044605.

[43] J. Aichelin, J. Hiifner and R. Ibarra, Phys. Rev. C **30** ( 1984) 107.

[44] D.J. Field, W.G. Lynch et al., Phys. Rev. C **30** (1984) 1912.

[45] B.E. Hasselquist et al., Phys. Rev. C **32** (1985) 145; Y. Shibata and T. Fujita, Phys. Lett. B **172** ( 1986) 283.

[46] J.W. Essam, Rep. Progr. Phys. **43** (1980) 833.

[47] X. Campi and J. Desbois, in: Proc. 23rd Int.Winter Meeting on Nucl.Phys., Bormio, 1985, p.497.

[48] W. Bauer, U. Post, D.R. Dean and U. Mosel, Nucl. Phys. A **452** (1986) 699.

[49] T.S. Biro, J. Knoll and J. Richert, Nucl. Phys. A **459** (1986) 692; 0. Knospe, R. Schmidt and H. Schulz, Phys. Lett. B **182** ( 1987) 293.

[50] A.S. Botvina, AS. Iljinov and IN. Mishustin, Pisma v ZhETF **42** (1985) 462; AS. Botvina, A.S. Iljinov and IN. Mishustin, Phys. Lett. B **205** (1988) 421.

[51] Chr. Jung, W. Cassing et al., Nucl. Phys. A **477** (1988) 256.

[52] S. Das Gupta, C. Gale and J. Gallego, Phys. Rev. C **33** (1986) 1634.

[53] K. Sneppen and L. Vinet, Nucl. Phys. A **480** (1988) 342.

[54] J. Desbois, R. Boisgard, G. Ngo and J. Nemeth, Z. Phys. A **328** (1987) 101.

[55] M. Colonna, N. Colonna, A. Bonasera and M. Di Toro, Nucl. Phys. A **541** ( 1992) 295.

[56] T.S. Sangster et al., Phys. Rev. C **46** (1992) 1404.

[57] S.R. Souza, L. de Paula, S. Leray, J. Nemeth, C. Ngo and H. Ngo, Nucl. Phys. A **571** (1994) 159 .

[58] G. H. Hardy and S. Ramanujan, 1917 Proc. London Math. Soc. 2 **16** 112; G. H. Hardy and S. Ramanujan, 1917 Proc. London Math. Soc. 2 **17** 75; G. H. Hardy and S. Ramanujan. Asymptotic formulae in combinatory analysis. Proc. London Math. Soc. (2), 17:75115, 1918.

[59] G.F. Peaslee *et al.*, Phys. Rev C **49** (1994) R 2271.

[60] D.H.E. Gross, L. Satpathy, Meng Ta-chung, M. Satpathy, Z. Physics A **309** (1982) 41.

# Chapter 2

# Statistical Physics: Overview

*"Statistical mechanics is a probabilistic approach to equilibrium macroscopic properties of large numbers of degrees of freedom"* [1]. In this chapter we have tried to sketch an outline of the basic concepts of statistical mechanics. Starting from the idea of equilibrium, we gradually develop the theory of ensembles and see how the probabilistic approach is incorporated here. In the context of this, we have discussed, briefly, the ideas of micro-states and macro-states, phase-space representation etc.

In the beginning, one needs to clarify the system size in the background of statistical mechanics. The term macroscopic is related to the size of the system of interest, and it means a large scale. A macroscopic system is big enough (roughly greater than 1 micron) so that it could be observed in the ordinary sense, at least with a microscope using ordinary light. On the other hand, microscopic means small scale so that a microscopic system is one, the size of which is of the order of atomic dimension or less (1 Angstrom or less). In statistical physics or thermodynamics, all the systems of interests are macroscopic, consist of a large number of particles (of the order of Avogadro's number $10^{23}$). Therefore, it is time-honoured, for all theoretical purposes, to do the analysis in the so-called 'thermodynamic limit', viz., $N \to \infty, V \to \infty$ so that particle density ($n = N/V$) remains fixed; all the extensive properties of the system will then be proportional to the system size (N or V).

## 2.1 Phase Space Representation and Definition of Equilibrium

In thermodynamics, equilibrium means the particular situation where the state variables of a system such as pressure (P), energy (E), temperature (T) etc. (which describe the macroscopic properties of the system) are independent of time. To define it in a more sophisticated way, one needs to consider the system from a microscopic point of view. At the microscopic level, all the macroscopic objects are composed of interacting atoms or molecules. The interaction between the atoms or molecules are known in principle, and their dynamics are governed by the more fundamental laws (laws of classical or quantum mechanics).

We consider the simplest system of ideal gas consisting of N particles. At any time t, the classical system can be completely described by specifying the instantaneous position $\vec{q}(t)$ and momentum $\vec{p}(t)$ of each particle of the system. This set of information of the system from the microscopic level, i.e., the microscopic configuration defines the micro-state of the system at the time t. Thus, the definition of micro-state requires, for N-particle system, 3N position coordinates $q_1$, $q_2$, ..., $q_{3N}$ and 3N momentum coordinates $p_1$, $p_2$, ..., $p_{3N}$. The set of coordinates ($q_i$, $p_i$), i=1, 2, ..., 3N, geometrically can be regarded as a point in a 6N-dimensional space which is referred to as phase space $\Gamma$. A point ($q_i$, $p_i$) on the phase space is a representative point of the system that represents micro-state $\mu(t)$ of the system at time t. Now, as time passes, all the particles of the system change, continuously, their position, and momenta also get changed. Thus the system switches from one micro-state to another, and the representative point moves accordingly in the 6N-dimensional phase space. The trajectory of the point in phase space is governed by the canonical equations of motion,

$$\begin{aligned} \frac{d\vec{q_i}}{dt} &= \frac{\partial H}{\partial \vec{p_i}} \\ \frac{d\vec{p_i}}{dt} &= -\frac{\partial H}{\partial \vec{q_i}} \end{aligned} \tag{2.1}$$

with i=1, 2, ..., 3N; where $H$ ($\mathbf{q}$, $\mathbf{p}$) is the Hamiltonian of the system in terms of the set of position coordinates $\mathbf{q}$ ($q_1$, $q_2$, ..., $q_{3N}$) and momenta $\mathbf{p}$ ($q_1$, $q_2$, ..., $p_{3N}$). Naturally, the trajectory, being restricted by the constraints of the system, remains confined within a certain region in the phase space. The macrostate M of a thermodynamic system is defined by prescribing the values of the state functions E, P, V, N etc. The macro-state cannot be defined unless the system is in equilibrium. There are a large number of micro-states $\mu$ under the same macroscopic configuration M. This 'many-to-one' connection between micro-states and macro-states leads to consider a set (statistical ensemble which will be discussed latter) of micro-states. Now if we consider a set of $N$ copies of a given macro-state $M$, at a particular instant each having different micro-state, i.e., each of them corresponds to a different representative point $\mu(t)$ in the phase space $\Gamma$. Let there are $d\,N(\mathbf{q},\ \mathbf{p},\ t)$ representative points within an elementary volume $d\Gamma = \prod_{i=1}^{N} d^3\vec{q_i}\ d^3\vec{p_i}$ around the point $(\mathbf{q}, \mathbf{p})$ in the phase space. Then phase space density or the probability density is defined by the objective probability as,

$$\rho(\mathbf{q}, \mathbf{p}, t)d\Gamma = Lim_{N\to\infty}\frac{dN(\mathbf{q}, \mathbf{p}, t)}{N}. \tag{2.2}$$

$\rho$ is a normalized probability density, $\int_\Gamma \rho\ d\Gamma = 1$. In general, this probability density distribution is not uniform throughout the phase space $\Gamma$; in other words, all the representative points are not equally probable. Therefore to obtain the value of any macroscopic quantity O $(\mathbf{q}, \mathbf{p}, t)$ from microscopic configurations, one needs to take an average over the entire phase space,

$$\langle O(\mathbf{q}, \mathbf{p}, t)\,\rangle = \int_\Gamma O(\mathbf{q}, \mathbf{p}, t)\ \rho(\mathbf{q}, \mathbf{p}, t)\ d\Gamma, \tag{2.3}$$

and thus the probabilistic description comes into the picture.

Now when a system is characterised by a particular micro-state $\mu$, it is said that the system is in a pure state. Again, when the description of the system is probabilistic, in terms of the probability density function $\rho(\mathbf{q}, \mathbf{p}, t)$ for a set of micro-states, the system is said to be in a mixed state. For pure state, $\mu(t)$ in phase space changes continuously with time following Eq. 2.1, so the definition of equilibrium cannot be given easily considering a pure state. While for a mixed state, one can conveniently define the state of equilibrium in terms of the time evolution of the phase space density, which follows the Liouville Equation.

**Liouville's Theorem and Consequences**

According to the Liouville's theorem, *the phase space density* $\rho(\Gamma, t)$ *behaves like an incompressible fluid* and its time evolution is given by the equation,

$$\frac{d\rho}{dt} = \frac{\partial \rho}{\partial t} + \{\rho, H\} = 0 \tag{2.4}$$

Now, the time evolution of a macroscopic physical quantity can be evaluated as,

$$\begin{aligned} \frac{d\langle O\rangle}{dt} &= \frac{d}{dt}\int_{\Gamma} O(\mathbf{q},\mathbf{p})\,.\,\rho(\mathbf{q},\mathbf{p},t)d\Gamma \\ &= \int_{\Gamma} O(\mathbf{q},\mathbf{p})\frac{\partial \rho(\mathbf{q},\mathbf{p},t)}{\partial t}d\Gamma. \end{aligned} \tag{2.5}$$

The ensemble will describe an equilibrium scenario i.e., the system under consideration will be in equilibrium if the phase space average is independent of time, $\frac{d\langle \mathbf{O}\rangle}{dt} = 0$. This can be reached if $\frac{\partial \rho_{eq}(\mathbf{q},\mathbf{p},t)}{\partial t} = 0$ i.e., phase space density distribution is stationary. Thus we get the more basic definition of a equilibrium state, where the distribution of probability density over the phase space is independent of time; so that macroscopic quantities will take time-independent values and the macro-states can be defined. From Liouville's equation, this implies,

$$\{\rho_{eq}, H\} = 0.$$

A first possible $\rho_{eq}$ that satisfy the above equation could be any function $\rho_{eq}(\mathbf{q},\mathbf{p}) = \rho\left(H\left(\mathbf{q},\mathbf{p}\right)\right)$, then it can be shown that

$$\begin{aligned} & \{\rho_{eq}(H), H\} \\ =& \frac{\partial \rho}{\partial H}\{H, H\} \\ =& 0. \end{aligned} \tag{2.6}$$

Then, at all the phase space points where H takes the same value, $\rho_{eq}$ will also be equal. The equilibrium probability density $\rho_{eq}$ takes the same value over a constant energy surface ($H(\mathbf{q},\mathbf{p}) = \text{const.}$). It can also be shown that if there are other conserved quantities ($L_i(\mathbf{q},\mathbf{p})$'s) apart from the total energy H, the equilibrium probability density function can be written as $\rho_{eq}(\mathbf{q}, \mathbf{p}) = \rho(H, L_1, L_2, ...L_i...)$. The probability density will take the same value at all phase space points where the conservations are maintained. In other words, all the accessible micro-states, satisfying the conservation laws, are equally likely and is referred as postulates of "equal a priori probabilities" of possible micro-states (this is the case of a micro-canonical ensemble in next section); which is one of the basic postulates of statistical mechanics.

## 2.2 Theory of Statistical Ensemble

Consider a thermodynamic system at any time t, which is in equilibrium, i.e., in a definite macro-state M. Now, the system is not a static one; it evolves with time. At the microscopic dimension, all of its constituting particles are moving, and thereby, changing their positions and momenta. Microscopic configuration changes continually as time passes. We know, there are a very large number of accessible micro-states under a macro-state satisfying the same macroscopic condition. As time evolves, the system switches from one micro-state to another thus moves over all the accessible region of phase space. In this region, apart from the fixed conserved quantities, other macroscopic observables can vary time to time leaving their time-average value, over a sufficiently long time, stationary. What we observe is this time averaged stationary values of the macroscopic observables. Naturally, all these micro-states are not equally probable in general. The probability that the system will be in a particular micro-state $P_M(\mu)$ is proportional to how much time it spends in that state, i.e., within the volume element around the corresponding representative point in phase space. So all we need is this probability which is extremely difficult to obtain. In statistical mechanics, instead of studying the evolution of a single system (pure state $\mu(t)$) over a long time duration one considers a collection of a large (theoretically infinite) number of identical copies of the given system at a particular instant. Each system in this collection will then be characterised by the same macro-state M as the original one but in different micro-states. This collection is known as the ensemble of micro-states, and the probability $P_M(\mu)$ is reflected in the phase space probability density function $\rho(\mathbf{q}, \mathbf{p})$ (defined earlier). Time evolution of a system in equilibrium is, thus, represented by an ensemble of accessible micro-states in association with the correct probabilities $P_M(\mu)$. In other words time evolution can be represented by the distribution of probability density in phase space. It is assumed that the average behaviour of an equilibrated system over a sufficiently long-time is same as, therefore, can be replaced by, the average over ensemble. This is the so-called ergodic hypothesis, one of the basic postulates of statistical mechanics. The primary aim of the ensemble theory is therefore to estimate these probabilities ($P_M(\mu)$) for systems under various equilibrium conditions (which leads to different representative ensembles). Then, one can easily get all the average macroscopic observables of interest. Now we consider different equilibrated system under different external conditions.

### 2.2.1 Isolated System: Microcanonical Ensemble

First, we consider an isolated thermodynamic system with a perfectly rigid and adiabatic wall so that neither its energy nor the volume can be changed. The system, in this condition, is completely isolated from its surroundings. It can be completely described by specifying its total internal energy E, volume V and number of particles N. Thus, the macro-state M of this system is defined by (E, N, V). The micro-states then lie on the constant energy surface $H(\mathbf{q}, \mathbf{p}) = E$, as all the microstates are restricted to have the same energy. All the micro-states of an isolated system in equilibrium are then equally probable and distributed uniformly with uniform probability density distribution in phase space, $\rho_{eq}(\mu) = \rho(H) = \text{const}$. Normalized probability of any micro-state at equilibrium will be,

$$\begin{aligned} P_M(\mu) &= \frac{1}{\Omega(E, N, V)}, \quad \text{if H}(\mu) = \text{E} \\ &= 0, \quad \text{otherwise} \end{aligned} \tag{2.7}$$

$\Omega(E, N, V)$ is the area of the constant energy surface in the phase space, which is proportional to the number of phase space points. The representative set of micro-states of an isolated system in equilibrium, distributed according to Eq. 2.7, is known as microcanonical ensemble.

The entropy of the uniform probability distribution is given by,

$$S(E,N,V) = k_B \log \Omega(E,N,V). \tag{2.8}$$

### 2.2.2 Closed System: Canonical Ensemble

The next system of interest is a closed system with rigid diathermic walls which allow heat exchange but not particle exchange. The total number of particles in the system N and its volume V are constrained to have fixed values. In equilibrium, the system will be at a temperature T which is equal to the temperature of the surroundings. The total energy E of the system can fluctuate, from E=0 to E=$\infty$ in principle, but the average ($\bar{E}$) of it over a reasonable time span should be constant (independent of time). The macro-state of the system, therefore, is defined by (T, N, V). The collection of all the accessible micro-states under M is called the canonical ensemble. As the energy can fluctuate in the different members of the ensemble, we see that from Liouville's theorem, equilibrium phase space density $\rho_{eq}(\mathbf{q},\mathbf{p})$ is not constant but varies with energy $\rho_{eq}(E)$. In other words, all the micro-states are not equally probable, but their probability depends on the system energy $P_M(\mu) = f(E)$. The correct probability, in this case, can be obtained as,

$$P_M(\mu) = \frac{e^{-\beta E_\mu}}{Z} \tag{2.9}$$

where $\beta = \frac{1}{K_B T}$, $K_B$ being the universal Boltzmann constant, $E_\mu$ is the energy of the system at a micro-state $\mu$. The normalization constant Z is given by,

$$Z = \sum_\mu e^{-\beta E_\mu} \tag{2.10}$$

which is the so-called canonical partition function or Gibbs partition function. One can essentially calculate all the thermodynamic quantities if the partition function is known. To get the probability, that the system has energy E at any moment t, one needs to add up the probability of all the micro-states where the total energy is E, i.e., $P(E) = \sum_{\mu(E)} P_M(\mu)$. All these micro-states are equally probable, designated by the same Boltzmann factor $e^{-\beta E}$. So, it simply becomes, number of possible micro-states having energy E times the probability of a micro-state having energy E (g(E)) and thus the probability is,

$$P(E) = g(E)\,\frac{e^{-\beta E}}{Z}. \tag{2.11}$$

Now g(E) is a rapidly increasing function of energy E. In the presence of a rapidly decreasing factor $e^{-\beta E}$, the product $g(E)\,e^{-\beta E}$ or the probability results in a sharp maximum at some energy (most probable energy $\tilde{E}$). It can be shown that the probability shows a Gaussian distribution. The probability, alternatively, can be written as,

$$\begin{aligned} P(E) &= g(E)\,\frac{e^{-\beta E}}{Z} \\ &= \frac{1}{Z} e^{S(E)/K_B}.e^{-\beta E} \quad [S(E) = k_B \log g(E)] \\ &= \frac{e^{-\beta F(E)}}{Z} \end{aligned} \tag{2.12}$$

Where F=E-TS is the Helmholtz free-energy. The probability P(E) has a maximum at the most probable energy that minimises F. The partition function then can be given as,

$$\begin{aligned} Z &= \sum_{\mu} e^{-\beta E_\mu} \\ &= \sum_{E=0}^{\infty} g(E).e^{-\beta E} \\ &= \sum_{E=0}^{\infty} e^{-\beta F(E)} \\ &\approx e^{-\beta F(\tilde{E})}. \end{aligned} \tag{2.13}$$

In the last step, the summation has dropped because equilibrium P(E) distribution is sharply peaked at $\tilde{E}$. Therefore, apart from the term corresponding to $E = \tilde{E}$, all other terms in the summation contribute almost none. Average of any quantity can be calculated as,

$$\langle O \rangle = \sum_{\mu} O(\mu) \frac{e^{-\beta E_\mu}}{Z}. \tag{2.14}$$

Average energy can be obtained in terms of partition function as,

$$\langle E \rangle = -\frac{\partial \log Z}{\partial \beta} \tag{2.15}$$

and the energy fluctuation about mean,

$$\begin{aligned}
\langle (E - \langle E \rangle)^2 \rangle &= \langle E^2 \rangle - \langle E \rangle^2 \\
&= \frac{\partial^2 \log Z}{\partial \beta^2} \\
&= -\frac{\partial \langle E \rangle}{\partial \beta} \\
&= k_B T^2 \left[ \frac{\partial \langle E \rangle}{\partial T} \right]_V \\
&= K_B T^2 C_V, \qquad (2.16)
\end{aligned}$$

and it is related to the heat capacity ($C_V$). The relative fluctuation being O($N^{-1/2}$) is negligibly small for a thermodynamic system, giving a very sharp peak in distribution. Then, the average energy ($\langle E \rangle$), the most probable energy ($\tilde{E}$) and the instantaneous total energy (E) become interchangeable, so that the situation is practically the same as a micro-canonical ensemble (Sec. 2.2.4).

### 2.2.3 Open System: Grand Canonical Ensemble

The most general consideration is an open system which is allowed to interchange both energy and particle with the surroundings. The system continues to exchange energy with the surroundings until a thermal equilibrium is established between them, where they both acquire the same temperature T. Similarly, particle exchange will continue to happen between the system and the surroundings until a chemical equilibrium is attained, which is governed by the chemical potential $\mu$. Chemical equilibrium is established between the system and the surrounding when both of them have the same $\mu$. At equilibrium, the total energy E or the particle number N of the system can vary, in principle form 0 to $\infty$, but their average value over appropriate time span should be constant and related to T and $\mu$ respectively. In this case, the macro-state of the system is described by the variables (T, $\mu$, V). The set of all accessible micro-states(r) under M, representing the system, is called grand canonical ensemble. The micro-states(r) in the ensemble follow the probability distribution,

$$P_r(E_r, N_r) = \frac{e^{-\beta E_r - \beta\mu N_r}}{Z_g}. \tag{2.17}$$

$P_r$ is the probability of $r^{th}$ micro-state having energy $E_r$ and particle $N_r$, and $Z_g$ is the normalisation factor called Grand Partition Function, and it is given as,

$$Z_g = \sum_r e^{-\beta E_r - \beta\mu N_r}. \tag{2.18}$$

Average energy and particle number, in this case, will be,

$$\langle E \rangle = -\frac{\partial \log Z_g}{\partial \beta}, \tag{2.19}$$

and

$$\langle N \rangle = -\frac{\partial \log Z_g}{\partial \beta}, \tag{2.20}$$

similarly, all other quantities can be calculated. The grand partition function can be written, alternatively, assembling all the micro-states r with the same number of particles (N) together, in terms of canonical partition functions $Q(T, N, V)$ of different N as,

$$\begin{aligned} Z_g &= \sum_{N=0}^{\infty} e^{-\beta\mu N} \sum_{r(N)} e^{-\beta E_{r(N)}} \\ &= \sum_{N=0}^{\infty} e^{-\beta\mu N} Q(T, N, V). \end{aligned} \tag{2.21}$$

Particle number distribution or the probability distribution of the canonical ensembles of different N is,

$$P(N) = \frac{e^{-\beta\mu N} Q(T, N, V)}{Z_g}. \tag{2.22}$$

The mean of this distribution is given in Eq. 2.19 and Eq. 2.20, and the particle number fluctuation is related to the variance of this distribution,

$$\begin{aligned} \langle (N - \langle N \rangle)^2 \rangle &= \langle N^2 \rangle - \langle N \rangle^2 \\ &= \frac{\partial \langle N \rangle}{\partial (\beta\mu)}. \end{aligned} \tag{2.23}$$

The relative fluctuation being of the order of O$(N^{-1/2})$ vanishes for a large N at the thermodynamic limit. The density (n=N/V) fluctuation can be shown from Eq. 2.23 as,

$$= \frac{k_B T}{V} K_T, \tag{2.24}$$

where $K_T$ is the isothermal compressibility of the system. It is true for a thermodynamic system that the fluctuation in N is negligible, which implies the probability distribution P(N) is sharply peaked at a particular N ($\tilde{N}$). So, the instantaneous total number (N), average number ($\langle N \rangle$) and $\tilde{N}$ become effectively the same, and the ensemble converges to the canonical one. The grand partition function can, then alternatively, be written as,

$$\begin{aligned} Z_g &= \sum_N e^{-\beta\mu N} Q(T, N, V) \\ &\approx e^{-\beta\mu\tilde{N}} \,.\, Q(T, \tilde{N}, V) \\ &= e^{-\beta\mu\tilde{N}} \,.\, e^{-\beta F} \\ &= e^{-\beta\left(F - \mu\tilde{N}\right)} \\ &= e^{-\beta \boldsymbol{G}} \end{aligned} \tag{2.25}$$

Where $G(T, \mu, V) = E - TS - \mu N = -k_B T \ \log Z_g$ is the Grand Potential. In the second line, the summation over N has dropped, and for a thermodynamic system, it can be correctly approximated by the largest contribution from the term corresponds to $\tilde{N}(\approx \langle N \rangle)$.

### 2.2.4 Equivalence of Ensembles

We see that all the fluctuations, energy fluctuation in a canonical ensemble or the energy and particle number fluctuation in a grand canonical ensemble become negligibly small for a thermodynamic system. So, the canonical and the grand canonical ensembles converge to a micro-canonical ensemble where all the fluctuations are strictly zero, which implies all the ensembles are equivalent to each other, and therefore will give the same result.

To elaborate the situation in a more physical terms, let us consider a closed system A which is thermally connected to a heat reservoir. In that case, the energy of the system A will change continuously with time due to the energy exchange between the system and the reservoir. The net energy exchange will not be zero until the thermal equilibrium is established between the system and the reservoir. Both the system and the reservoir will be at the same temperature when the thermal equilibrium is reached. The energy exchange is still going on, but, in this case, energy exchange over a sufficiently long period will be zero, and the energy of the system fluctuates around a mean energy value. The micro-states of the system is then a physical realisation of a canonical ensemble. For a macroscopic system ($N$ is $\mathrm{O}(10^{23})$), we have seen earlier, the (relative) energy fluctuation at equilibrium, being $O(N^{-1/2})$, becomes very small ($\mathbf{O}(10^{-11})$). So, at any time, the energy of the system at equilibrium will take a value, very close to the mean value. Now, if system A is detached from the reservoir and is thermally isolated from the surroundings, its total energy cannot vary and assumes a value very close to the equilibrium mean value. This situation is different from the previous one in the sense that the energy cannot fluctuate here but will remain constant. For most of the practical purpose, though, the difference is irrelevant because all the mean values of the observables differ negligibly in the two cases. For a macroscopic system in equilibrium, it is then unimportant whether the mean values are obtained considering system as an isolated one, where all of its micro-states having the exact fixed energy are equally probable, or a system in contact with a heat reservoir, where micro-states are following the law of canonical distribution.

Similarly, when a macroscopic system is in contact with the reservoirs where it can exchange both energy and particle, relative energy or particle number fluctuations around their mean values become negligibly small. So, the physical properties of the system do not get changed considerably if the system is detached from the reservoir, and remains isolated where its energy and particle number are strictly fixed. Thus in a macroscopic system for all practical purposes, where only the mean values are important, there are no significant differences between the situations, whether it is an isolated system or in thermal contact with a heat reservoir or in contact with a reservoir with which it can exchange both energy and particle. Therefore, one can conclude for a macroscopic system in equilibrium can be described by any of the three ensembles and the three ensembles are equivalent to each other.

However, the situation is quite different and not true in the presence of a phase transition. We see that the energy fluctuation is related to the specific heat $C_V$ (Eq. 2.16) and particle number fluctuation is related to isothermal compressibility $K_T$ (Eq. 2.23), and both of them diverge when the system passes through a 1st order phase transition. Then energy and particle number fluctuations diverge, and the ensembles become completely inequivalent.

## 2.3 Phase Transition

One of the most important goals of the statistical mechanics is to derive the equation of state of a thermodynamic system starting from the microscopic level, considering its constituent particles and interaction between them. Derivation of the equation of states of any ordinary substances and thus explaining their condensation or solidification, i.e., the transition from one phase to other is one of the primary interests of statistical mechanics. We briefly discuss phase transition for ordinary substances here since these concepts will be used in latter chapters where the phase transition of the nuclear system will be studied. The phase of any substance can be defined as a spatially homogeneous state of aggregation [2]. The state of a homogeneous thermodynamic system (a single phase) is defined by any two of the thermodynamic variables, volume V and energy E say, but the vice versa is not true in general. Not every given set of values of E and V corresponding to the state of a system in thermodynamic equilibrium is homogeneous. In fact, for a given (E, V) pair two distinct (homogeneous) phases of a substance can exist, simultaneously, in contact, maintaining thermodynamic equilibrium between them. This is known as the co-existence of two phases and main characteristics of the first-order phase transition. The condition for equilibrium between two phases can be obtained [2] as, i. The

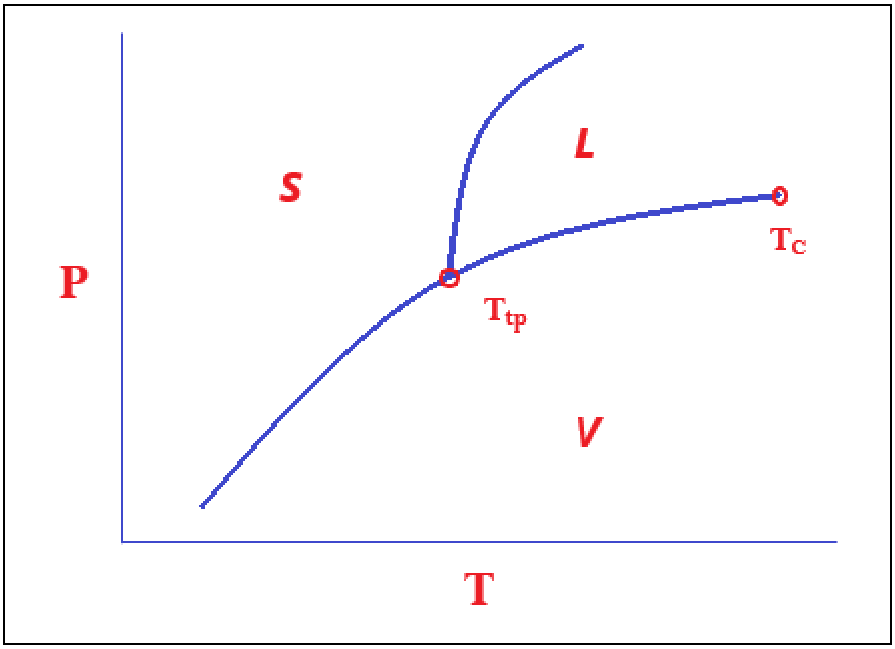

Figure 2.1: A typical P - T phase diagram of a ordinary substance

temperatures of the two phases are equal, $T_1 = T_2$. ii. Pressures in two phases are equal, $P_1 = P_2$. iii. Chemical potentials for the two phases should be the same, $\mu_1 = \mu_2$.

State of a thermodynamic system at any phase can be described by any two of the thermodynamic variables, but it is conventional to show the phase diagram either in P-T or P-V plane. A typical P-T diagram that most of the materials follow is shown in Fig. 2.1. In the figure solid, liquid and vapour phases are represented by $S$, $L$, $V$ respectively. Three lines, each separates two corresponding phases on the two side, are phase equilibrium lines along which the corresponding two phases exist simultaneously. Chemical potentials (which is equals to the Gibbs free energy per particle for a single component system) for two phases become equal on phase equilibrium curve. For example, consider liquid and vapour phases, and chemical potentials are expressed as a function of pressure and temperature. In the region of P-T plane denoted by L, the chemical potential for the liquid phase is smaller than the vapour phase, $\mu_L(P,T) < \mu_V(P,T)$ and the system will be in the liquid phase. On the other side, the chemical potential for vapour phase is smaller than the liquid phase, $\mu_L(P,T) > \mu_V(P,T)$ in the region V and the system will be in the vapour phase. Along the phase equilibrium line,

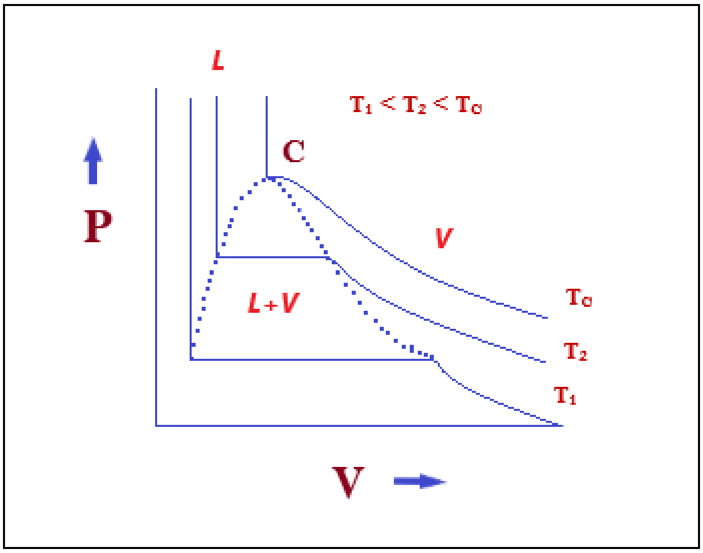

Figure 2.2: P Vs. V Phase diagram

$\mu_L(P, T) = \mu_V(P, T)$, liquid coexists with vapour for all (P, T). Three phase equilibrium curves meet at a point called the triple point where solid-liquid-vapour these three phases co-exist together. The liquid-vapour coexistence curve terminates at a point called the critical ($T_c$) point where the distinction between liquid and vapour phases vanish. Above the critical point, i.e., $P > P_c$ and $T > T_c$ only a single super-fluid phase exists.

The phase diagram in the P-V plane is shown in Fig. 2.2 where isotherms at several temperatures are drawn. The incompressible liquid phase, liquid-gas co-existence phase and vapour phase are indicated in the figure. At the low volume region, where the curves fall off almost vertically, is the region of incompressible liquid. The higher volume region, where the curves give a hyperbolic nature, is the vapour region. In between these two regions, isotherms are parallel to the volume axis, i.e., here pressure remains constant as volume increases. At this region, the liquid-gas phase transition occurs, and liquid and gas co-exist simultaneously. If a certain amount of energy is added to the system at this condition, the energy is then used as latent heat and convert some amount of liquid to vapour. As temperature increases, this parallel portion

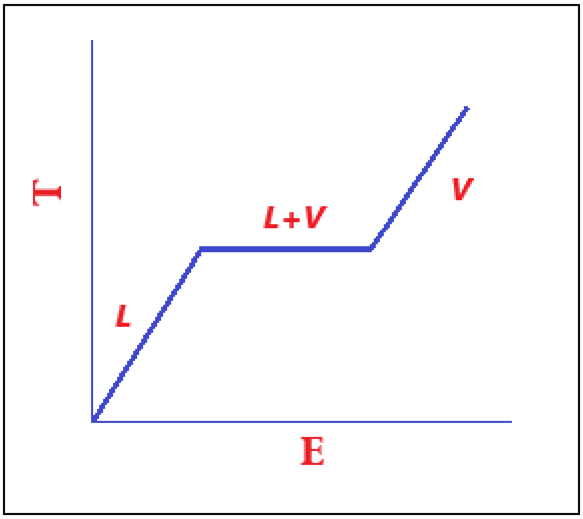

Figure 2.3: Variation of temperature (T) with energy (E) supplied to the system in case of an ordinary liquid.

of the curve, i.e., phase co-existence region becomes smaller and ultimately at the critical point this region becomes extinct. Theoretical equation of state for a real gas was given by Van Der Waals [4], and more rigorous treatment was done by Mayers [5] in his theory of cluster expansion. Two-body interaction with the Van der Waals potentials can give an approximate equation of state of real gas and explains phase transition. The order of phase transition, according to Ehrenfest, is determined by the lowest order of the derivative of free energy that shows a discontinuity. Now, free energy can be obtained in the method of statistical mechanics from partition function (Q) of the system, $F = -kT \, lnQ$ where F is the Helmholtz free energy. Plot showing the variation of F with temperature should be continuous. Its slope, i.e., 1st order derivative of F with respect to T gives a discontinuity at transition point if the system undergoes a 1st order phase transition. Entropy of the system is connected to the slope,

$$S = -T \left( \frac{\partial F}{\partial T} \right)_V \tag{2.26}$$

so entropy gives a finite discontinuity at the transition point. The discontinuity in S can be understood in terms of latent heat. The first-order transition involves latent heat, which is the energy required to convert a substance solely from one phase to another without affecting its temperature. This latent heat contributes to entropy and causes the discontinuity. It is evident from the above discussion that the second derivative of the free energy will diverge at the transition point. The second derivative is connected to the physical observable specific heat at constant volume ($C_V$),

$$\begin{aligned} C_V &= -T\left(\frac{\partial S}{\partial T}\right)_V && (2.27)\\ &= T^2\left(\frac{\partial F}{\partial T}\right)_V. && (2.28) \end{aligned}$$

Therefore, $C_V$ also diverges at the transition temperature.

A very well known curve, in connection to the phase transition, is Temperature Vs Energy curve (Fig. 2.3), and it is known as caloric curve. There is a region at low (T, E) values where the system is in a phase, say ‘A’, and where the temperature of the system increases linearly with the energy E supplied to the system. When T reaches a certain value the curve becomes parallel to the X-axis, T becomes constant even if energy is supplied to the system. Then the energy added to the system does not cause an increase of T but converts the system from phase “A” to phase “B”, and this energy is termed as latent heat. At the end of this flat line, the whole system in phase “A” is converted to phase “B”, and after that the temperature of phase “B” again rises linearly if energy is added further.

# Bibliography

[1] Mehran Kardar, **Statistical Physics of Particles**, Cambridge University Press. ISBN-13 978-0-511-28912-5

[2] F. Reif, **Fundamentals of Statistical and Thermal Physics**, McGRAW-HILL BOOK COMPANY, International Edition 1985.

[3] R. K. Pathria, Paul D. Beal; **Statistical Mechanics** Elsevier Ltd, Third Edition.

[4] J. D. Van der Waals, **On the Continuity of the Gaseous and Liquid States**. Ph.D. Dissertation, Universiteit Leiden, Leiden, The Netherlands, 1873 (English Translation by Threlfall and Adair 172); J. D. Van der Waals, **The equation of state for gases and liquids**, Nobel Lecture, December 12, 1910.

[5] Joseph E. Mayer, The J. of Chem. Phys. Vol **5** (1937) 67; The J. of Chem. Phys. Vol **5** (1937) 74.

# Chapter 3

# Statistical Models of Fragmentation of Nuclei

In nuclear multifragmentation, the projectile collides with the target, form a highly excited compound system which then decays, instantaneously, to several fragment nuclei (primary fragments). Then the whole system evolves with time, and finally reaches to a freeze-out condition. We know that for higher excitation energy, the system can decay in a large number of ways, so the statistical approach is reasonable. In this case, we are not interested in the exact dynamical process through which the fragments are produced. Our system of interest is the fragments at freeze-out where they are assumed to be in chemical and thermal equilibrium. According to Sec. 2.2, one needs to consider an ensemble of a large number of events giving all possible modes of decay. Then one needs to obtain the corresponding probability of occurrence of each decay channel correctly so that all the thermodynamic observables of the system can be evaluated taking an average on the ensemble. Now the probability of each decay mode contains a transition probability part from initial to final state and a phase space part, i.e., statistical weight. In the first part, the value of the relative matrix element is of the order of unity. The number of open decay channels, on the other side, is very large, so that the statistical weight part varies several orders of magnitude from channel to channel. The transition probability part can be, therefore, neglected compared to the statistical weight. According to the statistical model, the probability of a particular decay channel is solely given by its statistical weight [1]. Let there are N possible decay channels in the ensemble satisfying all conservations and a particular decay channel is given by 'y'. Thus, 'y' can vary from 1 to N, and the statistical weight corresponding to the channel y is $w_y$. Any physical quantity $O$, having value $O_y$ in the channel y, will have the average value over the ensemble (y; y=1,N),

$$\langle O \rangle = \frac{\sum_{y=1}^{N} O_y \,.\, w_y}{\sum_{y=1}^{N} w_y}. \tag{3.1}$$

Now we consider different statistical ensembles and proceed accordingly.

## 3.1 Micro-Canonical Model

A micro-canonical ensemble, according to Sec. 2.2.1, is where all the micro-states in the ensemble strictly obey the conservation of energy and particle number. So, for a fragmenting system given by mass $A_0$, charge $Z_0$, total energy $E_0$ and freeze-out volume $V_f$, the conservation conditions, that each of the micro-states is restricted to follow, are given by,

$$\begin{aligned} \sum A \,.\, n_{AZ} &= A_0 \\ \sum Z \,.\, n_{AZ} &= Z_0 \\ E_y &= E_0 \end{aligned}$$

All the micro-states are, therefore, equally probable so that the statistical weight of each partition or channel ($w_y$) will be determined by the number of micro-states under that partition ($\Omega_y$). The number of micro-states in this case can be given in terms of entropy as,

$$\Omega_y(A_0, Z_0, E_0, V_f) = \exp\left[S_y(A_0, Z_0, E_0, V_f)\right] \tag{3.2}$$

thus,

$$w_y \propto \exp\left[S_y\right]. \tag{3.3}$$

The normalized probability of a particular channel is given by,

$$P_y = \frac{\exp\ S_y}{\sum_y \exp\left[S_y\right]}; \tag{3.4}$$

denominator being the normalization constant. The implementation of this model is extremely difficult due to the constraints over energy and particle number, and require extensive computer simulation to obtain the break-up channels. There are some micro-canonical model calculations based on Monte Carlo sampling [[1]-[4]]. In the present work, we will not use any micro-canonical calculation.

## 3.2 Canonical Model

First, we shall describe the one component Canonical Thermodynamical Model [6], where we consider an ideal system of identical particles (nucleons) without distinguishing between neutron and proton. Then we extend it to the two-component case of real nuclei considering iso-spin.

### 3.2.1 One Component Canonical Thermodynamical Model

Consider an excited nuclear system of $A_0$ identical nucleons formed due to the collision in a nuclear reaction. This system, due to its high excitation energy, has expanded to a volume higher than normal nuclear volume $V_f$, produces fragments. In due course, the system containing all the fragments attains the freeze-out condition where the whole system is assumed to be in thermodynamic equilibrium, and the temperature of the system is T. The system can break up into various possible channels. In one channel, let there are

$n_1$ number of clusters of mass=1, i.e., monomer;

$n_2$ number of clusters of mass=2, i.e., dimer;

$n_3$ number of clusters of mass=3, i.e., trimer;

. . . . . . . . . . . . . . . . . . . . . . . . .;

$n_i$ number of clusters of mass=i;

. . . . . . . . . . . . . . . . . . . . . . . . .;

$n_{A_0}$ number of clusters of mass=$A_0$.

The set of numbers ($n_1$, $n_2$, $n_3$, . . ., $n_i$, . . ., $n_{A_0}$) represents this particular channel. The other possible channels can be obtained varying the values of the numbers $n_1$, $n_2$, $n_3$, . . . $n_{A_0}$, maintaining the conservation. For the canonical ensemble, the total number of particles is conserved and is equal to $A_0$. i.e.,

$$\sum_{i=1}^{A_0} i.n_i = A_0. \tag{3.5}$$

According to the statistical model assumption, the weight of a channel is proportional to the corresponding available phase space volume. Now, for the channel ($n_1$, $n_2$, $n_3$, . . . $n_{A_0}$), at freeze-out condition, non-interacting fragments ($n_1$ monomers, $n_2$ dimers, $n_3$ trimers, etc.) are enclosed within a volume $V_f$ at temperature T.

For 'n' non-interacting identical particles within a volume V, the partition function of the system will be,

$$Q_n = \frac{\omega^n}{n!}$$

where $\omega$ is the partition function of one particle. For a spin-less particle with no internal structure,

$$\begin{aligned} \omega &= \int \frac{d^3\vec{x}\, d^3\vec{p}}{h^3} \, . \, e^{-\beta\epsilon} \qquad\qquad [\epsilon = \frac{p^2}{2m}] \\ &= \frac{V}{h^3} . (2\pi m T)^{\frac{3}{2}}. \end{aligned}$$

m is the mass of the particle, V is the volume available to each particle for free motion and 'n!' is the correction factor of Gibbs paradox.

For the channel ($n_1$, $n_2$, $n_3$, . . ., $n_i$, . . ., $n_{A_0}$), there are $n_i$ identical non-interacting clusters of size 'i' and for them, the partition function is,

$$\frac{(\omega_i)^{n_i}}{n_i!}$$

where $\omega_i$ is the partition function of a i-size cluster. For monomer, i=1, as it is a spin-less structureless particle (nucleon), the partition function is,

$$\omega_i = \frac{V}{h^3}.(2\pi mT)^{\frac{3}{2}}.$$

m is the mass of the particle (nucleon), and V is the volume available for each fragment for their free motion. So, the partition function for the channel ($n_1$, $n_2$, $n_3$, . . ., $n_i$, . . ., $n_{A_0}$) is

$$\begin{aligned} Q_y &= \frac{(\omega_1)^{n_1}}{n_1!}.\frac{(\omega_2)^{n_2}}{n_2!}\cdots\frac{(\omega_i)^{n_i}}{n_i!}\cdots\frac{(\omega_{A_0})^{n_{A_0}}}{n_{A_0}!} \\ &= \prod_{i=1}^{A_0}\frac{(\omega_i)^{n_i}}{n_i!}. \end{aligned} \tag{3.6}$$

Therefore the total partition function considering all the channels,

$$\begin{aligned} Q_{A_0} &= \sum_y Q_y \\ &= \sum_y \prod_{i=1}^{A_0}\frac{(\omega_i)^{n_i}}{n_i!} \end{aligned} \tag{3.7}$$

where the sum is over all the possible channels, restricted by the constraint Eq. 3.5. The probability that the channel ($n_1$, $n_2$, $n_3$, . . ., $n_{A_0}$) will occur is,

$$\begin{aligned} P_y(n_1, \, , n_3, \, ..., n_{A_0}) &= \frac{Q_y}{Q_{A_0}} \\ &= \frac{1}{Q_{A_0}}.\prod_{i=1}^{A_0}\frac{\omega_i^{n_i}}{n_i!}. \end{aligned}$$

The average number of fragments of size 'i', i.e., average multiplicity is given as,

$$\begin{aligned} < n_i > &= \sum_y n_i \, . \, P_y(n_1, n_2, n_3, ..., n_{A_0}) \\ &= \omega_i \, . \, \frac{\partial \, ln \, Q_{A_0}}{\partial \, \omega_i}. \end{aligned} \tag{3.8}$$

It can be shown that

$$\frac{\partial \, Q_{A_0}}{\partial \, \omega_i} = Q_{A_0 - i}.$$

So that,

$$< n_i >= \frac{\omega_i \,.\, Q_{A_0-i}}{Q_{A_0}}. \tag{3.9}$$

Now, using Eq. 3.5, we arrive at,

$$Q_{A_0} = \frac{1}{Q_{A_0}} \,.\, \sum_{i=1}^{A_0} i\, \omega_i \, Q_{A-i}. \tag{3.10}$$

Starting from $Q_0 = 1$, $Q_1 = \omega_1$, one can easily calculate the partition functions for systems of different size using Eq. 3.10. This recursion relation makes the computation of CTM very easy. For a system like say 3000 particles of one kind, it takes a few seconds for partition function calculation on a normal computer. Otherwise, it is very difficult to calculate it using the basic equation Eq. 3.7 due to the summation over possible channels. Once the partition function is evaluated, one can get all the thermodynamic observables.

Up to this, the treatment is very general. Now we enter into the nuclear physics regime. We write down the explicit expression for $\omega$, which will carry the nuclear physics input. At freeze-out, now, nuclear fragments are non-interacting, no interaction potential (except Coulomb for real nuclei) is involved between the fragments so that they move freely within the freeze-out volume. They have kinetic energies due to the translational motion (motion of the centre of mass) as well as internal energies since they have internal structures. So, the partition function has two parts, one is the translational part ($\omega_t$), and the other is the internal one ($q_i$), and this will be,

$$\omega_k = \omega_t^k \,.\, q_i^k. \tag{3.11}$$

Translational part, as we have mentioned earlier, for a fragment of size 'k' is

$$\omega_t^k = \frac{V}{h^3} \,.\, (2\,\pi\, m_{CM}\, T)^{3/2} \tag{3.12}$$

where $m_{CM}$ is the mass of the fragment $= m \,.\, k$, m is the mass of one nucleon.

V is the volume available to the fragments for their free translational movement. This point needs a bit of illustration. We know nuclear force has a hard core (repulsive at short range) so any two nucleons cannot penetrate each other so as two nuclear fragments. Therefore, when a number of nuclear fragments are enclosed within a volume $V_f$ at freeze-out, the whole freeze-out volume $V_f$ will not be available to any fragment for its free motion; available volume (V) should be somewhat less than $V_f$. Remembering the concept of Van der Waals correction, $V = V_f - V_{ex}$ where $V_{ex}$ is the amount of reduction and is termed as 'excluded volume'. According to our assumption, at the freeze-out condition, the fragments are beyond the range of the nuclear force. So, there is no nuclear interaction between any two fragments, though they interact through the excluded volume. Hard core nature of nuclear force is incorporated in the model through this excluded volume. This excluded volume depends on total multiplicity, i.e., number of fragments present in the system, but a reasonable first approximation is $V_{ex} = V_0$ [7], [8]. $V_0$ is the normal nuclear volume of $A_0$ nucleons and is equal to $A_0/\rho_0$, $\rho_0$ being normal nuclear density, $\rho_0 = 0.16\ n/fm^3$. Throughout our calculation, this excluded volume is assumed to be constant, independent of multiplicity and is equal to $V_0$. This assumption will not be valid for a non-dilute system. Therefore, in this model, there is a restriction, quite arbitrarily, on the volume that $V_f \geq 2V_0$.

In the Intrinsic part, if k=1, $q_i^k = 1$. For all other fragments, $k \geq 2$, as the system is assumed to be at a constant temperature T, in contact with a heat reservoir at a fixed volume, $q_i^k = e^{-f/T}$. Where $f$ is the free-energy of the individual cluster, $f = E - TS$, S being entropy, and E is the total internal energy of the fragment, which can be written as a sum of ground-state binding energy ($E_{B.E.}$) plus excitation energy ($E^*$), $E = E_{B.E.} + E^*$. Entropy and excitation energy are taken from the Fermi-Gas model, $S = 2aT$ and $E^* = aT^2$, where $a = k/\epsilon_0$ is the level density parameter. $\epsilon_0$ is a constant, its value is taken to be 16 MeV. Ground-state binding energies are taken from the Liquid-drop model as,

$$E_{B.E.} = -W_0\, k + \sigma(T)\, k^{2/3}. \tag{3.13}$$

These are the volume and surface terms, respectively. All the other terms are absent because this is a single component system, and the Coulomb interaction is switched off. $W_0 = 16\,\text{MeV}$

and $\sigma(T)$ is the temperature dependent surface term, given as [1],

$$\sigma(T) = \sigma_0 \, . \left[\frac{T_c^2 - T^2}{T_c^2 + T^2}\right]^{5/4} , \tag{3.14}$$

where $\sigma_0 = 18$ MeV, and $T_c = 18$ MeV. The temperature dependence is taken because fragments are excited, and at a finite temperature T, not in the ground state at absolute zero. Many works [9], [10] show surface tension decreases with increasing temperature and ultimately goes to zero at a critical temperature ($T_c$). Now, intrinsic free-energy will be,

$$\begin{aligned} f &= E - TS \\ &= E_{B.E.} + E^* - TS \\ &= -W_0 \, k + \sigma(T) k^{3/2} + aT^2 - 2aT \, . \, T \\ &= -W_0 \, k + \sigma(T) k^{3/2} - \frac{k}{\epsilon_0} T^2 \qquad\qquad \left[a = \frac{k}{\epsilon_0}\right] \end{aligned}$$

and the intrinsic partition function will be,

$$\begin{aligned} q_i^k &= e^{-f/T} \\ &= \exp\left[\frac{1}{T}\left(W_0 \, k - \sigma(T) \, k^{2/3} + \frac{k}{\epsilon_0} T^2\right)\right] \end{aligned}$$

The final expression of the internal partition function of a fragment of size ‘k’ is,

$$\omega_k = \frac{V}{h^3} \left(2 \, \pi \, m \, k \, T\right)^{3/2} . \, \exp\left[\frac{1}{T}\left(W_0 \, k - \sigma(T) \, k^{2/3} + \frac{k}{\epsilon_0} T^2\right)\right] \tag{3.15}$$

Thus, we get the total partition function of the system, and now we can calculate all the relevant observables, some of them are given below.

### Multiplicity

Multiplicity means the total number of fragments. The average multiplicity of a particular fragment (Eq. 3.9) is

$$< n_i >= \frac{\omega_i \, . \, Q_{A_0 - i}}{Q_{A_0}},$$

and the total multiplicity (M), i.e., the average total number of fragments produced in the fragmentation is

$$\langle M\rangle = \sum_{i=1}^{A_0} \langle n_i\rangle \,.$$

The individual and total multiplicities are very basic observables in nuclear multifragmentation and can be measured in the experiment. The total multiplicity is, also, significant in the context of nuclear phase transition, which will be discussed later.

**Energy**

Average energy carried by a fragment of size-i is ,

$$\begin{aligned}
\langle E_i\rangle &= -\frac{\partial\, ln\, \omega_i}{\partial\, \beta} \\
&= T^2 \,.\, \frac{\partial\, ln\, \omega_i}{\partial\, T} \\
&= \frac{3}{2}T + i\left(-W_0 + \frac{T^2}{\epsilon_0}\right) + i^{2/3}\left(\sigma(T) - T\frac{\partial\sigma}{\partial T}\right),
\end{aligned} \tag{3.16}$$

where the first term is due to the centre of mass motion, and the others come from the intrinsic part of $\omega_i$. The energy of the entire system can be given by,

$$\langle E\rangle = -\frac{\partial\, ln\, Q_{A_0}}{\partial\, \beta}$$

and using Eq. 3.7 and Eq. 3.8 it can be shown that,

$$\langle E\rangle = \sum_{i=1}^{A_0} \langle n_i\rangle \;.\; \langle E_i\rangle \,. \tag{3.17}$$

Thus we get an expression for energy at a given temperature T, and this gives the caloric curve of a nuclear system which is measured in the experiment.

### Pressure

Thermodynamic pressure of the whole system can be obtained as,

$$\begin{aligned} P &= \frac{1}{\beta}.\frac{\partial \, ln \, Q_{A_0}}{\partial V} \\ &= \frac{T}{V}\sum \langle n_i \rangle \, . \end{aligned} \tag{3.18}$$

### Largest Cluster

If a channel has the largest cluster of size $Z_{max}$, this means there is at least one fragment of size $Z_{max}$ present in the channel, and no fragment present with the size greater than $Z_{max}$. The size of the largest cluster varies from channel to channel. The size can vary from 1 (where the entire system breaks up into nucleons) to $A_0$ (where the fragmenting system remains unexploded giving a single stable nucleus). Hence, each size has a finite probability of being the largest one when we consider all the possible channels. The average size of the largest fragment produced in fragmentation is therefore given by,

$$\langle Z_{max} \rangle = \sum_{Z_{max}=1}^{A_0} Z_{max} \, . \, Pr(Z_{max}) \tag{3.19}$$

where $Pr(Z_{max})$ is the probability of getting size $Z_{max}$ as the largest. To calculate this probability, we need to know the total partition function for those channels where size $Z_{max}$ is the largest one. Now, for the total partition function considering all the possible channels, different channels consist of different number of monomers ($\omega_1$), dimers ($\omega_2$),..., $\omega_i$,...up to a fragment as large as size-$A_0$ ($\omega_{A_0}$). So the total partition function is built up with all $\omega's$, up to $\omega_{A_0}$ and therefore, represented as $Q_{A_0}(\omega_1, \, \omega_2, \, \omega_3, \, \ldots, \, \omega_{A_0})$. Thus, here we include all the channels where the size of the largest cluster can be 1 or 2, or, ..., up to $A_0$. Similarly, consider $Q_{A_0}(\omega_1, \, \omega_2, \, \omega_3, \, \ldots, \, \omega_{Z_{max}}, \, 0, \, 0, \, 0, \, \ldots 0)$, which is built up with $\omega_1$, $\omega_2$,..., $\omega_{Z_{max}}$, 0, 0, 0,...,0. This is the total partition function including those channels where the size of the largest cluster can be 1, 2, 3, . . ., up to $Z_{max}$. Again, consider another one $Q_{A_0}(\omega_1, \, \omega_2, \, \omega_3, \, \ldots, \, \omega_{Z_{max}-1}, \, 0, \, 0, \, 0, \, \ldots 0)$, which represent the total partition function, considering those channels where the size of the largest cluster can be 1, or 2, or... up to $(Z_{max}-1)$. In the second case, all the previous channels are being considered, excluding only those where the size of the largest cluster is exactly $Z_{max}$. The difference, we define as,

$$\Delta Q_{A_0}(Z_{max}) = Q_{A_0}(\omega_1,\, \omega_2,\, \omega_3, ...,\, \omega_{Z_{max}},\, 0,\, 0, ...0) - Q_{A_0}(\omega_1,\, \omega_2,\, \omega_3, ..., \omega_{Z_{max}-1},\, 0,\, 0, ...0),$$

therefore, gives the total partition function, including only those channels where the largest cluster has $Z_{max}$ nucleons. This is valid for all $Z_{max}$ except $Z_{max}=1$. For $Z_{max}=1$, i.e., where each fragment is an individual nucleon, not cluster, the total partition function of the channels having largest cluster 1, is $\Delta Q_{A_0}(Z_{max}=1) = Q_{A_0}(\omega_1, 0, 0, ..., 0)$. So the probability will be,

$$Pr(Z_{max}) = \frac{Q_{A_0}(\omega_1, 0, 0, 0, ...0)}{Q_{A_0}(\omega_1,\, \omega_2,\, \omega_3,\, \ldots,\, \omega_{A_0})}, \qquad \text{if } \mathrm{Z_{max}} = 1$$

and

$$Pr(Z_{max}) = \frac{\Delta Q_{A_0}(Z_{max})}{Q_{A_0}(\omega_1,\, \omega_2,\, \omega_3,\, \ldots,\, \omega_{A_0})} \qquad \text{if } 2 \leq \mathrm{Z_{max}} \leq \mathrm{A_0}.$$

Thus, we get the average size of the largest cluster. This size will depend on the temperature, freeze-out volume, etc., and therefore has a significance in the context of phase transition in the nuclear system.

### 3.2.2 Two Component CTM

Now we switch to the case of real nuclei and extend the Canonical Thermodynamical Model to the two-component scenario [6]. We assume a similar system as before; the only difference is that there are total $N_0$ neutrons and $Z_0$ protons instead of all identical nucleons, but the total number is $A_0$. Here the fragments are real nuclei consisting of protons and neutrons. So each fragment is identified by two integers (i, j), giving the number of constituent protons and neutrons, respectively. For different composites 'i' runs from 0 to $Z_0$, and 'j' from 0 to $N_0$ though all combinations of (i, j) are not possible; only those combinations, which are within neutron and proton drip lines, give the real nuclei. The partition function for a composite having i-protons and j-neutrons will be $\omega_{i,j}$ instead of $\omega_i$, and the number of such fragments in a particular channel is $n_{i,j}$. The set of numbers $\{n_{i,j}\}$, i.e., ($n_{1,0}$, $n_{0,1}$, $n_{1,1}$,...$n_{i,j}$,...), satisfying two conservation equations, represents a channel. In this case, the conservation equations are

$$\sum_{i,j} i \,.\, n_{i,j} = Z_0 \tag{3.20}$$

for protons and

$$\sum_{i,j} j \,.\, n_{i,j} = N_0 \tag{3.21}$$

for neutrons, where the sum runs over all possible composites. The two-component picture is slightly different because of the presence of Coulomb interaction as nuclei carry Coulomb charges. The fragments are not free in this case. The partition function of a particular channel cannot be written as the product of the partition function of the individual fragment as before. The Coulomb interaction between the fragments is, though, managed by some realistic approximation (Wigner-Seitz approximation). So here we write all the expressions and equations as before. The total partition function can be written, from analogy to Eq. 3.7, as

$$Q_{A_0} = \sum \prod_{i,j} \frac{\omega_{i,j}^{n_{i,j}}}{n_{i,j}!} \tag{3.22}$$

where the product is over all possible composites, and the sum is over all possible channels satisfying the conservations. The average multiplicity can be written as,

$$\langle n_{i,j} \rangle = \frac{\omega_{i,j} Q_{Z_0-i,N_0-j}}{Q_{Z_0,N_0}}, \tag{3.23}$$

and using Eq. 3.20 and Eq. 3.21, we get two recursion relation as,

$$Q_{Z_0 N_0} = \frac{1}{Z_0} \cdot \sum_{i,j} i \,.\, \omega_{i,j} \,.\, Q_{Z_0-i,N_0-j} \tag{3.24}$$

and

$$Q_{Z_0 N_0} = \frac{1}{N_0} \cdot \sum_{i,j} j \,.\, \omega_{i,j} \,.\, Q_{Z_0-i,N_0-j}. \tag{3.25}$$

The partition function of a particular composite is

$$\omega_{i,j} = \frac{V}{h^3} \, . \, (2\pi m_{CM} T)^{3/2} \, . \, q_{i,j} \tag{3.26}$$

where $m_{CM} = (i+j)\,.\,m = A\,.\,m$, A being the mass number of the nuclei. $q_{i,j}$ is the internal partition function, and this will be, as before,

$$q_{i,j} = e^{-f/T}$$

where

$$\begin{aligned} f &= E - TS \\ &= E_{B.E.} + E^* - 2aT^2. \end{aligned}$$

Ground state binding energies ($E_{B.E.}$) are taken from the liquid drop model [6],

$$E_{B.E.} = -W_0 A + \sigma(T)\, A^{2/3} + \kappa \frac{i^2}{A^{1/3}} + s\frac{(i-j)^2}{A}, \tag{3.27}$$

and excitation energies from the Fermi-Gas model [6], $E^* = aT^2 = \frac{A}{\epsilon_0}T^2$. So,

$$q_{i,j} = \exp\left[\frac{1}{T}\left(W_0\, A - \sigma(T)\, A^{2/3} - \kappa\frac{i^2}{A^{1/3}} - s\frac{(i-j)^2}{A} + \frac{A}{\epsilon_0}T^2\right)\right]. \tag{3.28}$$

Liquid drop model is not applicable for the low mass nuclei, as low as A=2,3 etc.; so we have used this model for $A > 4$. For $A \leq 4$ nuclei, only ground states have been considered, and ground state binding energies are taken from experimental values along with spin degeneracy 2s+1. In Eq. 3.28, one can identify each term as, volume term $W_0 = 15.8 MeV$, temperature-dependent surface tension term, given explicitly in Eq. 3.14 with $\sigma_0 = 18.0 MeV$, $T_c = 18.0 MeV$, Coulomb energy term (Liquid drop model $\kappa$ = 0.72MeV but here its value is slightly modified (see **Appendix A**)), the symmetry energy term s=23.5 MeV and the last one is the contribution due to excitation. Besides thermodynamic equilibrium, the most important assumption is that the fragments are free, non-interacting. But in the case of real nuclei, this assumption is not true. At freeze-out, no short-range nuclear interaction is present between the fragments. But the nuclei carry charges and the Coulomb is a long-range interaction, so the fragments are not free but interacting with each other via Coulomb. Each fragment feels the Coulomb potential of all the other fragments. This interaction is not treated exactly in this model but through some approximation. One writes down all the expressions, as those are in one component case, treating as if the fragments are non-interacting. Then, one includes the Coulomb interaction, using Wigner-Seitz correction, modifying the Coulomb energy term in the liquid drop formula. So the next step is to calculate the modified Coulomb energy for each fragment using the approximation, which will be discussed in **Appendix A**. The total Coulomb energy of the entire system, from Appendix A (Eq. A.6), can be written as,

$$E_C = \frac{3}{5} \cdot \frac{Z_0^2 e^2}{R_f} + \sum_{i,j} \frac{3}{5} \cdot \frac{i^2 e^2}{R_{i,j}} (1 - \frac{R_0}{R_f}), \tag{3.29}$$

where $R_0$ is the normal radius, $R_f$ is the radius of the whole system at break up, and $R_{ij}$ is fragment radius (depends on fragment mass A=(i+j) only.) The first term in the expression has no significance as the freeze-out volume is constant, and the contribution from the second term needed is to be added in the expression of the corresponding $q_{ij}$. Finally, we see,

$$\kappa = \kappa_0 \cdot \frac{i^2}{A^{1/3}} \cdot \left[1 - \left(\frac{\rho}{\rho_0}\right)^{1/3}\right] \tag{3.30}$$

where $\kappa_0 = 0.72\text{MeV}$.

Now, the average multiplicity of (i, j) is,

$$\langle n_{i,j} \rangle = \omega_{i,j} \frac{Q_{Z_0-i,N_0-j}}{Q_{Z_0,N_0}} \tag{3.31}$$

and the total multiplicity will be,

$$\langle M \rangle = \sum_{ij} \langle n_{ij} \rangle . \tag{3.32}$$

All other observables can be obtained similarly as that have been given for the one-component system.

## 3.3 Two Component Grand-Canonical Thermodynamical Model

In this case, we consider a similar excited nuclear system as before, but here we assume that the system is in contact with a particle bath as well as a heat bath. At freeze-out condition, it has a finite temperature T, and its total number of particles can fluctuate, but the average values are fixed. The fixed average values of the total charge, total numbers of neutrons, and total mass are $Z_0$, $N_0$ and $A_0$ respectively. Therefore, the constrains, in this case, are,

$$\sum_{i,j} \langle n_{i,j} \rangle \, . \, i = Z_0, \tag{3.33}$$

$$\sum_{i,j} \langle n_{i,j} \rangle \, . \, j = N_0. \tag{3.34}$$

The partition function for a particular channel (y) is,

$$Q_{y(gc)} = \prod_{i,j} \frac{\tilde{\omega}_{ij}^{n_{i,j}}}{n_{ij}!}, \tag{3.35}$$

where $\tilde{\omega}_{ij}$ is the grand canonical partition function of a composite. In grand-canonical case, this partition function ($\tilde{\omega}_{ij}$) will be slightly different from canonical one ($\omega_{ij}$), and it is given by,

$$\begin{aligned} \tilde{\omega}_{ij} &= \frac{V}{h^3} . \, (2\,\pi\, m\, k\, T)^{3/2} \, . \, q_{int} \\ &= \frac{V}{h^3} . \, (2\,\pi\, m\, k\, T)^{3/2} \, . \, e^{-(f-\mu_z i-\mu_n j)/T} \\ &= \frac{V}{h^3} . \, (2\,\pi\, m\, k\, T)^{3/2} \, . \, e^{-f/T} \, . \, e^{\beta\mu_z i+\beta\mu_n j} \\ &= \omega_{ij}\, e^{\beta\mu_z i+\beta\mu_n j}.[6] \end{aligned} \tag{3.36}$$

Where, $\omega_{ij}$ is the canonical partition function of the composite (i,j). $\mu_z$ and $\mu_n$ are the proton and neutron chemical potentials, respectively, and those can be calculated from the two constraints (Eq. 3.33 and Eq. 3.34). The total partition function, in this case,

$$\mathbf{Q}_{gc} = \sum \prod \frac{\left(\omega_{ij} \,.\, e^{\beta\mu_z i + \beta\mu_n j}\right)^{n_{ij}}}{n_{ij}!}. \tag{3.37}$$

Where the summation is over all possible channels, without any restriction on total charge or mass, and the product is over all possible composites in a particular channel. So, the numbers of any particular composite ($n_{ij}$) in a channel in the grand-canonical ensemble can vary from 0 to $\infty$ to cover the entire ensemble. Thus, the above partition function can be written as,

$$\begin{aligned}
\mathbf{Q}_{gc} &= \sum_{n_{01}=0}^{\infty} \sum_{n_{11}=0}^{\infty} \sum_{n_{12}=0}^{\infty} ... \prod_{ij} \frac{\tilde{\omega}_{ij}^{n_{i,j}}}{n_{ij}!} \\
&= \prod_{ij} \sum_{n_{ij}=0}^{\infty} \frac{\tilde{\omega}_{ij}^{n_{ij}}}{n_{ij}!} \\
&= \prod_{ij} \exp(\tilde{\omega}_{ij}). \qquad (3.38)
\end{aligned}$$

Probability of occurring a particular channel y is

$$P_{y(gc)} = \frac{Q_{y(gc)}}{\mathbf{Q}_{gc}}. \tag{3.39}$$

The average number of a composite (i, j) will be,

$$\begin{aligned}
\langle n_{ij} \rangle &= \sum_{y} n_{ij}\, P_{y(gc)} \\
&= \sum_{y} n_{ij} \,.\, \frac{1}{\mathbf{Q}} \prod_{k,l} \frac{\tilde{\omega}_{kl}^{n_{kl}}}{n_{kl}!} \\
&= \sum_{n_{01}=0}^{\infty} \sum_{n_{11}=0}^{\infty} \sum_{n_{12}=0}^{\infty} ...\, n_{ij} \,.\, \frac{1}{\mathbf{Q}} \,.\, \prod_{kl} \frac{\tilde{\omega}_{kl}^{n_{kl}}}{n_{kl}!} \\
&= \frac{1}{\mathbf{Q}} \,.\, \sum_{n_{01}=0}^{\infty} \sum_{n_{11}=0}^{\infty} \sum_{n_{12}=0}^{\infty} ...\, \tilde{\omega}_{ij} \,.\, \frac{\tilde{\omega}_{ij}^{n_{ij}-1}}{(n_{ij}-1)!} \,.\, \prod_{k\neq i, l\neq j} \frac{\tilde{\omega}_{kl}^{n_{kl}}}{n_{kl}!} \\
&= \frac{1}{\mathbf{Q}} \,.\, \tilde{\omega_{ij}} \,.\, \mathbf{Q} \\
&= \tilde{\omega}_{ij} \\
&= \omega_{ij} \,.\, e^{\beta\mu_z i + \beta\mu_n j}. \qquad (3.40)
\end{aligned}$$

So, using Eq. 3.38, the total partition function can be written in terms of multiplicity as,

$$\begin{aligned}\mathbf{Q} &= \prod_{i,j} \exp\left(\tilde{\omega}_{ij}\right) \\ &= \prod_{i,j} \exp\left(\langle n_{ij}\rangle\right)\end{aligned} \tag{3.41}$$

and so,

$$\begin{aligned}\log_e \mathbf{Q} &= \log_e \prod_{i,j} exp\left(\langle n_{ij}\rangle\right) \\ &= \sum_{i,j} \langle n_{ij}\rangle \\ &= \text{total multiplicity } M.\end{aligned} \tag{3.42}$$

In this case, if one knows the chemical potentials and $\tilde{\omega}_{ij}$'s, then one can easily get multiplicities, the total partition function and other thermodynamic observables.

The size of the largest cluster in grand canonical case can be written, similar to its canonical version, as,

$$\langle Z_{max}\rangle = \sum_{Z_{max}} Z_{max} \,.\, P_{gc}\left(Z_{max}\right) \tag{3.43}$$

where $P_{gc}\left(Z_{max}\right)$ is the probability that the size $Z_{max}$ appears as largest, and can be written, in this case, as,

$$P_{gc}\left(Z_{max}\right) = \left[1 - \exp\left(-\sum_{i=Z_{max},\, j} \langle n_{ij}\rangle_{gc}\right)\right] . \prod_{i=Z_{max}+1,\, j}^{Z_{up}} \exp\left(-\langle n_{ij}\rangle_{gc}\right) . \tag{3.44}$$

# Bibliography

[1] J. P. Bondorf *et al.*, Phys. Rep. **257** (1995) 133.

[2] J. Randrup and S. E. Koonin , Nucl. Phys. A **471** (1987) 355c.

[3] S. E. Koonin and J. Randrup, Nucl. Phys. A **474** (1987) 173.

[4] D. H. E. Gross, Rep. Prog. Phys. **53** (1990) 605.

[5] D. H. E. Gross, Phys. Rep **279** (1997) 119.

[6] C. B. Das, S. Das Gupta, W. G. Lynch, A. Z. Mekjian and M. B. Tsang, Phys. Rep. **406** (2005) 1.

[7] D. Hahn and H. Stocker, Nucl. Phys. A **452** (1986) 723.

[8] A. Majumder and S. Das Gupta, Phys. Rev. C **59** (1999) 2.

[9] W. Stocker and J. Burzlaff, Nucl.Phys. A **202** (1973) 265.

[10] D.G. Ravenhall, C.J. Pethick and J.M. Lattimer, Nucl. Phys. A **407** (1983) 571; D.G. Ravenhall, C.J. Pethick and J.R. Wilson, Phys. Rev. Lett. **50** (1983) 2066.

# Chapter 4

# Ensemble Transformation

Statistical ensembles are known to become equivalent, hence, give the same result for a thermodynamic system at equilibrium, as discussed in Sec. 2.2.4. In handling the situation of a macroscopic system with specific energy, the micro-canonical ensemble is commonly replaced by a canonical or grand canonical one, in order to get the mean values, avoiding computational difficulties. Nuclear multifragmentation phenomenon in heavy ion collision at intermediate energy is often described using the statistical ensemble theory (Chapter 3). The micro-canonical ensemble is ideal for the actual laboratory condition in this case. The two constraints imposed on this ensemble make the computation extremely difficult, requiring extensive numerical techniques [1]. Due to this difficulty, the other ensembles are more frequently used for dealing with nuclear fragmentations. Even in the case of canonical calculation, the constraint on particle number makes it complicated than the grand canonical calculation, where no such constraints arise. That's why the grand canonical model is widely used, in spite of the canonical model being more appropriate for HIC. Heavy ion collisions in laboratories lead to the fragmentation of finite nuclei. For finite systems, statistical ensembles are not equivalent and different statistical models of fragmentation based on separate ensembles, actually, give different results. The term 'inequivalent' is not strictly appropriate, since, the results considering different ensembles are similar though not numerically same. Moreover, experimental multifragmentation data are observed to agree with the statistical model results, specifically with the canonical values. It is observed that [2] even in finite system, canonical and grand canonical model of nuclear multifragmentation give very similar result (thereby equivalent) under some conditions. The key condition is of greater fragment multiplicity, which lowers the effect of finiteness. It has been observed that the ensembles are completely inequivalent in the presence of phase transition.

The Sec. 2.2 shows that the ensembles are mathematically connected. The grand canonical ensemble can be thought of as a collection of different canonical ensembles of different size. Similarly, the canonical ensemble can be considered as a collection of a number of microcanonical ensembles. This mathematical connection between the ensembles leads one to find the connection between the average values of any observable, evaluated in different statistical models of fragmentation, based on different ensembles. Such an approximate expression, connecting the canonical average value of any observable to its grand canonical average, has already been developed in [3] for a single component ideal fragmenting system. The present work extends the mathematical approximation, that transforms grand canonical average to canonical, to the domain of real nuclei, through the inclusion of iso-spin [4].

It is mentioned that the complications, in the calculation with a micro-canonically or canonically distributed system, are usually circumvented by using grand canonical distribution, since all the ensembles are equivalent at the thermodynamic limit (Sec. 2.2.4). For cases like multifragmentation, dealing with a finite system, this direct replacement will not be correct. In that case, the grand canonical to canonical transformation relation will be very useful. Again, we mentioned that canonical and grand canonical model results of fragmentation of finite nuclei converge under certain conditions, which can be verified with the help of the transformation relation.

Besides this, the transformation will have some other practical uses. There are some parameters such as isoscaling [5],[6] and isobaric yield ratio parameters [7],[6], which are used to study the nuclear symmetry energy and its density dependence [9] [10] from heavy ion collision. Isotopic temperatures are conventionally measured using double isotope ratio method [8], [11]. The above-mentioned parameters or method are described using grand canonical yields of fragmentation. For example, grand canonical isotopic yields follow a scaling law, based on which the isoscaling parameters are defined (Sec. 4.2.3). Canonical yields show deviation from such scaling behaviour, whereas the experimental data are much closer to the canonical values. The parameters deduced in this way should not agree with the experimental results and need to be corrected. In such cases, the transformation relation can successfully connect the grand canonical parameter values to experimental data.

In the following sections, the mathematical relation between the average values of any observable, calculated in the grand canonical model and the same in the canonical model, is derived for the case of the two-component nuclear system. The relation is, then, applied to the nuclear multifragmentation phenomenon, the approximated results are compared with the exact values, and thus, the validity of the relation is checked.

## 4.1 Theoretical Formalism

The grand canonical ensemble of any statistical system can be thought, as a collection of a large number of canonical ensembles of different system size, starting from 0 to $\infty$, theoretically, along with respective probabilities. The partition function can be expressed, accordingly, as given in Eq. 2.21. This concept forms the basics upon which the transformation equation is built. We consider the excited fragmenting nuclear source contains $Z_0$ protons, $N_0$ neutrons; therefore, mass $A_0 = Z_0 + N_0$. The system of all fragments, produced in the decay of the source nucleus, attains the freeze-out at a volume $V_f$ and temperature $T_f$. Now the canonical and grand canonical partition functions of this system are denoted by $Q_{N_0,Z_0}$ and $Q_{f_n,f_z}$, respectively, where $f_n$ and $f_z$ are the chemical potentials for neutrons and protons. The Eq. 2.21 becomes, in this case,

$$Q_{f_n,f_z} = \sum_{N_0,Z_0=0}^{\infty} Q_{N_0,Z_0}\, e^{f_n N_0 + f_z Z_0}. \tag{4.1}$$

The probability distribution, of different canonical sources with different particle number $Z_0, N_0$, in the grand canonical ensemble is,

$$P_{f_n,f_z}(N_0, Z_0) = \frac{Q_{N_0,Z_0}\, e^{f_n\, N_0 + f_z\, Z_0}}{Q_{f_n,f_z}}. \tag{4.2}$$

The expression for canonical or grand canonical partition functions for the nuclear system are given in Eq. 3.22 and Eq. 3.38. The mean of the distribution, i.e., the grand canonical average of the source size can be expressed in terms of probability,

$$\langle N_0 \rangle_{f_n,f_z} = \sum_{N_0,Z_0=0}^{\infty} N_0 \,.\, P_{f_n,f_z}(N_0, Z_0) \tag{4.3}$$

$$\langle Z_0 \rangle_{f_n,f_z} = \sum_{N_0,Z_0=0}^{\infty} Z_0 \,.\, P_{f_n,f_z}(N_0, Z_0). \tag{4.4}$$

The variance of the distribution, in other words, the fluctuation in particle numbers are,

$$\sigma_n^2 = \frac{\partial^2 \log \boldsymbol{Q}_{f_n,f_z}}{\partial f_n^2} = \sum_{N_0,Z_0=0}^{\infty} \left(N_0 - \langle N_0 \rangle_{f_n,f_z}\right)^2 \,.\, P_{f_n,f_z}(N_0, Z_0) \tag{4.5}$$

$$\sigma_z^2 = \frac{\partial^2 \log \boldsymbol{Q}_{f_n,f_z}}{\partial f_z^2} = \sum_{N_0,Z_0=0}^{\infty} \left(Z_0 - \langle Z_0 \rangle_{f_n,f_z}\right)^2 \,.\, P_{f_n,f_z}(N_0, Z_0) \tag{4.6}$$

$$\sigma_{nz} = \frac{\partial^2 \log \boldsymbol{Q}_{f_n,f_z}}{\partial f_n\, \partial f_z} = \sum_{N_0,Z_0=0}^{\infty} \left(N_0 - \langle N_0 \rangle_{f_n,f_z}\right)\left(Z_0 - \langle Z_0 \rangle_{f_n,f_z}\right) \,.\, P_{f_n,f_z}(N_0, Z_0). \tag{4.7}$$

The analytical connection, between the canonical and grand canonical ensembles (Eq. 4.1), suggests that one should be able to extract grand canonical results from canonical ones and vice versa, provided the probability distribution is known, or it is completely described by a limited number of moments.

Now, we consider an observable R of the above mentioned nuclear system, which can be estimated both in the canonical ensemble and the grand canonical ensemble. When the system is at microstate r $(N_0, Z_0, E_r)$, this observable takes a value $R_r$. The average value of this observable, calculated in a canonical ensemble corresponding to the system of size $(N_0, Z_0)$, is $R_c(N_0, Z_0)$. Its average value calculated in the grand canonical ensemble associated with the system, where the system size can vary, but the average $(\langle N_0 \rangle, \langle Z_0 \rangle)$ is restricted to the original system size by the values of $f_n$ and $f_z$, is $R_{gc}(f_n, f_z)$. The canonical average can be written as,

$$R_c(N_0, Z_0) = \sum_r \frac{R_r(E_r)\; e^{-\beta E_r}}{\boldsymbol{Q}_{N_0,Z_0}}, \tag{4.8}$$

and the grand canonical average is,

$$\begin{aligned} R_{gc}(f_n, f_z) &= \sum_r \frac{R_r(N_{0r}, Z_{0r}, E_r)\; e^{-\beta E_r + f_n N_0 + f_z Z_0}}{\boldsymbol{Q}_{f_n,f_z}} \\ &= \sum_{N_0,Z_0=0}^{\infty} \frac{R_c(N_0, Z_0)\;\; \boldsymbol{Q}_{N_0,Z_0}\; e^{f_n N_0 + f_z Z_0}}{\boldsymbol{Q}_{f_n,f_z}} \\ &= \sum_{N_0,Z_0}^{\infty} R_c(N_0, Z_0)\,.\,P_{f_n,f_z}(N_0, Z_0). \end{aligned} \tag{4.9}$$

$R_r(N_{0r}, Z_{0r}, E_r)$ is the $r^{th}$ possible microstate in the grand canonical ensemble. Eq. 4.9 gives the grand canonical average of R in terms of its canonical averages with respective source probabilities. Now, we expand $R_c(N_0, Z_0)$ in Taylor's series about the point $(\langle N_0\rangle_{f_n,f_z}, \langle Z_0\rangle_{f_n,f_z})$,

$$\begin{aligned} R_c\,(N_0, Z_0) &= R_c\,(\langle N_0\rangle_{f_n,f_z}, \langle Z_0\rangle_{f_n,f_z}) + (N_0 - \langle N_0\rangle_{f_n,f_z})\;.\;\left(\frac{\partial R_c}{\partial N_0}\right)_{\langle N_0\rangle_{f_n,f_z}, \langle Z_0\rangle_{f_n,f_z}} \\ &+ (Z_0 - \langle Z_0\rangle_{f_n,f_z})\;.\;\left(\frac{\partial R_c}{\partial Z_0}\right)_{\langle N_0\rangle_{f_n,f_z}, \langle Z_0\rangle_{f_n,f_z}} \\ &+ \frac{1}{2!}\,(N_0 - \langle N_0\rangle_{f_n,f_z})^2\;.\;\left(\frac{\partial^2 R_c}{\partial N_0^2}\right)_{\langle N_0\rangle_{f_n,f_z}, \langle Z_0\rangle_{f_n,f_z}} \\ &+ \frac{1}{2!}\,(Z_0 - \langle Z_0\rangle_{f_n,f_z})^2\;.\;\left(\frac{\partial^2 R_c}{\partial N_0^2}\right)_{\langle N_0\rangle_{f_n,f_z}, \langle Z_0\rangle_{f_n,f_z}} \\ &+ (N_0 - \langle N_0\rangle_{f_n,f_z})\,(Z_0 - \langle Z_0\rangle_{f_n,f_z})\;.\;\left(\frac{\partial^2 R_c}{\partial N_0 \partial Z_0}\right)_{\langle N_0\rangle_{f_n,f_z}, \langle Z_0\rangle_{f_n,f_z}} + \ldots \end{aligned} \tag{4.10}$$

Putting this expression for $R_c(N_0, Z_0)$ in the above equation and taking up to 2nd order term we get,

$$\begin{aligned}
R_{gc} &\approx R_c\left(\langle N_0\rangle_{f_n,f_z},\, \langle Z_0\rangle_{f_n,f_z}\right) && (4.11)\\
&+ \frac{1}{2!}\sum_{N_0,Z_0=0}^{\infty} P_{f_n,f_z}(N_0,Z_0)\left(N_0-\langle N_0\rangle_{f_n,f_z}\right)^2 \,.\, \left(\frac{\partial^2 R_c}{\partial N_0^2}\right)_{\langle N_0\rangle_{f_n,f_z},\,\langle Z_0\rangle_{f_n,f_z}} \\
&+ \frac{1}{2!}\sum_{N_0,Z_0=0}^{\infty} P_{f_n,f_z}(N_0,Z_0)\left(Z_0-\langle Z_0\rangle_{f_n,f_z}\right)^2 \,.\, \left(\frac{\partial^2 R_c}{\partial N_0^2}\right)_{\langle N_0\rangle_{f_n,f_z},\,\langle Z_0\rangle_{f_n,f_z}} \\
&+ \sum_{N_0,Z_0=0}^{\infty} P_{f_n,f_z}(N_0,Z_0)\left(N_0-\langle N_0\rangle_{f_n,f_z}\right)\left(Z_0-\langle Z_0\rangle_{f_n,f_z}\right) \,.\, \left(\frac{\partial^2 R_c}{\partial N_0 \partial Z_0}\right)_{\langle N_0\rangle_{f_n,f_z},\,\langle Z_0\rangle_{f_n,f_z}} && (4.12)
\end{aligned}$$

where all the first order terms are identically zero. Using the definitions of particle number fluctuations of Eq. 4.6 to 4.7, we get,

$$\begin{aligned}
R_{gc} &= R_c\left(\langle N_0\rangle_{f_n,f_z}, \langle Z_0\rangle_{f_n,f_z}\right) + \frac{1}{2}\sigma_n^2 \left(\frac{\partial^2 R_c}{\partial N_0^2}\right)_{\langle N_0\rangle_{f_n,f_z},\,\langle Z_0\rangle_{f_n,f_z}} \\
&+ \frac{1}{2}\sigma_z^2 \left(\frac{\partial^2 R_c}{\partial Z_0^2}\right)_{\langle N_0\rangle_{f_n,f_z},\,\langle Z_0\rangle_{f_n,f_z}} + \sigma_{nz}\left(\frac{\partial^2 R_c}{\partial N_0 \partial Z_0}\right)_{\langle N_0\rangle_{f_n,f_z},\,\langle Z_0\rangle_{f_n,f_z}} . && (4.13)
\end{aligned}$$

Again, we define another observable as,

$$T_c^{n^2}\left(N_0, Z_0\right) = \frac{\partial^2 R_c\left(N_0, Z_0\right)}{\partial N_0^2}. \qquad (4.14)$$

Now, we expand this new observable $T_c^{n^2}$ in Taylor's series and then taking the grand canonical average, similar to $R_c$, using Eq. 4.13 as before,

$$\begin{aligned}
T_{gc}^{n^2}\left(f_n, f_z\right) &= T_c^{n^2}\left(\langle N_0\rangle_{f_n,f_z}, \langle Z_0\rangle_{f_n,f_z}\right) + \frac{1}{2}\sigma_n^2 \left(\frac{\partial^2 T_c^{n^2}}{\partial N_0^2}\right)_{\langle N_0\rangle_{f_n,f_z},\,\langle Z_0\rangle_{f_n,f_z}} \\
&+ \frac{1}{2}\sigma_z^2 \left(\frac{\partial^2 T_c^{n^2}}{\partial Z_0^2}\right)_{\langle N_0\rangle_{f_n,f_z},\,\langle Z_0\rangle_{f_n,f_z}} + \sigma_{nz}\left(\frac{\partial^2 T_c^{n^2}}{\partial N_0 \partial Z_0}\right)_{\langle N_0\rangle_{f_n,f_z},\,\langle Z_0\rangle_{f_n,f_z}} . && (4.15)
\end{aligned}$$

So, the canonical value can be written as,

$$\begin{aligned} T_c^{n^2}\left(\langle N_0\rangle_{f_n,f_z},\langle Z_0\rangle_{f_n,f_z}\right) &= T_{gc}^{n^2}\left(f_n,f_z\right)-\frac{1}{2}\sigma_n^2\left(\frac{\partial^2 T_c^{n^2}}{\partial N_0^2}\right)_{\langle N_0\rangle_{f_n,f_z},\langle Z_0\rangle_{f_n,f_z}} \\ &- \frac{1}{2}\sigma_z^2\left(\frac{\partial^2 T_c^{n^2}}{\partial Z_0^2}\right)_{\langle N_0\rangle_{f_n,f_z},\langle Z_0\rangle_{f_n,f_z}} - \sigma_{nz}\left(\frac{\partial^2 T_c^{n^2}}{\partial N_0 \partial Z_0}\right)_{\langle N_0\rangle_{f_n,f_z},\langle Z_0\rangle_{f_n,f_z}} \end{aligned} \quad (4.16)$$

This $T_c^{n^2}\left(\langle N_0\rangle_{f_n,f_z},\langle Z_0\rangle_{f_n,f_z}\right)$ is actually,

$$= \left(\frac{\partial^2 R_c\left(N_0,Z_0\right)}{\partial N_0^2}\right)_{\langle N_0\rangle_{f_n,f_z},\langle Z_0\rangle_{f_n,f_z}},$$

and we may replace this term in the 2nd term of Eq. 4.13 by the series 4.16. But there is a multiplicative factor $\sigma_n^2$ in the 2nd term of Eq. 4.13 so that,

$$\begin{aligned} \sigma_n^2\left(\frac{\partial^2 R_c}{\partial N_0^2}\right)_{\langle N_0\rangle_{f_n,f_z},\langle Z_0\rangle_{f_n,f_z}} &= \sigma_n^2\, T_{gc}^{n^2}\left(f_n,f_z\right)-\frac{1}{2}\sigma_n^4\left(\frac{\partial^4 R_c}{\partial N_0^4}\right)_{\langle N_0\rangle_{f_n,f_z},\langle Z_0\rangle_{f_n,f_z}} \\ &- \frac{1}{2}\sigma_z^2\sigma_n^2\left(\frac{\partial^4 R_c}{\partial Z_0^2\partial N_0^2}\right)_{\langle N_0\rangle_{f_n,f_z},\langle Z_0\rangle_{f_n,f_z}} \\ &- \sigma_n^2\sigma_{nz}\left(\frac{\partial^4 R_c}{\partial N_0^3\partial Z_0}\right)_{\langle N_0\rangle_{f_n,f_z},\langle Z_0\rangle_{f_n,f_z}}. \end{aligned} \quad (4.17)$$

We see in the above expression, apart from the first term, all the other terms contain $\sigma$ with more than 2nd order. We consider the limit of small particle number fluctuation i.e.,

$$\begin{aligned} \frac{\sigma_n^2}{\langle N_0^2\rangle_{f_n,f_z}} &\leq 1 \\ \frac{\sigma_z^2}{\langle Z_0^2\rangle_{f_n,f_z}} &\leq 1 \\ \frac{\sigma_{nz}^2}{\langle N_0\rangle_{f_n,f_z}\langle Z_0\rangle_{f_n,f_z}} &\leq 1, \end{aligned} \quad (4.18)$$

so, we neglect the higher order terms in Eq. 4.17, and approximated as,

$$\begin{aligned} \sigma_n^2\left(\frac{\partial^2 R_c}{\partial N_0^2}\right)_{\langle N_0\rangle_{f_n,f_z},\langle Z_0\rangle_{f_n,f_z}} &\approx \sigma_n^2\, T_{gc}^{n^2}\left(f_n,f_z\right) \\ &\approx \sigma_n^2\,\frac{\partial^2 R_{gc}\left(f_n,f_z\right)}{\partial\langle N_0\rangle_{f_n,f_z}^2}. \end{aligned} \quad (4.19)$$

In the similar way, it can be shown that,

$$
\begin{aligned}
\sigma_z^2\left(\frac{\partial^2 R_c}{\partial Z_0^2}\right)_{\langle N_0\rangle_{f_n,f_z},\langle Z_0\rangle_{f_n,f_z}} &\approx \sigma_z^2\,\frac{\partial^2 R_{gc}\left(f_n,f_z\right)}{\partial\langle Z_0\rangle^2_{f_n,f_z}} \qquad (4.20)\\
\sigma_{nz}\left(\frac{\partial^2 R_c}{\partial N_0\partial Z_0}\right)_{\langle N_0\rangle_{f_n,f_z},\langle Z_0\rangle_{f_n,f_z}} &\approx \sigma_{nz}\,\frac{\partial^2 R_{gc}\left(f_n,f_z\right)}{\partial\langle N_0\rangle_{f_n,f_z}\partial\langle Z_0\rangle_{f_n,f_z}}. \qquad (4.21)
\end{aligned}
$$

Now, we can replace the last three terms of Eq. 4.13 by their approximate grand canonical values, taking from Eq. 4.19 to Eq. 4.21,

$$
\begin{aligned}
R_{gc} &= R_c\left(\langle N_0\rangle_{f_n,f_z},\langle Z_0\rangle_{f_n,f_z}\right)+\frac{1}{2}\sigma_n^2\left(\frac{\partial^2 R_{gc}(f_n,f_z)}{\partial\langle N_0\rangle^2_{f_n,f_z}}\right)_{f_n,f_z}\\
&+ \frac{1}{2}\sigma_z^2\left(\frac{\partial^2 R_{gc}(f_n,f_z)}{\partial\langle Z_0\rangle^2_{f_n,f_z}}\right)_{f_n,f_z}+\sigma_{nz}\left(\frac{\partial^2 R_{gc}(f_n,f_z)}{\partial\langle N_0\rangle_{f_n,f_z}\partial\langle Z_0\rangle_{f_n,f_z}}\right)_{f_n,f_z}. \qquad (4.22)
\end{aligned}
$$

or,

$$
\begin{aligned}
R_c\left(\langle N_0\rangle_{f_n,f_z},\langle Z_0\rangle_{f_n,f_z}\right) &= R_{gc}(f_n,f_z)-\frac{1}{2}\sigma_n^2\left(\frac{\partial^2 R_{gc}}{\partial\langle N_0\rangle^2}\right)_{f_n,f_z}\\
&- \frac{1}{2}\sigma_z^2\left(\frac{\partial^2 R_{gc}}{\partial\langle Z_0\rangle^2}\right)_{f_n,f_z}-\sigma_{nz}\left(\frac{\partial^2 R_{gc}}{\partial\langle N_0\rangle\partial\langle Z_0\rangle}\right)_{f_n,f_z}. \qquad (4.23)
\end{aligned}
$$

In the last equation, all the terms in the right-hand side are calculated in the grand canonical ensemble, while the left-hand side is the canonical average of the observable, $R_c$. Thus, the average value of an observable in the canonical ensemble can be approximated from grand canonical calculations, using Eq. 4.23. The assumptions made in our calculation are i. the low particle number fluctuation, and ii. the observable that we consider should be of low convexity (second order derivatives with respect to neutron or proton number). Otherwise, the higher order terms in the Taylor expansion become important. We see that if the probability distribution $P_{f_n,f_z}(N_0,Z_0)$ is a Gaussian, which is completely described by it's mean and variance ($\sigma^2$), all the higher order moments other than 2nd order are either zero (odd moments) or can be given in terms of $\sigma^2$ (even moments). Then, Eq. 4.23 gives the correct canonical results. As the distribution deviates more from the Gaussian, the higher moments/higher order terms will become more important, and the Eq. 4.23 will be less accurate. Evidently, this approximation is not valid unless the probability distribution is entirely described by the limited number of moments. In the presence of the 1st order phase transition, particle number fluctuation (which is related to the isothermal compressibility $K_T$) diverges. Hence, this equation is not valid in the presence of phase transition, and $P_{f_n,f_z}(N_0, Z_0)$ at such condition may deviate widely from Gaussian.

## 4.2 Results

In this section, we show the results obtained using the transformation relation Eq. 4.23, for different fragmentation observables. Both the canonical and grand canonical thermodynamical model for fragmentation is exactly solvable so that one can check the accuracy of the transformation equation. All the results are shown for the system of all the fragments produced in fragmentation of the fragmenting source $Z_0 = 28, N_0 = 30$ at freeze-out volume $V_f = 3V_0$.

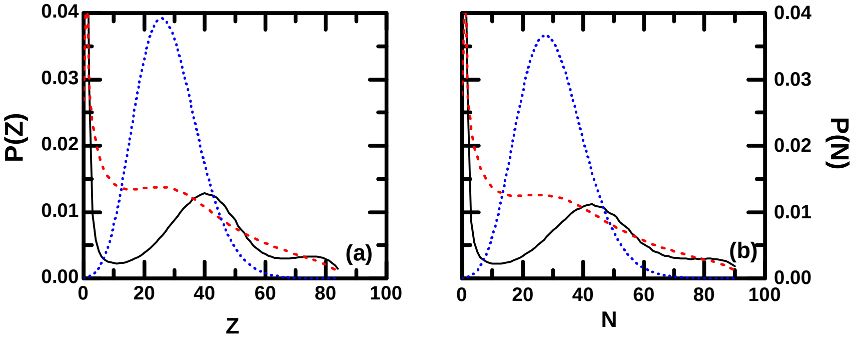

Figure 4.1: Grand canonical (a) proton, and (b) neutron number distributions for fragmenting source $Z_0 = 28$, $N_0 = 30$ at three different temperatures, T =3.6 MeV (black solid line), 4.5 MeV (red dashed line), 10.0 MeV (blue dotted line).

Before the application of the transformation equation Eq. 4.23, we should examine its region of validity. For this purpose, we have shown the grand canonical particle number distributions at different freeze-out temperatures. The variance of the distribution (which is the square of particle number fluctuation) $\sigma^2$ has, also, been plotted against the freeze-out temperature. Fig. 4.1 shows the particle number distribution for proton ( 4.1(a)) and neutron ( 4.1(b)). We see that at higher freeze-out temperature (T=10.0 MeV) the distribution is very near to a

Gaussian distribution. As temperature decreases, the system enters into the region of phase transition, and the grand canonical particle number distribution deviates from the Gaussian shape.

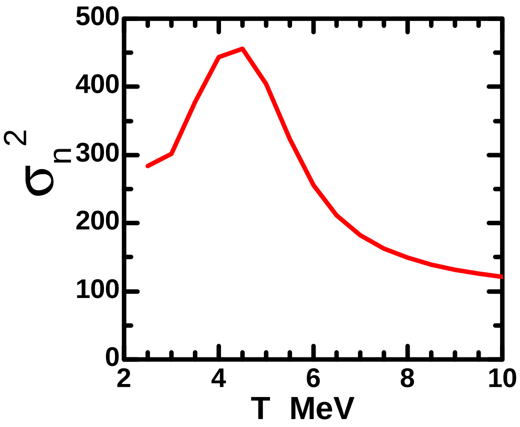

Figure 4.2: Variation of $\sigma_n^2$ with freeze-out temperature (T) for the fragmenting system of charge 28 and mass 58. [4]

In Fig. 4.2, the variance is plotted with temperature. It shows that the particle number fluctuation gives a peak at low temperature where phase transition has occurred. It is expected from the discussion of Chapter 2 that the particle number fluctuation will diverge in the phase transition region. For the present system, because of its finiteness, the divergence is replaced by a maximum. Therefore, at the low-temperature region, where the system undergoes a 1st order phase transition, transformation from grand canonical to canonical averages, following the above mentioned procedure, will not be appropriate. Figure 4.3 shows 2D plot of $P_{f_n,f_z}(N_0, Z_0)$. Next, we have shown different important observables of fragmentation, obtained from the exact canonical calculation, exact grand canonical calculation, and compared them with the extracted canonical results from grand canonical values, using Eq. 4.23.

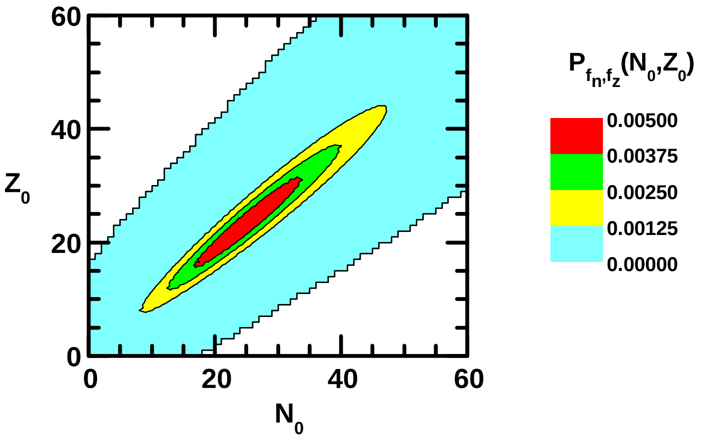

Figure 4.3: Grand canonical proton and neutron number distributions for fragmenting source $Z_0 = 28$, $N_0 = 30$ at temperature T =8 MeV. [4]

### 4.2.1 Multiplicity

#### Mass distribution

The mass distribution, i.e., the plot of the multiplicity $n_{\mathbf{a}}$ of various fragments produced in fragmentation of nucleus with their fragment mass **a**, is one of the important plots of nuclear multi-fragmentation. The Fig. 4.4 shows mass distribution at two different temperatures, 6MeV and 8MeV. For each temperature, three different lines are shown, which corresponds to the exact canonical model calculation, exact grand canonical calculation and the extracted canonical results using Eq. 4.23. Evidently, the canonical results obtained using the transformation equation, agree with the exact canonical model results, except for the region, where the value of the multiplicity is very low. In that case, as the value itself is very small, the contribution from the higher order terms in the expansion may not be negligible, so that the above relation may not be valid.

#### Isotopic distribution

To study the multiplicity of the individual fragment nuclei, we have plotted isotopic distribution (Fig. 4.5) which can be obtained experimentally. It shows how correctly one can extrapolate the individual fragment multiplicity. We have shown it for fragments, having two different atomic

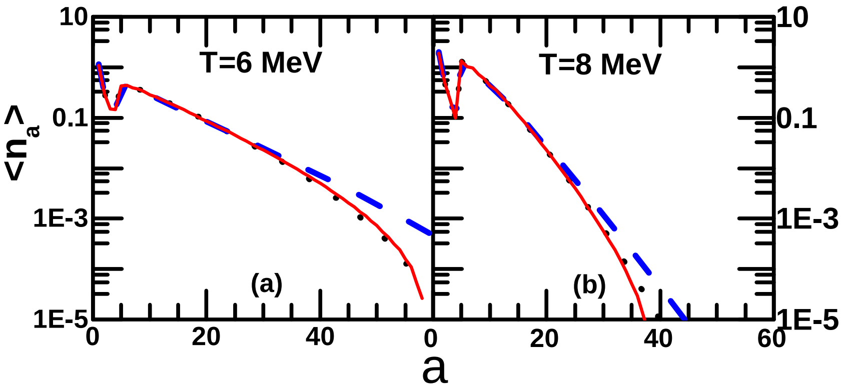

Figure 4.4: Mass distribution of the fragments produced from disassembly of a source of mass number 58 and proton number 28, calculated from canonical (black dotted line) and grand canonical (blue dashed line) models for two different temperatures, T =6MeV (left panel) and 8MeV (right panel). There solid lines represent the canonical result obtained from the grand canonical model by using Eq. 4.23.[4]

number, z=7 and z=12, formed in fragmentation of two fragmenting sources, containing the same number of protons but different neutrons. This fragment multiplicity, or more explicitly, the set of the multiplicities of different isotopes or isotones will be used latter to extract the isoscaling parameters. These are also widely used to extract the valuable parameters, like isobaric yield ratio, temperature, etc., other than isoscaling. We see that the transformation equation successfully gives the canonical multiplicities. The deviation is observed, only where, as before, the value is as low as $\approx 10^{-5}$.

### 4.2.2 Largest Cluster

The average size of the largest cluster (concerning the charge of the fragment) formed in fragmentation (can be given similar to the Sec. 3.2.1) is plotted with temperature in Fig. 4.6. The predicted canonical results from the grand canonical calculation, are very close to the exact canonical results in the high-temperature region. In the region, where the temperature is low, lower than 5 MeV, Eq. 4.23 fails because, in this region, as it is explained earlier, the system undergoes a 1st order phase transition.

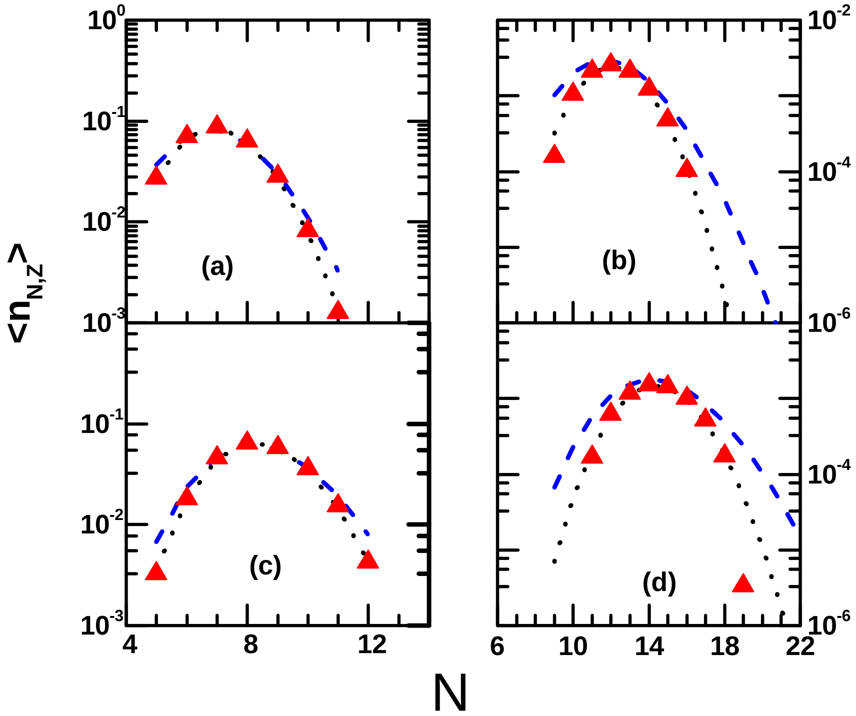

Figure 4.5: Multiplicities of Z =7 (left panels) and Z =12 (right panels) isotopes produced from two fragmenting systems of the same atomic number 28, but different mass numbers 58 (upper panels) and 64 (lower panels), calculated from canonical (black dotted line) and grand canonical (blue dashed line) models. The freeze-out temperature for both the system is T = 8 MeV. The red triangles represent the canonical result obtained from the grand canonical model by using Eq. 4.23.[4]

### 4.2.3 Isoscaling Parameters

We consider two different fragmentation reactions, reaction 1 and reaction 2, where two different fragmenting sources of the two reactions have different isospin asymmetry (source 2 is more neutron-rich compared to 1). $R_{21}$ is defined as the ratio of multiplicities of a nucleus (N,Z) produced in the two different fragmentation reaction.

$$R_{21} = \frac{n_2(N,Z)}{n_1(N,Z)} \tag{4.24}$$

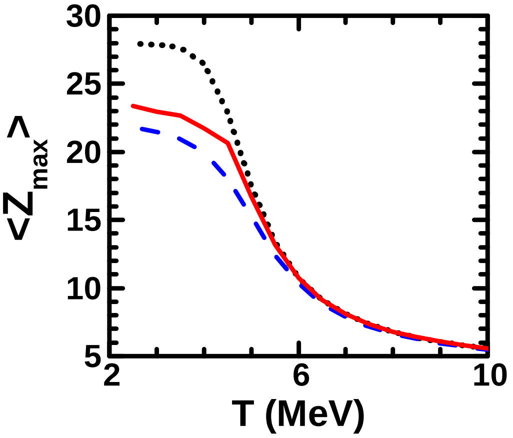

Figure 4.6: Variation of average size of the largest cluster ($Z_{max}$) with temperature (T) for the fragmenting system of charge 28 and mass 58 calculated from canonical (black dotted line) and grand canonical (blue dashed line) models. There solid lines represent the canonical result obtained from the grand canonical model by using Eq. 4.23.[4]

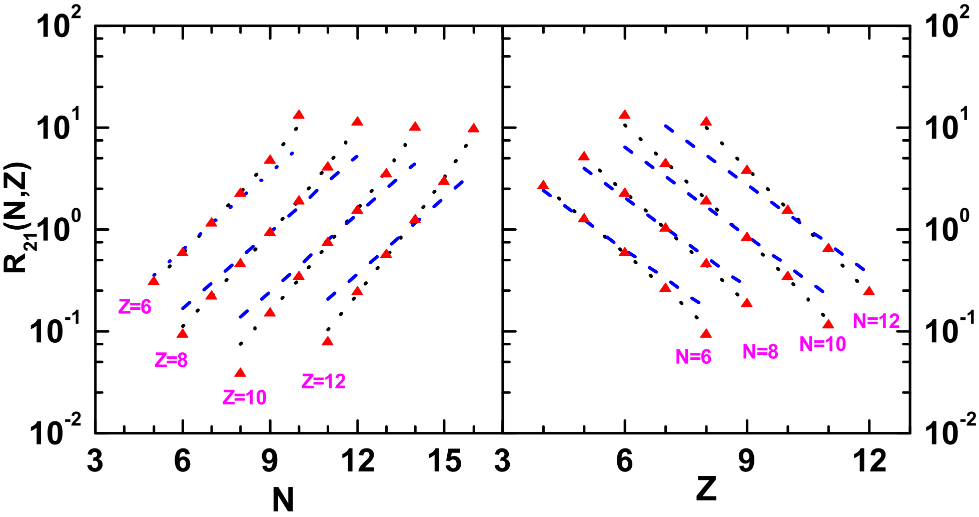

Figure 4.7: Ratios ($R_{21}$) of multiplicities of fragments (N,Z) where mass and charge of the fragmenting system for reaction 1 are 58 and 28 respectively and those for reaction 2 are 64 and 28. The freeze-out temperature for both the fragmenting systems is T =8MeV. The left panel shows the ratios as a function of neutron number N for fixed Z values, while the right panel displays the ratios as a function of proton number Z for fixed neutron numbers (N) calculated from canonical (black dotted line) and grand canonical (blue dashed line) models. The red triangles represent the canonical result obtained from the grand canonical model by using Eq. 4.23. [4]

Where $n_2$ and $n_1$ are multiplicities from reaction 2 and reaction 1 respectively. Now the ratio follows a universal scaling law,

$$R_{21} = \frac{n_2(N,Z)}{n_1(N,Z)} = C\,exp\,(\alpha\,Z + \beta\,N) \tag{4.25}$$

where $\alpha$, $\beta$ are known as isoscaling parameters, and C is a normalization constant. Evidently, for different isotopes corresponding to a particular Z, $R_{21}$ follows a straight line. A set of isotopes of different Z gives a set of parallel straight lines, as shown in the left of Fig. 4.7, all having the same slope $\alpha$. Similarly, isotones having the same N give another set of parallel straight lines, as in the right panel of the figure, with slope $\beta$. In Fig. 4.7, $R_{21}$ is plotted for four different Z (left) and N (right). For each Z or N, three lines are drawn with the exact canonical values, grand canonical values and the approximate canonical value using transformation equation. One can get the value of isoscaling parameters from the slopes. We see that the canonical lines deviate from the straight nature of grand canonical lines, but are successfully recovered from the grand canonical values. This deviation is expected, since the isoscaling relation is theoretically derived in the grand canonical model, so the canonical values may not follow it. Important point needed to be mentioned is that the laboratory conditions are more close to canonical conditions than grand canonical, and the experimental results closely agree with the canonical results. Further discussion can be found in [12], [13]. The apparent disagreement between canonical and grand canonical or experimental results are merely because of the difference in the model description, and the connection between them is possible via transformation relation. Similarly, the transformation relation will also be useful for other parameters, like isotope temperature, etc., which, too, are obtained using grand canonical yields.

### 4.2.4 Table

At the end, all the important results are summarised and compared in the TABLE. The results are given for two different temperatures (6 MeV and 8 MeV). The observables that have been examined are the total multiplicity $\langle n\rangle_{tot}$, average size (charge) of the largest cluster, and isoscaling parameters $\alpha$ and $\beta$. The agreement is very good at both the temperatures, irre-

Table 4.1: The grand canonical result, as well as the approximation, Eq. 4.23, of the canonical result from the grand canonical ensemble are compared to the exact canonical calculation for different observables obtained from fragmentation of the source of mass number 58 and proton number 28 at freeze-out volume $V_f = 3V_0$ and two different temperatures T =6 and 8 MeV.

| Observables | Temperature (MeV) (MeV) | Grand Canonical Canonical Model Result | Canonical Model Result | Transformation relation Using Eq. 4.23 |
|---|---|---|---|---|
| $\langle n_{tot} \rangle$ | 6 | 5.994 | 6.155 | 6.116 |
| | 8 | 9.131 | 9.184 | 9.171 |
| $\langle Z_{max} \rangle$ | 6 | 10.293 | 10.752 | 10.724 |
| | 8 | 6.653 | 6.796 | 6.798 |
| $\alpha$ | 6 | 0.668 | 0.958 | 0.942 |
| | 8 | 0.578 | 0.786 | 0.801 |
| $\beta$ | 6 | -0.780 | -1.035 | -1.048 |
| | 8 | -0.670 | -0.856 | -0.867 |

spective of the observable used, which ensures the accurateness of the ensemble transformation relation, for finite nuclei formed in the fragmentation reactions at intermediate energies.

# Bibliography

[1] D. H. E. Gross, Phys. Rep **279**, 119 (1997).

[2] S. Mallik and G. Chaudhuri, Phys. Lett. B **718** (2012) 189.

[3] G. Chaudhuri, F. Gulminelli, and S. Mallik, Phys. Lett. B **724** (2013) 115.

[4] P. Das, S. Mallik, and G. Chaudhuri, Phys. Rev C **96** (2017) 034609.

[5] M. B. Tsang, W. A. Friedman, C. K. Gelbke, W. G. Lynch, G. Verde, and H. S. Xu, Phys. Rev. Lett. **86** (2001) 5023.

[6] S. Mallik and G. Chaudhuri, Phys. Rev. C **87** (2013) 011602(R).

[7] M.Huang, Z.Chen, S.Kowalski, Y.G.Ma, R.Wada, T.Keutgen, K. Hagel, M. Barbui, A. Bonasera, C. Bottosso, T. Materna, J. B. Natowitz, L. Qin, M. R. D. Rodrigues, P. K. Sahu, and J. Wang, Phys. Rev. C **81** (2010) 044620.

[8] S. Albergo, S. Costa, E. Costanzo, and A. Rubbino, Nuovo Cimento A 89 (1985) 1.

[9] B.-A. Li, L.-W. Chen, and C. M. Ko, Phys. Rep. **464** (2008) 113.

[10] M. Baldo, G. F. Burgio, Progress in Particle and Nuclear Physics **91** (2016) 203.

[11] S. R. Souza, W. P. Tanb, R. Donangeloa, C. K. Gelbkeb, W. G. Lynchb and M. B. Tsang, arXiv:nucl-th/0005030v3 18 Jul 2000.

[12] G.Chaudhuri, S.Das Gupta, and M.Mocko, Nucl. Phys. A **813** (2008) 293.

[13] S. Mallik and G. Chaudhuri, Phys. Lett. B **727** (2013) 282.

# Chapter 5

# Proposition of New Observables to Study Nuclear Phase Transistion

Atomic nuclei are often treated as the incompressible liquid. Various nuclear phenomena are successfully described by the liquid-drop model. The standard nature of nucleon-nucleon strong interaction potential, which is an attractive potential with a repulsive core, is very similar to the Van Der Waals potential, except for the scale of the depth. This type of molecular interaction successfully describes the phenomenon of phase transition in ordinary liquid, and thus, one may expect such phase transition in the nuclear system also. In the case of ordinary liquid, it is very well known that if energy is added continually to the system, its temperature rises until the boiling point is attained. Then, if energy is added further, the temperature does not rise, and the liquid starts to become vapour instead. The temperature will remain constant until the whole amount of liquid changes to vapour, and during this transition, the liquid and vapour phase co-exist together in equilibrium. When the entire liquid becomes vapour, the system temperature starts to increase with the addition of energy.

To observe phase transition in the nuclear system, similarly, one has to pump energy to the system, and the possible way is a nuclear collision. In a very high energy nuclear (heavy ion) collision, a phase transition is expected to occur at very high nuclear density (much higher than the normal nuclear density) and temperature ($\approx 150$ MeV) where normal hadronic phase transfers to Quark Gluon Plasma (QGP) phase. At comparatively low energy collision, in the intermediate energy regime, multifragmentation process is observed to happen in the nuclear system. This can be associated with a liquid-gas kind of transition at sub-saturation nuclear density and transition temperature below 10 MeV, which is the subject of interest in the present discussion.

Phase transition in a nuclear system in association with the fragmentation of the nucleus in intermediate energy heavy ion collisions has drawn the attention of the nuclear physics community for the past several decades. Theoretical models of multi-fragmentation predict the existence of phase transition in infinite nuclear matter. Experimental evidence associated with multi-fragmentation, also, provide signatures of change of state in finite nuclei, and this is interpreted as finite size counterpart of the 1st order phase transition in the nuclear matter.

In the present chapter, we have proposed some new observables, which can be satisfactorily measured in experiments, and that may furnish the signature of phase transition in the nuclear system. We will begin with the conventional theoretical or experimental signatures of phase transition in the nuclear system and will discuss the ambiguity in them. In Sec. 5.2 we have proposed new observables, finding some similarities with the conventional ones, in the framework of Canonical Thermodynamical Model (Sec. 3.2.2). In the next section, we have attempted to extract phase transition signals from the proposed observables using the same model and thus established them as observables of phase transition.

## 5.1 Existing Signatures of Nuclear Phase Transition

Different theoretical models predict, and experimental results indicate the occurrence of phase transition in heavy ion collision if the beam energy is chosen appropriately. Here we are presenting some of the theoretical and experimental signatures.

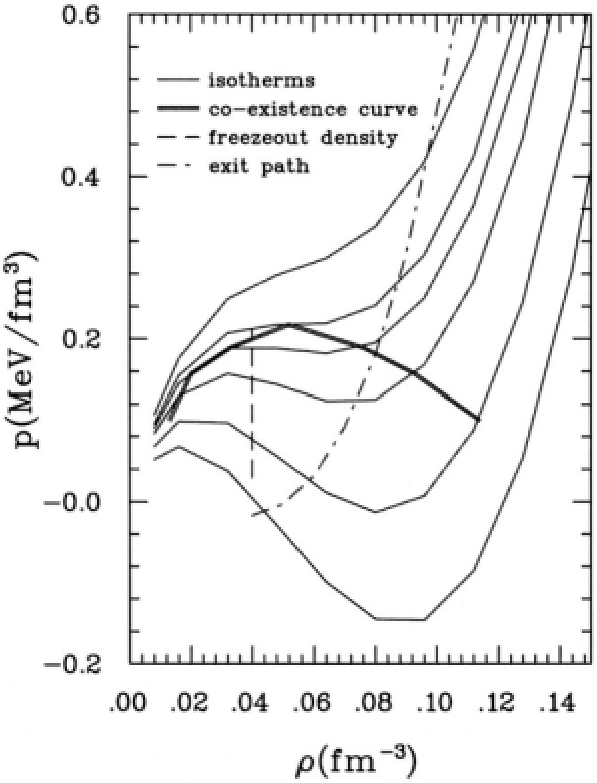

Figure 5.1: Equation of state of nuclear matter obtained from the Nuclear Mean Field theory considering Skyrme interaction with compressibility 201MeV.[1]

### 5.1.1 Signatures of Nuclear Phase Transition Obtained in Theoretical Models

Study of phase transition of any thermodynamic system involves thermodynamic variables like free-energy, specific heat, pressure, energy, etc., as discussed in Sec. 2.3. All these are equally relevant to the theoretical study of the nuclear phase transition. Mean field calculation using Skyrme parametrisation gives an equation of state of nuclear matter, which is very similar to the Van der Waals EOS and is shown in Fig. 5.1 [1].

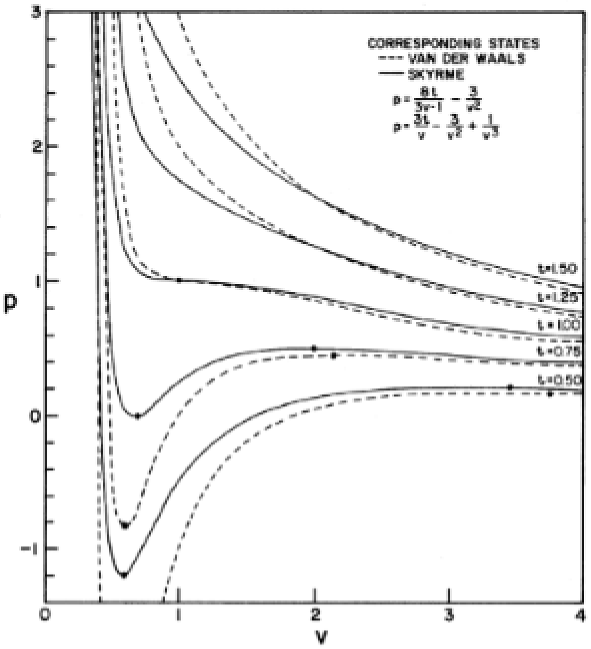

Figure 5.2: Comparition between EOS for a Van der Waals gas and a system interacting via Skyrme interaction.[2]

A quantitative comparison with Van der Waals EOS can be found in [2] (Fig. 5.2) where the authors have investigated the condensation of a gas of nucleons interacting via a zero-range Skyrme effective interaction. Equation of state is calculated using finite temperature Hartree-Fock theory. They have studied both the infinite nuclear matter and finite nuclei. Hartree-Fock calculations in [3] also give similar results. Mean field models alone cannot give the common experimental observables like multiplicity, cluster composition, excitation, etc. Some realistic model calculations [[4]-[9]] considering finite nuclei, find a peak in specific heat at around 5MeV temperature, which is supported by experiments. Canonical Thermodynamical Model calculations give thermodynamic functions like free-energy, specific heat, excitation energy that shows signatures of 1st order phase transition [[6]-[9]]. Fragments yield calculated in this model, shown in Fig. 5.3, indicates transition between phases.

Variation of free-energy(F), entropy (S), specific heat ($C_V$) (all per particle) with temperature for different systems are shown in Fig. 5.4.

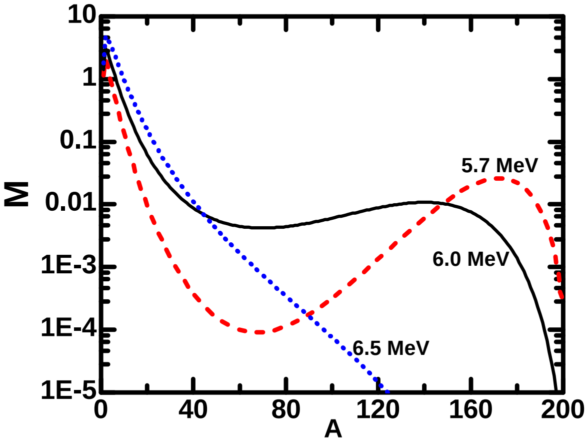

Figure 5.3: Mass distribution of the fragments produced in fragmentation of a source of size $A_0 = 200$ at three temperatures, 3.5MeV (black solid line), 4.0MeV (red dashed line) and 5.0MeV (blue dotted line).

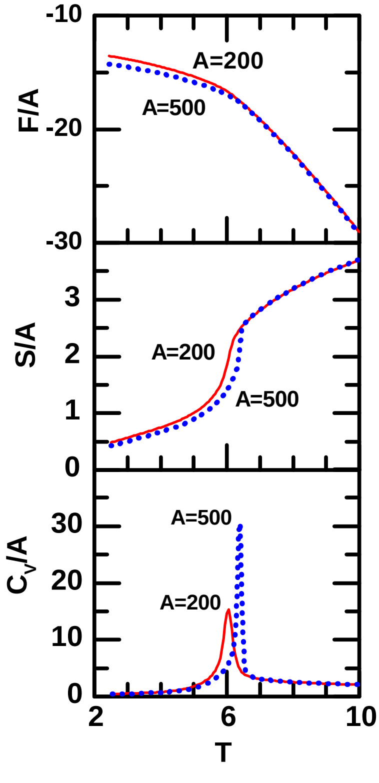

Figure 5.4: Variation of free-energy (F/A), entropy (S/A) and specific heat ($C_V/A$) with temperature T in the upper, middle and lower panel, respectively, for two fragmenting sources $A = 200$, $A = 500$. T, F, S, $C_V$ all are plotted in MeV.

One can see a break in free-energy at a certain temperature, where entropy jumps sharply from very low to a very high value, and $C_V$ shows a maximum. It is observed that the temperature at which $C_V$ gives the peak, coincides with the temperature where fragment yield starts to deviate from U shape. Ideally, phase transition should be observed in an infinite system. For a first-order phase transition, entropy should give a finite discontinuity, and specific heat a divergence at the transition temperature. Here for finite nuclei, instead of discontinuity or divergence, we get a sharp jump and maximum. We see, as system size increases, jump in entropy, and the peak of $C_V$ becomes sharper. Thus, one can extrapolate that the system will show a 1st order phase transition at the thermodynamic limit. In other words, jump in entropy, peak in $C_V$ are the finite size-counterpart of the phase transition signals. Another important

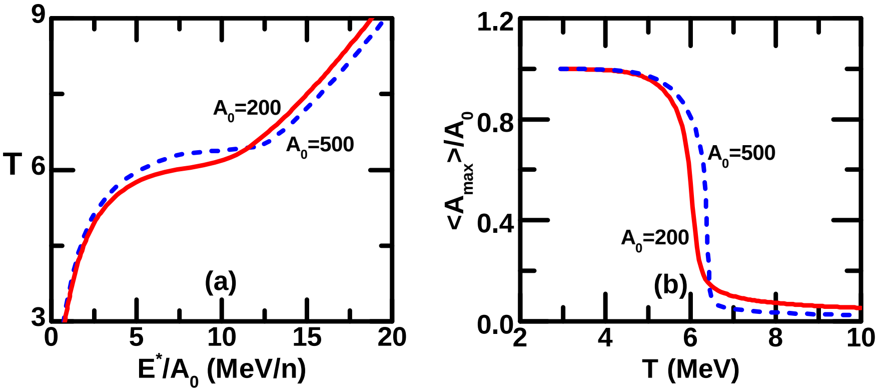

Figure 5.5: (a) Caloric curve and (b) the variation of normalised size of the average largest cluster $\langle A_{max}\rangle/A_0$ with temperature are plotted for two different fragmenting system of size $A_0 = 200$ and $A_0 = 500$ using CTM.

observable for a phase transition is the average size of the largest cluster ($\langle A_{max}\rangle$), which is considered as an order parameter of the nuclear phase transition. A normalised size of the largest cluster ($\langle A_{max}\rangle/A_0$) is plotted with T in Fig. 5.5(b). One can find here that at a very low T, the normalised size is 1, that means the size of the largest cluster is practically the same as the fragmenting source size. As the temperature increases from a low value, the size falls off rapidly (around T=6MeV) from 1 to a very low value. Thus, $\langle A_{max}\rangle/A_0$ can distinguish the nuclear liquid and gas phases. Caloric curves are very important to study 1st order phase transition in ordinary liquid-gas transition as well as in the nuclear system. For the nuclear case, it means excitation energy per particle ($E*$/A) versus temperature T plot, which is shown in Fig. 5.5(a). It shows a small plateau region near T=6MeV where one can find T increases remarkably slowly with increasing $E^*$. It is expected that the temperature of this plateau region is the same, where $C_v$ gives a peak, or $\langle A_{max}\rangle/A_0$ falls rapidly. The plots shown above have been drawn using CTM, and without considering the Coulomb interaction. Coulomb is neglected because we are interested in the signatures of phase transition in the nuclear system, while the coulomb being a long-range interaction, suppress the phase transition signals.

Again, theoretically, another signature of the first-order phase transition was proposed to be observed when it occurs in a finite system. The probability distribution of the order parameter ($A_{max}$, $\mathbf{a}_2$ defined latter) will show a bimodality, near the transition temperature due to the finiteness of the system . Bimodality means the appearance of two distinct peaks corresponding to two different phases. The transition temperature is the temperature where the two peaks assume the same height. Bimodality is established in theoretical calculations [[10]-[14]] as well as in experimental signatures [15], [16]. There can be some ambiguity, both experimentally and theoretically, regarding the identification of equal heights of the peaks, since the largest cluster distribution loose sharpness due to the finite size of the system.

### 5.1.2 Experimental Signatures of Nuclear Phase Transition

Experimental studies of multifragmentation began methodically from the mid-eighties. The fundamental problem with experimental detection is the time scale of the event. The actual nuclear collision procedure, where the nuclear matter produces fragments in different phases, occurs within $10^{-22}$ sec. Only the end products are detected in the detector, and one has to reconstruct the actual collision conditions from them. However, there are a few experimental observables that have been measured to study the multifragmentation process and nuclear liquid-gas phase transition. Those are, multiplicities (i.e., charge particle multiplicity ($N_c$), low charge fragment multiplicity ($N_{LCP}$), intermediate mass fragment multiplicity ($N_{IMF}$), etc.), energy, the momentum of the fragments, size of the largest fragment etc. Among these, we will briefly discuss those observables, which are the most important concerning the phase transition study. An extensive discussion can be found in [1].

Intermediate mass fragment (IMF) (fragments of charge $3 \leqslant Z \leqslant 20$) production is predicted by the statistical as well as transport models, as a consequence of liquid-gas phase transition in nuclear matter. Experimentally, it is observed that the IMFs are produced, and their multiplicity show a "rise and fall" nature in both the central and peripheral collision (Fig. 5.6[17](left),[18](right)) [[17]-[19]]. IMF multiplicity increases with excitation energy, attains a maximum and then falls indicating vaporisation of nuclear liquid into nucleons and light fragments.

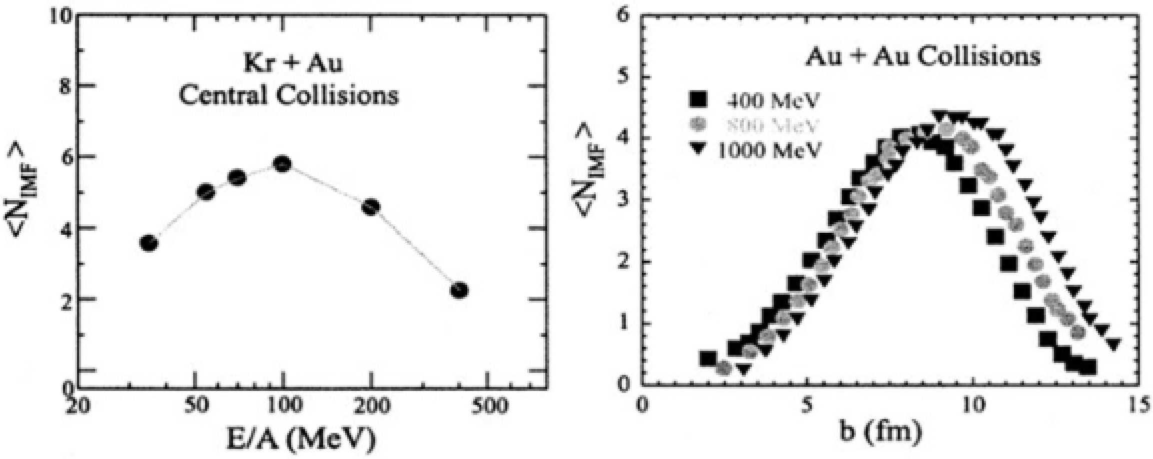

Figure 5.6: Variation of IMF multiplicity with incident energy for the central collision of Kr+Au (left) [17], and with impact parameters for "Au+Au" projectile fragmentation reaction. (right)[18].

Another crucial experimental signature of phase transition is the caloric curve, and experimentally, this has been measured for decades [20],[1]. Such plots have been shown in Fig. 5.7 [1]. The caloric curve is significant because the slope of this curve gives a measure of the specific heat $C_V$. Otherwise, $C_V$ or any other thermodynamic functions (F, S, P etc.) can not be measured directly in the experiments.

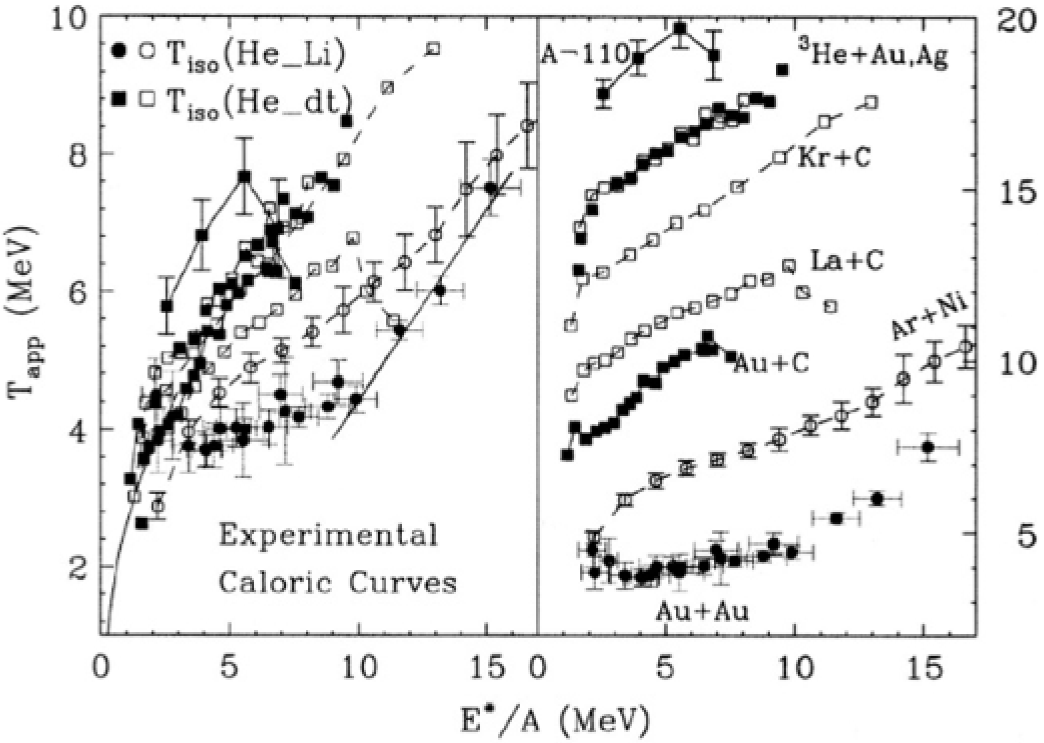

Figure 5.7: Caloric curves measured in the experiments. [1]

"Au+Au" curve at the bottom of the right panel is the most interesting plot, where the temperature is almost constant over the energy $E^*/A$ range 3 to 10 MeV and increases rapidly if $E^*/A$ increases further. This curve is very similar to the caloric curve for ordinary liquid-gas transition, and therefore, caused much excitement in the community. Although one can observe here, a possible signal of 1st order transition, it involves many problems and inconsistencies. It is evident from the Fig. 5.7, that in all the other plots, except "Au+Au", temperature increases smoothly with the excitation energy. Such observations are not quite consistent with the nature of the "Au+Au" plot. Since the caloric curve is considered as a significant experimental signal of nuclear liquid-gas phase transition, we will discuss its measurement briefly.

There are many uncertainties involved in the experimental measurement of excitation energy and temperature. Concept of temperature in case of heavy ion collision is not as traditional, and it cannot be measured in a conventional way, keeping a thermometer in contact with the system. In this case, instead, temperatures are being measured (or deduced), comparing experimental data with theoretical model calculation; it is more like a model parameter. Based on different phenomenological models, describing heavy ion collision at intermediate energies, several thermometers have been developed. For, example, kinetic temperatures are measured from the slope of the particle kinetic energy spectra. Excited state temperatures of excited nuclear systems are measured from the thermometers, based on the relative populations of the emitted particles in excited states. Isotope temperature $T_{iso}$ is deduced from the double isotope yield ratio, considering the grand canonical model. But different factors make the measurements inaccurate and inconsistent. One main factor is the sequential decay. Significant differences are observed between different thermometers. Further details can be found in [1]. The total excitation energy of a hot system can be measured, by summing up the energies of each and every fragment, produced from that particular fragmenting source. Identification of all the fragments produced in a specific event, correctly, is not trivial. Moreover, the excited source sometimes get de-excited through pre-equilibrium particles (neutron or light charged) emission in a very short time ($< 30$ fm/c). This amount of energy, lost in the very early stage of the reaction, is always absent in the energy measurement of the fragmenting system. If we assume that all the fragments from a particular source are detected, and identified, the total excitation energy of the system can be written from energy conservation as,

$$E^* = \sum_i E_i + \sum_n E_n + \sum E_\gamma + Q.$$

There are different sources of errors in the measurement of kinetic energies ($E_i$) of the emitted charged particles, and Q (the mass difference between the parent nucleus and daughters). This is because $4\pi$ detector coverage is not available in most of the experiments, and the detection arrays have energy thresholds. The energy of neutrons $E_n$ is challenging to measure, as it rarely interacts with the matter compared to charged particles; so in most of the cases they aren't considered. So, $\sum E_n$ is the primary source of inaccuracy in excitation energy measurement. Thus, we see, vagueness and various doubts are involved in the temperature and excitation energy measurements, and therefore, in the experimental caloric curves. Experimental caloric curves (Fig. 5.7), thus, cannot provide very satisfactory evidence of first-order phase transition.

## 5.2 Search for Alternatives

In view of the uncertainties mentioned above, involving experimental detection of signals of nuclear phase transition, one needs to think about alternatives. One can think of the observables that can be measured with comparatively greater accuracy in experiments, and from which one may be able to extract the signals of phase transition. Among the various observables, a similarity can be found between the theoretical caloric curves and the variation of total multiplicity (M) with temperature. We have shown them side by side in Fig. 5.8. Again, it is self-evident that there exists an (anti) correlation between the total multiplicity and the size of the largest cluster. More the system will fragment, less will be the size of the largest cluster. We have shown three curves together in Fig. 5.8.

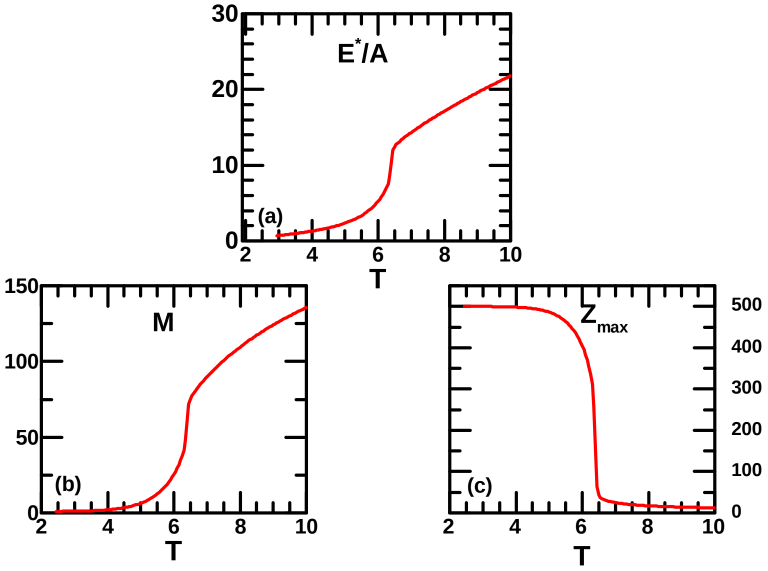

Figure 5.8: Variation of (a) excitation energy $E^*/A$ (MeV/A), (b) total multiplicity M, (c) average size of the largest cluster $Z_{max}$ with temperature T (MeV) for the fragments produced in the fragmentation of an ideal one-component system of size A=500.

## 5.3 Observables Proposed

Motivated by the similarities and the correlations discussed above, we will continue our study of nuclear phase transition, and extraction of its signatures from these multiplicity and largest cluster variables.

### 5.3.1 Multiplicity

Panel (a) and (b) of Fig. 5.8 show the variation of M and $E^*/A$ with temperature, for a one-component source of size A=500, at the same fragmentation condition (excitation, freeze-out volume). We see that both of them take a very low value at a low temperature. They increase slowly with temperature up to a particular temperature value (around 6MeV) and then increase very rapidly within a small range of temperature. After that, they again increase slowly. It is the same temperature range, where the two variables increase rapidly in the two plots. The slope of the $E^*/A$ vs. T curve gives specific heat per particle. Observing the similarity between total multiplicity and the excitation energy, we can draw a parallel between specific heat and the slope in multiplicity curve (dM/dT). We expect a maximum in the multiplicity derivative at the transition temperature, just like the specific heat. Now to investigate further, we have drawn variation of multiplicity (M) and its temperature derivative (dM/dT) with temperature for different fragmentation conditions, e.g., various fragmenting sources, incorporating or without incorporating Coulomb interaction. Then, we have compared M and dM/dT plots with the specific heat and the entropy.

#### M and dM/dT for different fragmenting system

We have drawn the total multiplicity M and dM/dT for a fragmenting system having 82 protons (Z=82) and 126 neutrons (N=126) in Fig. 5.9. To see the effect of Coulomb interaction, we have plotted them for two-component real nucleus as well as a single component system of the same mass, only switching off the Coulomb. As it is expected, the sudden rise of multiplicity

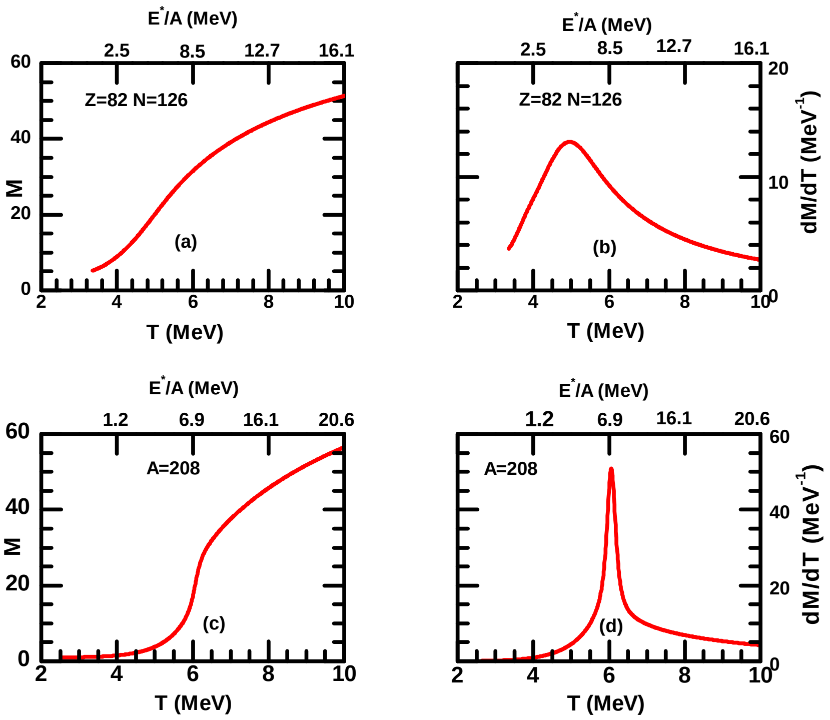

Figure 5.9: Variation of multiplicity M (left panels) and dM/dT (right panels) with temperature (bottom x axes) and excitation per nucleon (top x axes) from the CTM calculation for fragmenting systems having Z =82 and N =126 (top panels). Bottom panels represent the same but for a hypothetical system of one kind of particle with no Coulomb interaction but the same mass number (A =208). $E^* = E - E_0$, where $E_0$ is the ground-state energy of the dissociating system in the liquid drop model whose parameters are given in Ref. [21].[23]

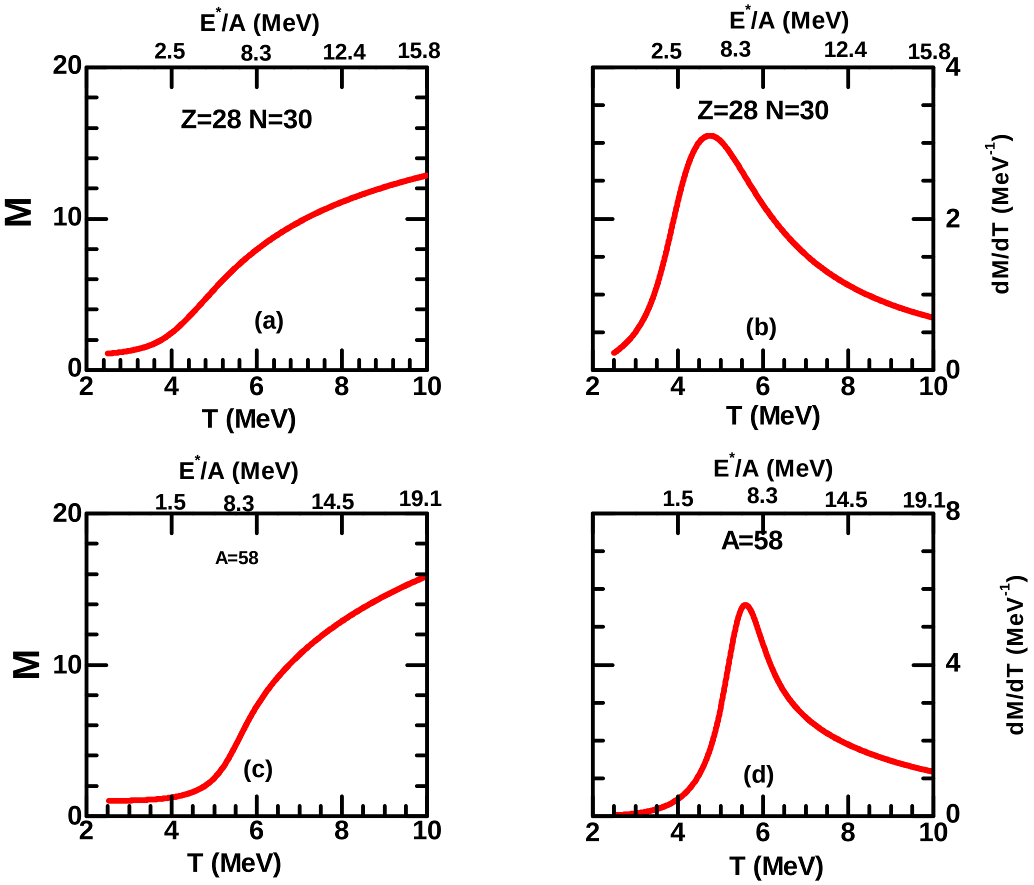

Figure 5.10: Same as Fig. 5.9 but the fragmenting systems are Z =28 and N =30 (top panels) and A =58 (bottom panels). [23]

and peak in dM/dT are much sharper in the absence of Coulomb. In Fig. 5.10, we have drawn the same plot as Fig. 5.9, except for the system size, which is smaller, Z=28, N=30 in this case. In the smaller system, we still observe a rapid jump in M and a peak in its temperature derivative. Though the sharpness of the jump and the peak is lesser for the smaller system.

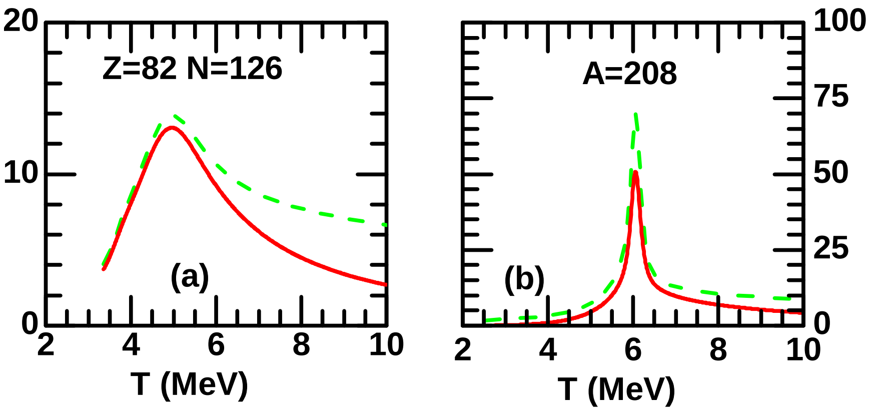

Figure 5.11: Variation of dM/dT (red solid lines) and $C_v$ (green dashed lines) with temperature from CTM for fragmenting systems having Z =82 and N =126 (left panel) and for hypothetical systems of one kind of particle with no Coulomb interaction of mass number A =208. To draw dM/dT and $C_v$ in the same scale, Cv is normalized by a factor of 1/50. [23]

### dM/dT and $C_V$

In the next two figures, Fig. 5.11 and Fig. 5.12, we compare dM/dT and the specific heat per particle $C_V$ for the two systems of size Z=82, N=126 and Z=28, N=30, respectively. In each case, we also consider the situation where the Coulomb interaction is switched off. We notice that the peak of dM/dT coincides with the peak of specific heat ($C_V$) in all the cases. The variation of $C_V$ with the temperature shows a maximum at the transition temperature, and this is a signature of the 1st order phase transition. From the last two figures, we may say that dM/dT can possibly give a signature of phase transition alternative to $C_V$. Even where bimodality develops, it may be easier to locate the position of the maxima in the derivative of M since the bimodal region is very narrow. The maximum of dM/dT, thus, can, possibly, be used as a signature of the occurrence of 1st order phase transition in Heavy Ion Collision.

Again, the temperature at which specific heat maximises, that is the transition temperature of phase transition. Since peaks of $C_V$ and dM/dT occur at the same temperature, the peak of dM/dT gives the transition temperature, too.

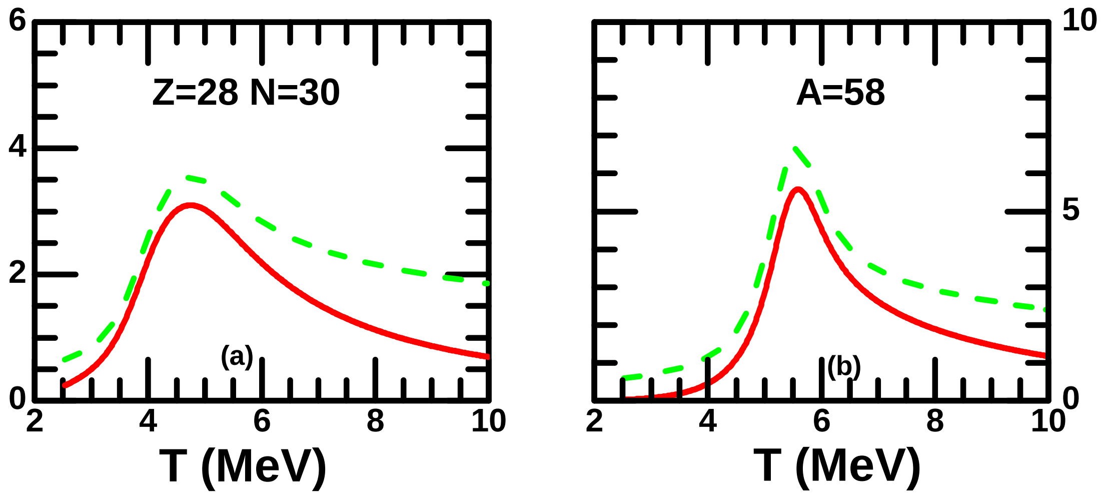

Figure 5.12: Same as in Fig. 5.11, but the fragmenting systems are Z =28 and N =30 (left panel) and A =58 (right panel). [23]

### dM/dT and Entropy

It is well known that (Fig. 5.4) in case of a first-order transition, entropy shows a rapid jump in the vicinity of the transition temperature, very similar to the total multiplicity. In the next plot (Fig. 5.13), we have compared the temperature variation of dM/dT and the entropy for the fragmenting system Z=82, N=126, and also for an ideal condition, neglecting the Coulomb interaction. It is evident, for both the cases, that the region in temperature scale where dM/dT exhibits a maximum, exactly there the entropy changes rapidly. The presence of Coulomb effect in a real system, only, smears the rise of entropy and the peak in dM/dT. This behaviour, further, establishes that dM/dT is giving the signature of phase transition.

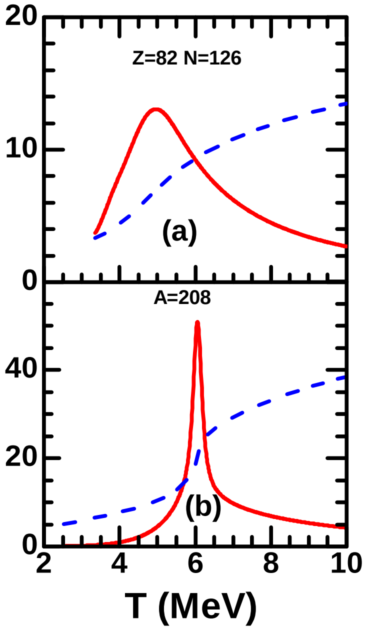

Figure 5.13: Variation of entropy (blue dashed lines) and dM/dT (red solid lines) with temperature from CTM for fragmenting systems having Z =82and N =126 (top panel) and for hypothetical system of one kind of particle with no Coulomb interaction of mass number A =208 (bottom panel). To draw S and dM/dT in the same scale, S is normalized by a factor of 1/20 for Z =82 and N =126 system and 1/50 for hypothetical system of one kind of particle. [23]

### Study with IMF multiplicity

The multiplicity of the intermediate mass fragments ($M_{IMF}$) in HIC can indicate the occurrence of phase transition (as discussed in Sec. 5.1.2). It is an important observable of multifragmentation, which is measured in the experiment, sometimes, instead of the total multiplicity M. Therefore, a similar study has been done on $M_{IMF}$. We have plotted the variation of $M_{IMF}$ and its temperature derivative with temperature for the system Z=82, N=126 in Fig. 5.14, and compared $dM_{IMF}$/dT with $C_V$. $M_{IMF}$ and $dM_{IMF}$/dT display a similar behaviour as that of the total multiplicity and its derivative. Only the exception is that the position of the two peaks, obtained from $dM_{IMF}/dT$ and $C_V$, do not coincide with each other. This is expected because the calculation of $C_V$ involves all the fragments irrespective of their mass or charge, but in $M_{IMF}$, only selected fragments are included.

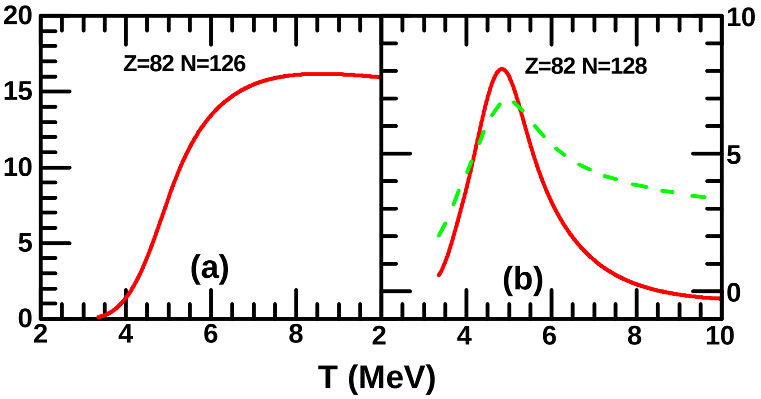

Figure 5.14: Variation of intermediate-massfragment(IMF) multiplicity $M_{IMF}$ (left panels) and first-order derivative of IMF multiplicity $dM_{IMF}/dT$ (right panels) with temperature from CTM calculation for fragmenting systems having Z =82 and N =126. Variation of $C_v$ with temperature (T) is shown by green dashed line in right panel. To draw d$M_{IMF}/dT$ and $C_v$ in the same scale, $C_v$ is normalized by a factor of 1/100. [23]

### Effects of secondary decay

In a heavy ion collision, when a nucleus instantaneously breaks up through the process of nuclear multifragmentation, giving various composites, these composites are called primary fragments. The primary fragments are excited in general, and lose excitation through sequential two-body decay, and thus affect the total multiplicity. The final cold fragments, called secondary fragments, are detected in the laboratory. The fragments that we are dealing with in our study (using CTM), are all primary fragments. The secondary decay may affect the total multiplicity in such a way that alters the behaviour of multiplicity discussed above. As we are interested in the experimental signature, we assimilate the secondary decay in our calculation (detail discussion is given in **Appendix C**), and do the same study with the multiplicity of the secondary fragments. We have plotted the multiplicities of the primary and the secondary fragments and their derivatives in Fig. 5.15. It is apparent that the effect of secondary decay does not alter our previous observation. Moreover, it enhances the signals, the total multiplicity jumps more rapidly, and the peak in $dM/dT$ is sharper in case of the secondary fragments. Thus the maxima of multiplicity derivative can be obtained successfully in experiments with a possibly unaltered transition temperature.

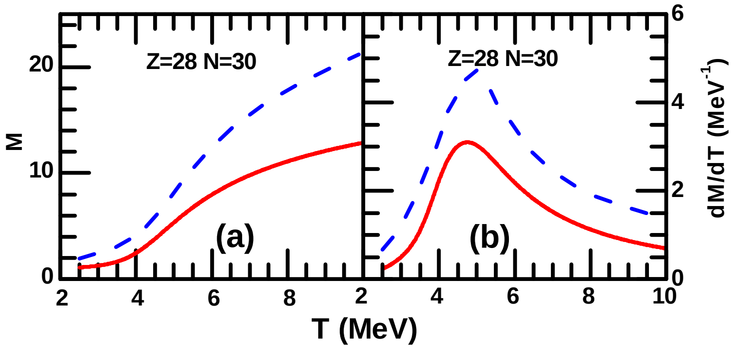

Figure 5.15: Effect of secondary decay on M (left panel) and dM/dT (right panel) for fragmenting systems having Z =28 and N =30. Red solid lines show the results after the multifragmentation stage (calculated from CTM), whereas blue dashed lines represent the results after secondary decay of the excited fragments. [23]

### 5.3.2 Largest Cluster

Now, we will concentrate on the observables, the average size of the largest cluster $\langle A_{max}\rangle$ and a normalized variable $\mathbf{a}_2$. $\langle A_{max}\rangle$ is defined in Sec. 3.2.1 and $\mathbf{a}_2$, measures the asymmetry between the two largest fragments, is defined as [16],

$$\mathbf{a}_2=\frac{\langle A_{max}\rangle\ -\ \langle A_{max-1}\rangle}{\langle A_{max}\rangle\ +\ \langle A_{max-1}\rangle}.$$

$A_{max-1}$ is the size of the second largest cluster produced in the fragmentation, and we estimate it using CTM in Appendix B. We have shown the connection between the multiplicity and the size of the largest cluster in Sec. 5.2. The behaviour of $\mathbf{a}_2$ being very similar to the largest cluster size, is often considered as an order parameter of the phase transition, and is measured in the experiments.

Throughout the rest of our study, we consider an ideal system of A=200 identical nucleons with no Coulomb force acting between them. Left panels of Fig. 5.16 ((a) to (d)) display the variations of the four variables, the normalised size of the average largest cluster $\mathbf{a}_{max}$, $\mathbf{a}_2$, total multiplicity M and entropy per particle (S/A) with temperature.

$$\mathbf{a}_{max}=\frac{\langle A_{max}\rangle}{A}. \tag{5.1}$$

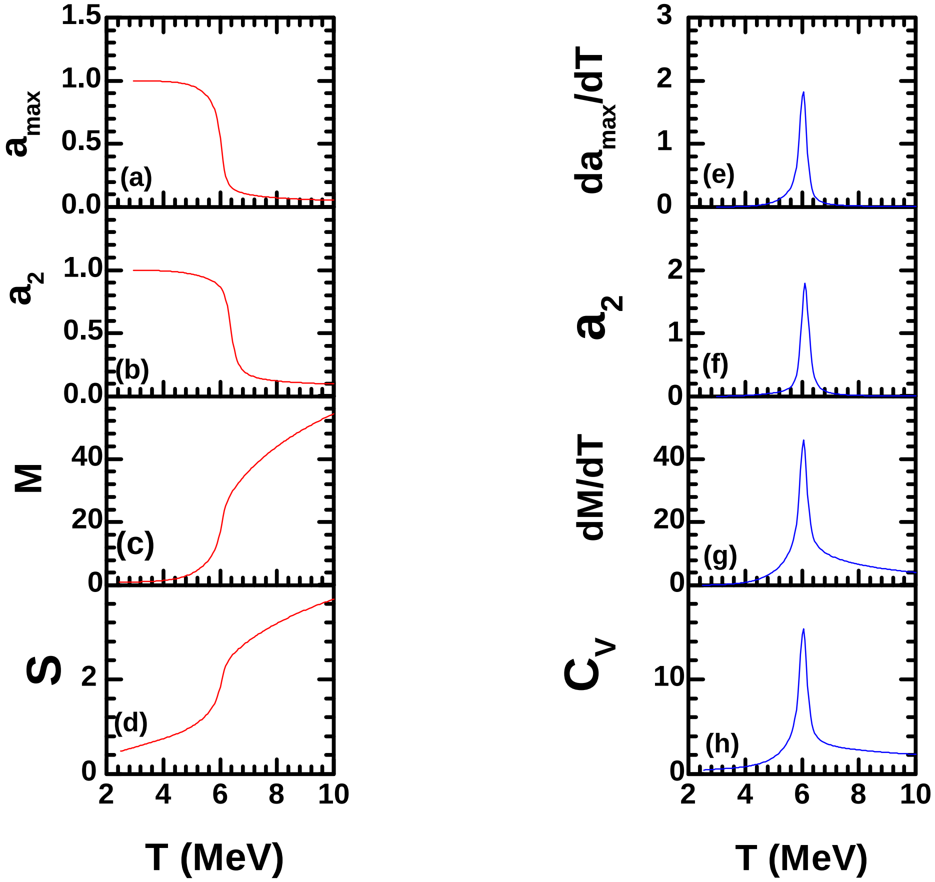

Figure 5.16: Variation of (a) $\mathbf{a}_{max}$, (b) $\mathbf{a}_2$, (c) M, (d) S, (e) -$d\mathbf{a}_{max}/dT$, (f) -$d\mathbf{a}_2/dT$, (g) dM/dT and (h) $C_v$ with temperature for fragmenting system of mass A=200. [24]

Over a temperature interval in the lower portion of the scale, up to approximately 5 MeV, $\mathbf{a}_{max}$ and $\mathbf{a}_2$ are almost constant and assume a value $\approx 1$. This implies that in this temperature range, the size of the largest fragment produced is almost the same as the size of the fragmenting source. Around T=6 MeV, both of them fall suddenly to a very low value near zero, which indicate the entire system fragments into the light mass nuclei. After that, they remain almost unchanged. These observables, clearly, give a sharp transition near T=6 MeV and therefore behave as an order parameter of the nuclear phase transition. Now, the last two panels ((c) and (d)) in the left of Fig. 5.16, show the variation of the total multiplicity and entropy per nucleon with temperature. $\mathbf{a}_{max}$ and $\mathbf{a}_2$ display similar behaviour as that of the multiplicity and the entropy; the sudden jump (or fall) of these four variables occur almost at the same temperature around 6 MeV. This similarity motivates us to investigate the behaviour of the derivatives of $\mathbf{a}_{max}$ and $\mathbf{a}_2$. In the right panel of Fig. 5.16, temperature derivatives of all the four quantities are plotted with the temperature. In the right bottom panel Fig. 5.16(h), we have plotted $C_V$, which is related to the temperature derivative of the entropy (S). The derivatives of $\mathbf{a}_{max}$ and $\mathbf{a}_2$ exhibit maxima just like total multiplicity and specific heat, and almost at the same temperature. Therefore the position of these maxima also gives the transition temperature.

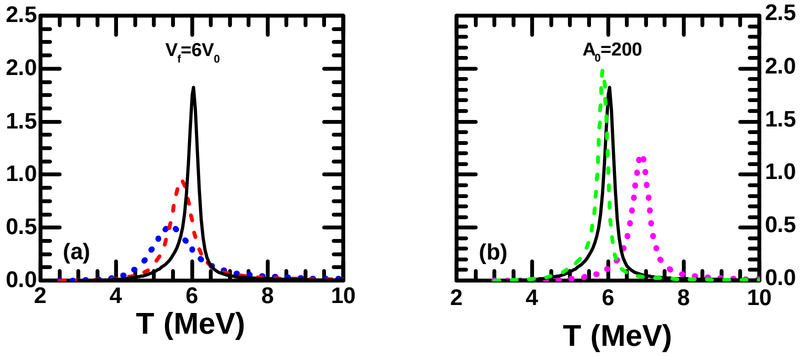

Figure 5.17: Variation of $d\mathbf{a}_{max}/dT$ with temperature (a) at constant freeze-out volume $V_f = 6V_0$ but for three fragmenting system of mass 50 (blue dotted line), 100 (red dashed line) and 200 (black solid line) and (b) for same fragmenting system of mass 200 but at three constant freeze-out volumes $V_f = 2V_0$ (magenta dotted line), $V_f = 6V_0$ (black solid line) anf $V_f = 8V_0$ (green dashed line). [24]

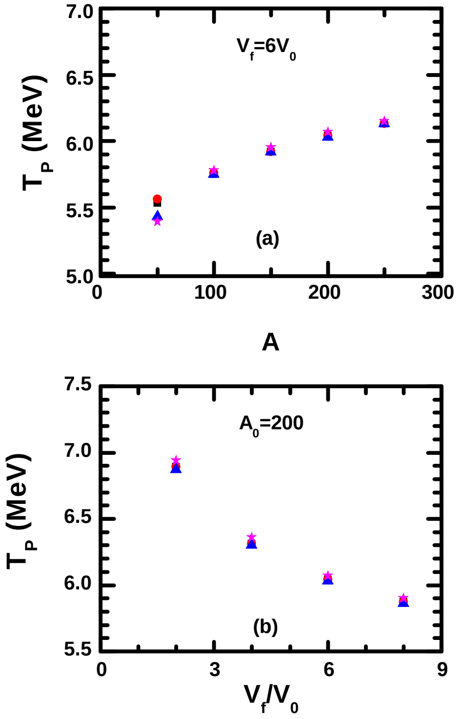

Figure 5.18: Dependence of the peak position of -$d\mathbf{a}_{max}/dT$, -$d\mathbf{a}_2/dT$, dM/dT and $C_v$ on fragmenting system size (upper panel) and freeze-out volume (lower panel). [24]

Next, we have investigated how the position of the maximum in temperature axis varies with the source size and the freeze-out volume. We have plotted the variation of d$\mathbf{a}_{max}$/dT with T for three different fragmenting systems of size A=50, 100, 200 at a fixed freeze-out volume $V_f = 6V_0$ in Fig. 5.17(a), and the same for three freeze-out volume $V_f$=$3V_0$, $4V_0$, $8V_0$ with fixed source A=200 in Fig. 5.17(b). We see that the peaks are sharper for the more massive source and the higher freeze-out volume. The position of the peak is observed to shift at right towards the upper-temperature region for the greater source size, and the lower temperature side for the greater freeze-out volume. This implies that the smaller system fragments more easily at a lower transition temperature as compared to its bigger counterparts. For freeze-out volume, the result that we have obtained is expected, since higher freeze-out volume (lower density) will favour the disintegration of the nucleus, resulting in lower transition temperature.

At the end, we have plotted the transition temperatures as a function of system size at fixed freeze-out volume (upper panel (a)), and as a function of freeze-out volume for a fixed system (lower panel (b)) in Fig. 5.18. In each panel, four different sets of transition temperatures are plotted. Those sets are obtained from the position of the maxima in $d\mathbf{a}_{max}/dT$, $d\mathbf{a}_2/dT$, dM/dT and $C_V$. The transition temperatures obtained from all the four observables give consistent results. Small differences between them attributed to the finiteness of the fragmenting system.

# Bibliography

[1] S. Das Gupta, A. Z. Mekjian, M. B. Tsang, **arXiv:nucl-th/0009033v2**, (2000).

[2] H. Jaquaman, A.Z. Mekjian and L. Zamick, Phys. Rev. C, **27**, (1983) 2782.

[3] L. Satpathy, M. Mishra and R. Nayak, Phys. Rev. C, **39**, (1988) 1.

[4] J.P. Bondorf, R. Donangelo, I.M. Mishustin, and H. Schulz, Nucl. Phys. A, **444**, (1985) 460.

[5] J.P. Bondorf, A.S. Botvina, A.S. Iljinov, I.N. Mishustin, and K. Sneppen, Phys. Rep. **257** (1995) 133.

[6] S. Das Gupta and A.Z. Mekjian, Phys. Rev. C **57** (1998) 1361.

[7] P. Bhattacharyya, S. Das Gupta and A. Z. Mekjian, Phys. Rev. C **60** (1999) 054616.

[8] C. B. Das, S. Das Gupta and A. Z. Mekjian, Phys. Rev. C **67** (2003) 064607.

[9] C. B. Das, S. Das Gupta and A. Z. Mekjian, Phys. Rev. C **68** (2003) 031601(R).

[10] G. Chaudhuri and S. Das Gupta, Phys. Rev. C **76** (2007) 014619.

[11] G. Chaudhuri and S. Das Gupta and F. Gulminelli, Nucl. Phys. A **815** (2009) 89.

[12] M. Bruno, F. Gulminelli, F. Cannata, M. D. Agostino, F. Gramegna, G. Vannini, Nucl. Phys. A **807** (2008) 48.

[13] A. Le Fe‘vre and J. AichelinPhys. Rev. Lett., **100** (2008) 042701.

[14] A. Le F‘evre *et al.*, Phys. Rev. C **80** (2009) 044615.

[15] M. Pichon, B. Tamain, R. Bougault, O. Lopez, Nucl. Phys. A **749** (2005) 93c.

[16] M. Pichon *et al.*, Nucl. Phys. A **779** (2006) 267.

[17] G. F. Peaslee *et al.*, Phys. Rev C **49** (1994) 2271(R).

[18] C. A. Ogilvie *et al.*, Phys. Rev. Lett. **67** (1991) 1214.

[19] M. B. Tsang *et al.*, Phys. Rev. Lett. **71** (1993) 1502.

[20] J. Pochodzalla, *et al.* Phys. Rev. Lett. **75(6)** (1995) 1040.

[21] C. B. Das, S. D. Gupta, W. G. Lynch, A. Z. Mekjian, and M. B. Tsang, Phys. Rep. **406** (2005) 1.

[22] Gargi Chaudhuri, Swagata Mallik, Nucl. Phys. A **849** (2011) 190.

[23] S. Mallik, G. Chaudhuri, P. Das, and S. Das Gupta, Phys. Rev. C **95** (2017) 061601(R).

[24] P. Das, S. Mallik, G. Chaudhuri, Phys. Lett. B **783** (2018) 364.

# Chapter 6

# Phase Transition in Hypernuclei

Hypernuclei, similar to normal nuclei, are the bound states of hyperons (strange baryons) in addition to the ordinary nucleons, e.g., neutrons and protons [1]. This is an obvious extension of the normal nuclear sector. Hypernuclei are discovered in 1952, in the experiment of fragmentation of emulsion nucleus, induced by high energy cosmic radiation [[1]-[3]]. In the laboratory, they are produced in a relativistic nuclear collision [[4]-[7]]. The motivation for the study of hypernuclei is to understand hyperon-nucleon (Y-N) and hyperon-hyperon (Y-Y) interaction (where Y: $\Lambda$, $\Sigma$, $\Omega$, $\Xi$ hyperons), which are of fundamental interest in nuclear physics and nuclear astrophysics. It helps us to understand the conventional nuclei [8], extend normal nuclear chart, and thus, leads towards hadron physics from traditional nuclear physics. These (hadronic equation of states) are important for the studies of astrophysical objects like neutron stars. Because, different theoretical models predict the dominant presence of hyperons within the core of neutron stars, where dense nuclear matter causes the abundance of hyperons [9]. There is no means of direct study of these N-Y or Y-Y interactions through the rudimentary hyperon-nucleon scattering experiments since hyperons are quite short-lived particles (decay time of the order of pico second). Instead of this, when hyperons form hypernuclei, being captured in the atomic nuclei, their formation cross-section or decay lifetime can provide the information about Y-N interaction or properties of strange matter, indirectly. Multi-strange hypernuclei, especially, can reveal Y-Y interaction and strange-matter properties.

The main problems in this study are extremely small formation probability and the lifetime of the hypernuclei. For example, in the reaction with 3.7 GeV/n $\mathrm{He}^4$ and 3.7 GeV/n $\mathrm{Li}^6$ beams projected on carbon target, the production cross section of $\mathrm{H}^4_\Lambda$ is obtained as approximately 0.3 $\mu$b and the lifetime of $\mathrm{H}^4_\Lambda$ is 0.22 ns [6]. For the other hypernuclei consisting of massive hyperons other than $\Lambda$, the probability and decay time are lower than $\Lambda$-hypernuclei. More than 30 single-$\Lambda$ hyperons, such as $\mathrm{H}^3_\Lambda$, $\mathrm{He}^4_\Lambda$,...$\mathrm{Bi}^{210}_\Lambda$, some double-$\Lambda$ hypernuclei, e.g., $\mathrm{He}^6_{\Lambda\Lambda}$, $\mathrm{Be}^{11}_{\Lambda\Lambda}$, $\mathrm{C}^{15}_{\Lambda\Lambda}$, etc. [10], and very few hypernuclei, involving hyperons other than $\Lambda$, are observed till the present day. Most of the experimental data of hypernuclei production, therefore, involves lambda hyperons. Since they are the lightest hyperons, they decay only via weak interaction. Their lifetime is higher compared to the reaction time, so, they can be detected in the nuclear collision experiments.

There are several theoretical approaches to the formation of hypernuclei. Those are Ultra-relativistic Quantum Molecular Dynamics (Ur QMD) [11], Dubna cascade model [11], Covariant Transport Model [12] based on coalescence picture [13], starting from the first theoretical proposition by Kerman and Weiss [14]. These theoretical models can explain the experimental results, quite satisfactorily.

In all the models, the physical picture is same as discussed below. The conventional picture of high energy heavy ion collision with a general impact parameter, established in different experimental and theoretical studies, is described in terms of participant spectator model. According to that, the collision occurs only at the overlapping region of the target and the projectile (participating region). The non-overlapping portions of the target and the projectile, being excited mildly, fly off and pass through without any interaction; they are called the target like fragment (TLF) and projectile-like fragment (PLF), respectively. Physical situation of both the PLF and TLF are similar for a symmetric collision; they are slightly excited and due to this excitation, break into fragments. Study of PLF is more advantageous since the fragment velocities are centred around the projectile velocity. In the fixed target experiments, they are emitted in the forward direction and therefore, can be detected easily. In the participating zone, profound interactions occur between nucleons themselves and with the other hadrons produced in the primary and secondary collision. In all the transport models, hyperons are considered to be produced in the participating zone due to nucleon-nucleon collision (B-B interaction) and interaction of baryons with the secondary meson (B-M) beam (secondary pion beam)($B+B \rightarrow B+Y+K, p+n \rightarrow n+\Lambda+K^{+}$; $B+M \rightarrow Y+K, \pi^{+}+n \rightarrow \Lambda+K^{+}$). Momenta of the produced Λs are distributed over a wide range. Some of the produced Λs, in the momentum range close to that of the projectile, having total momenta in PLF frame up to the Fermi momentum ($p_{tot} < 250MeV/c$), can be trapped in the PLF and form hypernuclear matter. Eventually, this mildly excited hypermatter decays to several normal and hyper fragments [15]. Experimental evidence shows hypernuclei are produced both in a central and peripheral collision. But the latter is preferred more since the detection of the hypernuclei is easier. In addition to that, the formation of heavy hypernuclei is possible in the peripheral collision, while in a central collision, mainly small fragments are produced due to high energy deposition.

Again, we mentioned that most of the experimental data are of Λ-hyperons, and very few involve other hyperons. So, we have considered Λ-hyperons only in our study and in the rest of the chapter, the term 'hyperon' indicates Λ unless it is mentioned.

Here, we explore the multifragmentation of a hypernuclear matter, which may be produced in the laboratory in a high energy heavy ion collision. Multifragmentation, as discussed in the previous chapters, is often described as a nuclear liquid-gas phase transition. In the present study, we will describe the effect of hyperons (Λ) on the transition, using Canonical Thermodynamical Model of multifragmentation. The Canonical Thermodynamical Model(CTM), already, has been extended to the three component system [16], and a recent study using three component CTM shows the existence of phase transition in this case [17]. A "U"-shaped mass distribution of the normal and hyper-fragments has been obtained in the fragmentation of the hyper-nuclear system. The "U"-shape indicates a liquid-gas (nuclear) phase co-existence, which is a well-known signature of the first-order phase transition [Chapter 5]. Here, that study has been continued further, analysing the relevant thermodynamic observables and the order parameters of the phase transition.

## 6.1 Three-component Canonical Thermodynamical Model

The theory used here is the same as the 2-component CTM in the Chapter 3, with an additional degree of freedom. The general statistical behaviour is assumed to be unchanged due to the presence of hyperons. We consider a fragmenting system, consists of $A_0$ baryons, $Z_0$ protons, and $H_0$ hyperons, produces different fragments of normal nuclei as well as hyper nuclei. The total system of the fragments is at freeze-out, where its temperature is T and volume is $V_f$ $(> V_0)$. The total canonical partition function is given by [16],

$$Q_{A_0,Z_0,H_0} = \sum \prod \frac{(\omega_{a,z,h})^{n_{a,z,h}}}{n_{a,z,h}!}, \tag{6.1}$$

where the product is over all the possible fragments in one decay channel. The sum is over the all possible decay channels, satisfying baryon, proton and hyperon number conservations,

$$\begin{aligned} \sum a\ .n_{a,z,h} &= A_0 && (6.2) \\ \sum z\ .n_{a,z,h} &= Z_0 && (6.3) \\ \sum h\ .n_{a,z,h} &= H_0. && (6.4) \end{aligned}$$

$n_{a,z,h}$ is the number of hyper-nuclei in a break-up channel that contains 'a' baryons, 'z' protons and 'h' hyperons, and $\omega_{a,z,h}$ is the partition function of such composite. The partition function $Q_{A_0,Z_0,H_0}$ is calculated, using the recursion relation,

$$Q_{A_0,Z_0,H_0} = \frac{1}{A_0} \sum_{a,z,h} a \cdot \omega_{a,z,h} \cdot Q_{A_0-a,Z_0-z,H_0-h}. \tag{6.5}$$

The average number of composites, having mass 'a', charge 'z', hyperons 'h', is given as,

$$\langle n_{a,z,h} \rangle = \frac{\omega_{a,z,h} \cdot Q_{A_0-a,Z_0-z,H_0-h}}{Q_{A_0,Z_0,H_0}}. \tag{6.6}$$

The partition function of a composite $\omega_{a,z,h}$ is given by,

$$\omega_{a,z,h} = \frac{V}{h^3}(2\pi T)^{3/2} \left\{(a-h)m_n + hm_h\right\}^{3/2}\ .\ Z_{a,z,h}(int), \tag{6.7}$$

where $m_n$ and $m_h$ are masses of the nucleons (938 MeV) and hyperons (1116 MeV for $\Lambda$), respectively. The volume V and the intrinsic partition function $Z_{int}$ is similar to that of the Chapter 3. The fundamental building blocks, in this case, are proton, neutron and $\Lambda$, and therefore $z_{int}(1,0,0) = z_{int}(1,1,0) = z_{int}(1,0,1) = 1$. For the composites, the intrinsic partition functions are derived in the following way, using the nuclear ground state energies and the excitations. In case of low mass composites, $1 < a \leq 5$, both for h=0 and $h > 0$, experimental binding energies are used. For others, $a > 5$, ground state energies are obtained from a liquid drop formula with a modification [20] due to the presence of hyperons. The excitation energies for these composites and entropies are derived using the Fermi-gas model. The expression for the ground state energy is [20],

$$E_0(T) = -16a + \sigma(T)a^{2/3} + 0.72\frac{\kappa z^2}{a^{1/3}} + 25.\frac{(a-h-2z)^2}{a-h} - 10.68h + 21.27\frac{h}{a^{1/3}}, \tag{6.8}$$

where the surface tension at finite temperature $\sigma(T)$ and the Wigner-Seitz correction factor $\kappa$ are given in the chapter 3.

Here we should mention the composite nuclei that are being considered, since all possible combinations between n, p, and h are not physically acceptable. For heavy fragments $a > 8$, the composites, that have been included, are guided by the lines of stability for neutrons and protons. The stability lines are calculated using the liquid-drop mass formula (Eq. 6.8), where the neutron and proton separation energies become zero, respectively. For low mass composites, $1 < a \leq 8$, we have taken the same set as mentioned in [18]. Another well-known parametrisation of binding energy for hypernuclei was proposed by Samanta et al. in [19]. A comparative study of these two formulae in case of hyper nuclear fragmentation was described in Ref. [20], and finally, the one used here was chosen because it produces results closer to the experimental data.

## 6.2 Results and Discussions

To get a clear picture of the phase transition in the strange nuclear system, we consider a system of clusters produced in the fragmentation of a strange nucleus. We have studied the thermodynamic observables, e.g., free energy, entropy and specific heat, the variation of pressure with volume and the order parameter (size of the largest cluster) for that system. Throughout the study, the fragmenting source that has been taken, is of charge 50 and baryon number 128. To observe the effect of hyperons on phase transition, both the normal system with no hyperons (H=0) as well as a strange system with H=8 hyperons have been considered, and the results have been compared. The Coulomb interaction is known to distort the phase transition signals. Therefore, in each case, until the last one, we have switched off the Coulomb interaction, since the primary interest of the study is to get the nature of the interaction of hyperons and their effects on phase transition. At the end, the Coulomb interaction is considered, in order to observe whether the signatures of phase transition in strange nuclear system persist in the presence of Coulomb, and how far the signals are distorted by it.

### 6.2.1 Free Energy, Entropy, Specific Heat

Free energy (F), and its first and second order derivatives with respect to temperature are the basic thermodynamic observables to study the phase transition (Sec. 2.3). The Helmholtz's free energy of the fragmenting hyper system can be calculated from the partition function,

$$F = -T \, . \, \ln Q_{A_0,Z_0,H_0}, \tag{6.9}$$

and is plotted against temperature, in the upper panel of Fig. 6.1. Entropy can be obtained from the derivative of F,

$$S = -\left[\frac{\partial F}{\partial T}\right]_V, \tag{6.10}$$

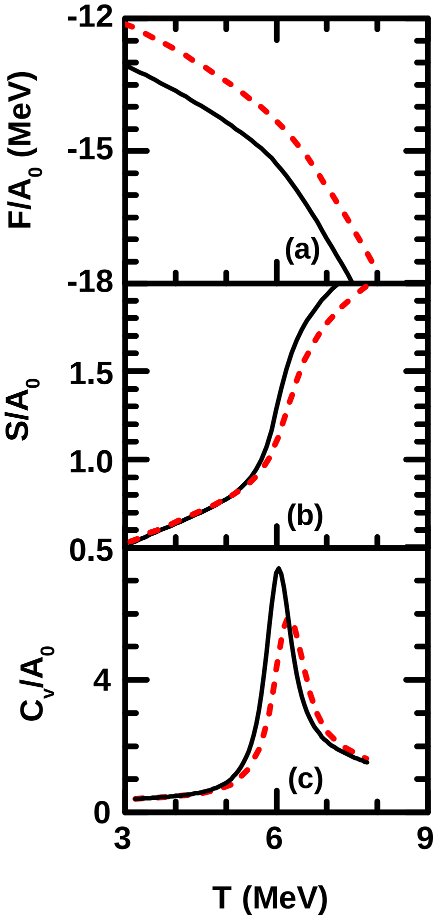

Figure 6.1: Variation of Helmholtzs free energy per nucleon (upper panel), entropy per nucleon (middle panel), and specic heat per nucleon (bottom panel) with temperature for two fragmenting systems having the same $A_0 = 128$, $Z_0 = 50$ but different $H_0 = 8$ (black solid lines) and $H_0 = 0$ (red dashed lines).[21]

and its variation with temperature is plotted in the mid-panel of Fig. 6.1. In the lowest panel of the Fig. 6.1, we have plotted the specific heat, which is given by

$$C_v = T\left(\frac{\partial S}{\partial T}\right)_V, \tag{6.11}$$

with temperature. We do not observe much qualitative difference between the plots of normal (solid lines) nuclei and strange (dashed lines) nuclei. Thermodynamic potential (F) shows a continuous trend, while entropy exhibits a sudden jump around T=6 MeV. The specific heat gives a prominent peak near the same temperature, for both the systems, as expected for a system undergoing the first-order phase transition. It is evident from the figures that the jump in entropy is more profound, and the peak in the specific heat plot is sharper for the strange system than the normal system. Therefore, it is clearly observed that the presence of hyperons enhances the signature of phase transition. The temperature at which entropy jumps suddenly, or specific heat gives peak, is the transition temperature. We see that the transition temperature is lower for the strange nuclear system than the normal one. This lowering of transition temperature is due to the presence of hyperons in the system. Therefore, the effect of the addition of hyperons in the nuclear system can be thought of equivalent to an increase of excitation energy of the nuclear system. Hence, the system disintegrates at a lower temperature.

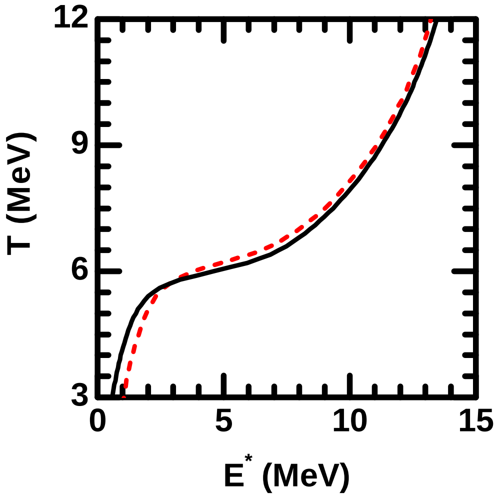

Figure 6.2: Variation of temperature (T) with excitation energy ($E$) for two fragmenting systems having the same $A_0 = 128$, $Z_0 = 50$ but different $H_0 = 8$ (black solid line) and $H_0 = 0$ (red dashed line).[21]

### 6.2.2 Caloric Curve

The excitation energy of the strange fragmenting system at a given temperature can be obtained from,

$$E^*_{A_0,Z_0,H_0} = T^2 \frac{1}{Q_{A_0,Z_0,H_0}} \left( \frac{\partial Q_{A_0,Z_0,H_0}}{\partial T} \right) - E_{A_0,Z_0,H_0}(T = 0). \tag{6.12}$$

The variation of temperature with the excitation energy is plotted in Fig. 6.2. Initially, the temperature rises steeply with the excitation, then it slows down during the phase transition process and again, starts to increase rapidly. For a system in the thermodynamic limit, the temperature is expected to remain constant with increasing excitation energy in the transition region. The nuclei being much smaller in size, the signatures are suppressed; one observes a remarkable slowing down in the rate of change of temperature, instead of T remaining constant for a macroscopic system.

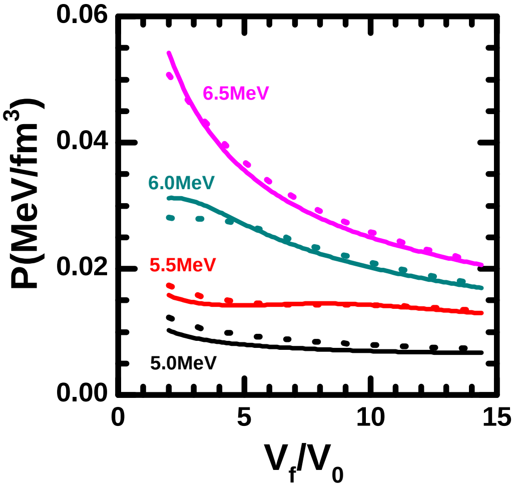

Figure 6.3: Variation of pressure with volume for two fragmenting systems having the same $A_0 = 128$, $Z_0 = 50$ but different $H_0 = 8$ (solid lines) and $H_0 = 0$ (dashed lines) at four different temperatures T =5.0, 5.5, 6.0, and 6.5 MeV.[21]

### 6.2.3 P Vs V : Isotherms

Figure 6.3 shows isotherms, i.e., pressure vs volume plots for four different temperatures, which are very important in case of a phase transition study. At a very low temperature, T=5 MeV, we get a flat region where pressure is almost unchanged with increasing volume. At this physical condition, both the systems (strange as well as a normal system) are in the liquid-gas co-existence phase. It is well known that as temperature increases, the co-existence region becomes smaller, and at the temperature where it just vanishes is the critical temperature. Now, at a comparatively higher temperature, T=6.0 MeV, we get a small portion of the curve in the lower volume, where the pressure is almost constant. This is the region of liquid-gas phase co-existence. Beyond this small region, as volume increases, pressure gradually decreases, and the system enters into the gaseous phase from the region of co-existence. At high temperature T=6.5 MeV, no region of phase co-existence is observed. The P-V plots show a rectangular hyperbolic nature that indicates both the normal nuclear system as well as the hyper nuclear system are completely in the gaseous phase. We have found an important observation at an intermediate temperature, T=6 MeV, where the flat portion, i.e., the region of phase co-existence is smaller for the hyper-system than the normal system. It implies, at this temperature, the strange nuclear system is more close to the gaseous phase than the normal one. In other words, the strange system disintegrates at a smaller volume as compared to a normal system.

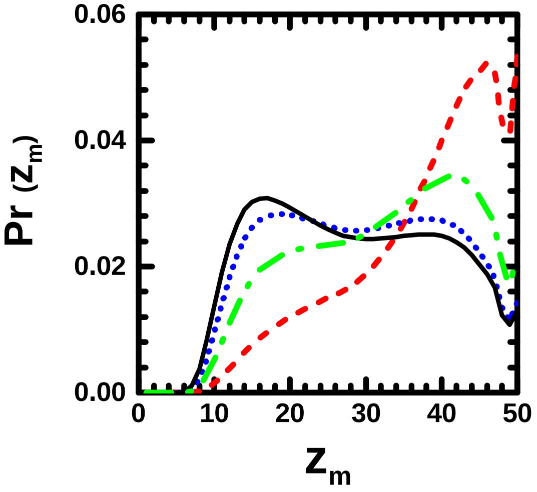

Figure 6.4: Largest cluster probability distribution for four different fragmenting systems having same $A_0 = 128$, $Z_0 = 50$ but different $H_0 = 8$ (black solid line), $H_0 = 4$ (blue dotted line), $H_0 = 2$ (green dash-dotted line), and $H_0 = 0$ (red dashed line). Calculations are done at constant temperature T =6.065 MeV.[21]

### 6.2.4 Largest Cluster and Bimodality

The average size of the largest cluster is an order parameter (Chapter 5) for a nuclear phase transition. It is given by the Eq. 3.19 where the probability $Pr(Z_m)$ for the strange nuclear

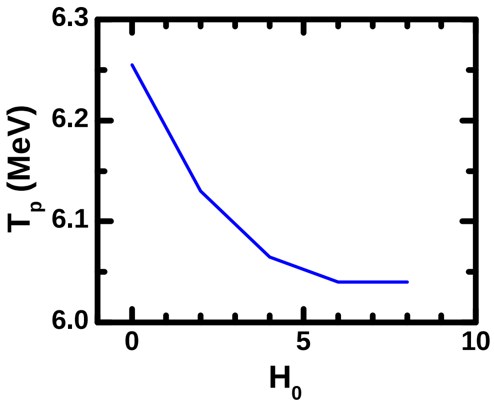

Figure 6.5: Variation of transition temperature ($T_p$) with the total strangeness content of the fragmenting system.[21]

system is,

$$Pr(Z_m) = \frac{Q_{A_0,Z_0,H_0}(Z_m) - Q_{A_0,Z_0,H_0}(Z_m - 1)}{Q_{A_0,Z_0,H_0}(Z_0)}, \tag{6.13}$$

which is very similar to the Eq. 3.20. The detailed discussion of the terms of Eq. 3.20 is applicable here also. The probability distribution of the largest cluster size is plotted at temperature T=6.065 MeV, in Fig. 6.4, for four different fragmenting systems containing different strangeness content, e.g., H=0 (normal system), H=2, H=4, H=8. The theoretical calculation shows the bimodality in the distribution of order parameter is a signature of the first-order phase transition for a finite system. The probability distribution, hence, is expected to give a bimodal behaviour, that means, a two-peaked curve around the transition temperature, in the present case. At the transition point, the height of the two peaks become exactly equal. In the figure one can see, at that temperature, the probability distribution gives a maximum around a small value of $Z_m$ for the strange system containing 8 hyperons. For the normal nuclear system, it exhibits a maximum near the high value of $Z_m$. So, it is clear from the figure that at this temperature, the hyper system containing 8 hyperons is more close to the gaseous phase, and the normal system remains in the liquid phase. The system with 4 hyperons, at T=6.065 MeV, is very close to the transition point since the peaks are almost of equal height. Therefore, the transition temperature varies with the strangeness content, and is less for the

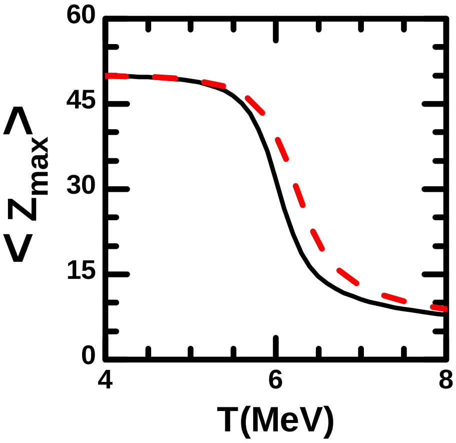

Figure 6.6: Variation of average charge of the largest cluster ($Z_{max}$) with temperature (T) for two fragmenting systems having the same $A_0 = 128$, $Z_0 = 50$ but different $H_0 = 8$ (black solid line) and $H_0 = 0$ (red dashed line).[21]

more strange system, as the system with more hyperons breaks down more easily. The bimodal behaviour [[22]-[25]] of the size of the largest cluster probability distribution, establishes the occurrence of the first-order phase transition in the system. Variation of transition temperature with the strangeness content of the fragmenting system is displayed in Fig. 6.5, where the transition temperatures are calculated from the bimodality of $Pr(Z_m)$. It further confirms the observation, already obtained from the Fig. 6.4, that the phase transition temperature is less for the more strange system, indicating that the strangeness aids in the disintegration of the system. In the next figure (Fig. 6.6), we have shown the variation of the order parameter, i.e., the average size of the largest cluster with temperature. The variation for the strange system is exactly similar to that of the normal system, except for the sharpness of the change of $\langle Z_{max} \rangle$ with the temperature near the phase transition region. Change of $\langle Z_{max} \rangle$ is more pronounced, and the transition temperature is smaller for the strange system, which is consistent with the previous observations.

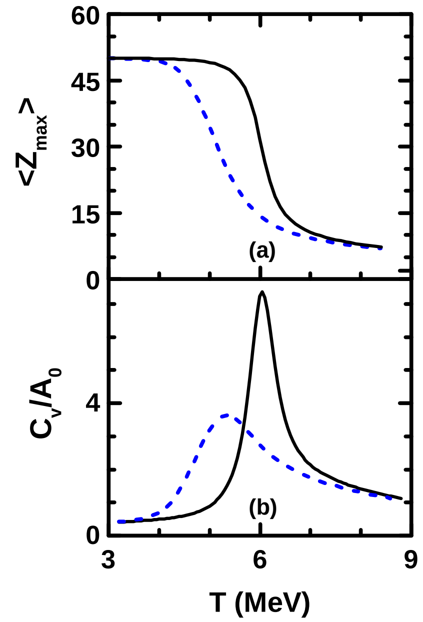

Figure 6.7: Variation of average charge of the largest cluster ($Z_{max}$) (upper panel) and specific heat per nucleon (lower panel) with temperature (T) by switching on (blue dashed lines) and switching off (black solid lines) the Coulomb interaction. All the calculations are done for the fragmentation of a hypernucleus having $A_0 = 128$ baryons, $Z_0 = 50$ protons, and $H_0 = 8$ hyperons.[21]

### 6.2.5 Effect of coulomb interaction

In the end, we examine the effect of the long-range Coulomb interaction on the hypernuclear phase transition, and how the signals get disturbed due to its presence. For this purpose, the variation of the order parameter $\langle Z_{max} \rangle$ and specific heat $C_V$ are plotted with temperature for the strange system in Fig. 6.7. Two lines corresponding to two different situations, one where the Coulomb has been taken into consideration and the other where the Coulomb interaction is switched off, are compared. Effect of Coulomb on ordinary nuclear phase transition is well established, and known to suppress the signals of phase transition as mentioned earlier. The Fig. 6.7 indicates, this effect is unaltered in the case of hyper-nuclear transition. It is observed from the figure that the size of the largest cluster falls more abruptly, and the specific heat peak is sharper in the absence of the Coulomb interaction. Further, the region where $\langle Z_{max} \rangle$ falls rapidly or $C_V$ gives peak, i.e., the transition region is shifted to the lower side of the temperature scale. Since the repulsive Coulomb interaction tries to break the nuclei into fragments to minimise the Coulomb potential, the transition occurs at a lower temperature in its presence. Thus, the effect of the Coulomb interaction in the case of hyper-nuclear phase transition is the same as that for a normal nuclear system.

# Bibliography

[1] J. Pniewski, Discovery of Hypernuclei: the Beginnings, in: Early History of Cosmic Ray Studies, eds. Yataro Sekido, Harry Elliot, D. Reidel Publishing Company, Dodrecht 1985, p. 323.

[2] M. Danysz and J. Pniewski, Philos. Mag. **44** (1953) 348.

[3] ACTA PHYSICA POLONICA B, **35** (2004) 3.

[4] K. J. Nield *et al.*, Phys. Rev. C **13** (1976) 3.

[5] S. A. Avramenko *et al.*, Pis'ma Zh. Eksp. Tero. Fiz. **48**, 9 (1988) 474.

[6] S. A. Avramenko, *et al.*, Nucl. Phys. A **547** (1992) 95c.

[7] T. R. Saito *et al.*, Nucl. Phys. A **881** (2021) 218.

[8] O. Hashimoto and H. Tamura, Prog. Part. Nucl. Phys. **57** (2006) 564.

[9] J. Schaffner-Bielich, Nucl. Phys. A **804** (2008) 309.

[10] J. K. Ahn, Phys. Rev. C **88** (2013) 014003.

[11] A. S. Botvina, K. K. Gudima, J. Steinheimer, M. Bleicher, and I. N. Mishustin, Phys. Rev. C **84** (2001) 064904.

[12] T. Gaitanos, H. Lenske, U. Mosel, Phys. Lett. B **675** (2009) 297.

[13] M. Wakai, H. Bando, M. Sano, Phys. Rev. C **38** (1988) 2.

[14] A. K. Kerman and M. S. Weiss, Phys. Rev. C **8** (1973) 408.

[15] N. Buyukcizmeci, A. S. Botvina, J. Pochodzalla, and M. Bleicher Phys. Rev. C **88** (2013) 014611.

[16] S. Das Gupta, Nucl. Phs. A **822** (2009) 41.

[17] S. Mallik and G. Chaudhuri Phys. Rev. C **91** (2015) 054603.

[18] V. Topor Pop and S. Das Gupta, Phys. Rev. C **81** (2010) 054911.

[19] C.Samanta,P.R.Chowdhurry,andD.N.Basu,J.Phys.G.Nucl. Part. Phys. **32** (2006) 363.

[20] A. S. Botvina and J. Pochodzalla, Phys. Rev. C **76** (2007) 024909.

[21] P. Das, S. Mallik, and G. Chaudhuri, Phys. Rev. C **95** (2017) 014603.

[22] F. Gulminelli and Ph. Chomaz, Phys. Rev. C **71** (2005) 054607.

[23] G. Chaudhuri, S. Das Gupta, and F. Gulminelli, Nucl. Phys. A **815** (2009) 89.

[24] S. Mallik, S. Das Gupta, and G. Chaudhuri, Phys. Rev. C **93** (2016) 041603(R).

[25] E. Bonnet *et al.*, (INDRA and ALADIN Collaborations), Phys. Rev. Lett. **103** (2009) 072701.

# Chapter 7

# Summary and outlook

In this dissertation, some of the aspects of the fragmentation of nuclei in heavy ion collision at intermediate energy has been explored in the framework of the statistical model, a brief summary of which is given here:

In **Chapter 4**, a mathematical relation has been obtained to extract the canonical average of an observable, knowing its grand canonical average values, in case of fragmentation of a finite nuclear system. The approximate canonical results, obtained using the transformation, agree nicely with the exact canonical values. The method of approximation has a few limitations. Firstly, one should consider an observable that varies only linearly or quadratically with the number of nucleons. Secondly, the method fails when the value of the observable itself is very small. Also, the transformation relation (Eq. 4.23) will not be valid in the temperature or the density region where fluctuations get maximised due to the presence of the 1st order phase transition. In the presence of long-rang Coulomb interaction, though, the signature of phase transition is quenched, so that the performance of the approximation is not too bad near the phase transition temperature. In spite of these limitations, we hope the relation connecting canonical and grand canonical averages will be useful for the extraction of certain parameters, e.g., isoscaling parameters $\alpha$, $\beta$, isotope temperature, etc. from experimental data. At last, it should be mentioned that the laboratory condition of intermediate energy heavy ion collision is consistent with the microcanonical ensemble distribution, though, its exact calculation is extremely difficult. In this context, the extension of this method of approximation to connect microcanonical and canonical averages of observables will be very interesting, and of great practical use.

In **Chapter 5**, we aimed to find new observables that can be used to observe the unique signatures of nuclear phase transition, experimentally. We have done our investigation using CTM. We chose the fragmentation observables the total multiplicity M, the average largest cluster size $\mathbf{a}_{max}$ (normalised by the system size), and a normalised variable $\mathbf{a}_2$, which assume distinctly different values in the liquid and gas phases of a nuclear system, and thus can distinguish between the two phases. Specially, they are accessible in the experiment, and can be measured more accurately than the existing observables of phase transition (e.g., excitation energy and T in the caloric curve). We observe that the total multiplicity behaves very similarly as entropy (or excitation energy), and its temperature derivative as specific heat. dM/dT peaks at the same temperature as $C_V$. So, the transition temperature can be measured theoretically from the maximum of dM/dT, just like it is obtained from specific heat. Even in the presence of Coulomb interaction, that is a long-range interaction which suppresses phase transition signals, the performance of dM/dT is quite satisfactory. The signature of phase transition is not distorted, rather, it gets enhanced, when we consider the multiplicity of the cold fragments, produced after the secondary decay of the primary fragments. Thus we see, this signature of phase transition can be extracted experimentally, measuring the total multiplicity.

The present work on the derivative of fragment multiplicity (total or IMF multiplicity) led to some recent theoretical and experimental exploration in this area of research. In [1], [2] the multiplicity derivative (dM/dT) has been studied in the Statistical Multifragmentation model for various fragmentation conditions (different source size, freeze-out volume, N/Z asymmetry, etc.). They have found the maximum in dM/dT as in the present work. They have also shown, within the framework of SMM model [3], that the multiplicity derivative measures the transition point most accurately in comparison to the other phase transition probes, both considering primary and the secondary fragments. Other works [4] and [5], too, using the Isospin-dependent Quantum Molecular Dynamics (IQMD) model [6] and the modified Nuclear Statistical Equilibrium (NSE) model [7], respectively, on the multiplicity derivative reveal the observations more or less consistent to the present study. Besides the theoretical studies, an experimental investigation has also been performed in [8], where the charge particle multiplicity of the Quasi-Projectile source exhibit the same behaviour as that of the specific heat, which is in close agreement to our observation. A similar study has been done in case of the lattice gas model as well as percolation model [9]. These theoretical and experimental investigations and the observed behaviour consistent to ours establish, further, the proposition that the multiplicity derivative can be treated as a signature of nuclear liquid-gas phase transition.

Study with the other two observables, $\mathbf{a}_{max}$ and $\mathbf{a}_2$, reveals that they provide the phase transition signals and the transition temperature, similar to multiplicity when we consider the fragmentation of an ideal one-component system, turning-off the Coulomb effect. It is sometimes easier to measure the largest cluster size than to count the total multiplicity, covering all the produced nuclei in the experiment. Extensive work with these variables for real nuclei with two types of nucleons has not been done. We will continue the study in future.

In **Chapter 6**, the liquid-gas phase transition has been examined for a strange nuclear system, using the 3-component CTM, and the results obtained can be summarised into the following points:
i. The thermodynamic variables and the order parameter show the persistence of phase transition in the presence of hyperons.
ii. Signals of the phase transition get enhanced in the presence of strangeness, while the transition temperature gets lowered.
iii. Ideally, the entropy should have a discontinuity, and the specific heat should diverge at the transition point when a thermodynamic system undergoes a first-order phase transition but, as discussed previously, the signals get softened here due to the finiteness of the system.
iv. Bimodal behaviour of the probability distribution of the order parameter $\langle Z_{max} \rangle$ is observed, which is a signature of the first-order phase transition for a finite system.
v. The effect of long-range Coulomb interaction on the phase transition of strange matter has also been investigated, and the result obtained is the same as that of a normal nuclear system.

Apart from the above-mentioned points, some other points are worth mentioning. It is obvious that the observed effect of hyperons on the nuclear phase transition should give valuable information about Y-N and Y-Y interaction. But the observations made here, such as the enhancement of phase transition signature, the decrease of the transition temperature, or the flat portion of the Fig. 6.5, are not unambiguous. The only input of the nature of hyperons or Y-N/Y-Y interaction comes in the model through the hyper-nuclear binding energy. The liquid-drop hyper term is based on the parametrisation using the experimental data, where the experimental data are not available in sufficient amount to do such parametrisation correctly. Therefore, in order to get the effects more reliably and in order to explain them correctly, we need more rigorous treatment in the form of microscopic calculation. There are some works in the literature, where the multi-strange nuclear system has been studied, and binding energies are calculated using Relativistic Mean-Field(RMF) theory [10],[11]. These may be incorporated in 3-component CTM model. In [12] a generalised Bethe-Weizsacker mass formula has been developed for strange hadronic system, that also, may be employed to the present model. Further investigation incorporating this in 3-component CTM may provide interesting results.

# Bibliography

[1] W. Lin, P. Ren, H. Zheng, X. Liu, M. Huang, R. Wada, and G. Qu; Phys. Rev. C **97** (2018) 054615.

[2] W. Lin, P. Ren, H. Zheng, X. Liu, M. Huang, K. Yang, G. Qu and R. Wada; Phys. Rev. C **99** (2019) 054616.

[3] J. P. Bondorf *et al.*, Phys. Rep. **257** (1995) 133.

[4] H. L. Liu, Y. G. Ma and D. Q. Fang; Phys. Rev. C **99** (2019) 054614.

[5] Rula Bakeer, Waad Awad and H R Jaqaman; J. Phys. G: Nucl. Part. Phys. **46** (2019) 025105.

[6] C. Hartnack et al., Eur. phys. J. A **1** (1998) 151.

[7] S. Talahmeh and H. R. Jaqaman; J Phys. G: Nucl. Part. Phys. **40** (2013) 015103.

[8] R. Wada, W. Lin, P. Ren, H. Zheng, X. Liu, M. Huang, K. Yang and K. Hagel; Phys. Rev. C **99** (2019) 024616.

[9] S. Das Gupta, S. Mallik and G. Chaudhuri; Phys. Rev. C **97** (2018) 044605.

[10] LAN Mi-Xiang, LI Lei, NING Ping-Zhi; arXiv:0903.0769v3 [nucl-th] 2009.

[11] M. Ikram, S. K. Singh, A. A. Usmani, S. K. Patra; International Journal of Modern Physics E Vol. **23**, No. 9 (2014) 1450052.

[12] Carl B. Dover and A. Gal; Nucl. Phys. A **560** (1993) 559.

# Appendix A

# Wigner - Seitz Approximation

Here we shall present the calculation used to get the estimate of Coulomb energy of the system of several fragments at freeze-out, using Wigner-Seitz approximation. We consider a fragmenting system of mass number $A_0$, the atomic number $Z_0$ (charge $=Z_0$e), goes through the process of nuclear fragmentation and reaches the freeze-out condition. This is, basically, a system of a number of charged fragments enclosed within a spherical region, of volume equal to freeze-out volume $V_f$, with radius $R_f$. The number of fragments varies from channel to channel, satisfying the two conservations, that total charge must be $Z_0$, total mass $A_0$. We calculate the approximate Coulomb energy for a particular channel ($\{n_{ij}\}$).

The total Coulomb energy ($E_C$) of such a system can be approximated as the sum of two terms,

$$E_C = E_C^0 + E_C'. \tag{A.1}$$

$E_C^0$ is the Coulomb energy of a charged sphere of volume $V_f$, where the total $Z_0$ charge is distributed uniformly over this volume with a charge density $\rho_f^{ch}$. $E_C'$ is the total Coulomb energy of a system, shown in Fig. A.1. To calculate the latter, we divide the entire freeze-out volume into different spherical cells of different size, containing only one fragment in each, the centre of each fragment being at its centre. The assumption is that the cells are not interacting with each other. Even for two consecutive cells, there exists no Coulomb interaction between them. Size of each cell is determined by the charge contained within it, i.e., the charge of the

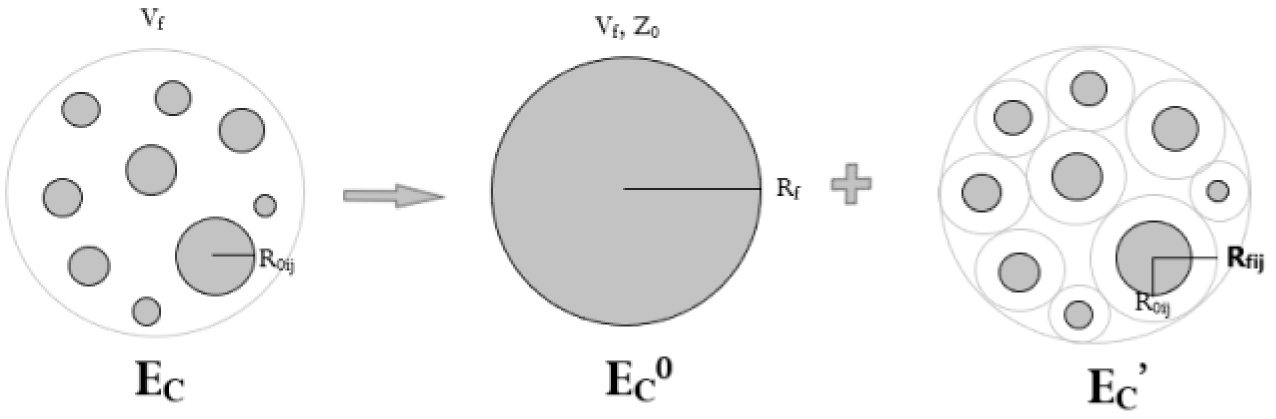

Figure A.1: Wigner-Seitz approximation

fragment in it. A cell containing a composite (i, j) has a volume, over which the charge 'i' can be distributed if it is distributed uniformly at a density $\rho_f^{ch}$. Then, we calculate the Coulomb energy, to shrink this dilute charged cell to make it a denser blob, of a normal nucleus at normal nuclear density $\rho_0$. Then the sum of these energies over all the fragments will give $E_C'$.

Mass $A_0$ as well as charge $Z_0$ is distributed over $V_f$. So, the freeze-out mass density is defined as, $\rho_f^{mass} = \frac{A_0}{V_f}$, freeze-out charge density will be $\rho_f^{ch} = \frac{Z_0}{V_f}$. If $R_f$ be the radius of the sphere of volume $V_f$ then,
$V_f = \frac{4}{3}\pi R_f^3 = \frac{Z_0}{\rho_f^{ch}} = \frac{A_0}{\rho_f^{mass}}$. First term, the Coulomb energy of a uniformly charged sphere of total charge $Z_0.e$ will be,

$$E_C^0 = \frac{1}{4\pi\epsilon_0} \cdot \frac{3}{5} \cdot \frac{Z_0^2 e^2}{R_f}. \tag{A.2}$$

Now, we calculate the second term. For a fragment (i, j), let its normal nuclear radius be $R_{0ij}$, so the normal nuclear volume of this nucleus is

$$V_{0ij} = \frac{A}{\rho_0^m} = \frac{i}{\rho_0^{ch}} = \frac{4}{3}\pi R_{0ij}^3 \qquad [A = i + j, \text{mass of the nucleus}]$$

Let the radius of the cell corresponding to this (i, j) fragment is $R_{fij}$, which is at freeze-out density. The total amount of charge within this cell is i (actually = $i.e$), and we can write,

$$V_{fij} = \frac{A}{\rho_f^m} = \frac{i}{\rho_f^{ch}} = \frac{4}{3}\pi R_{fij}^3.$$

The energy, required to shrink this dilute cell to make a normal nucleus (i, j), is the difference in Coulomb energy between the two states, the cell at a density $\rho_f$ ($U_{fij}$) and the nucleus at normal nuclear density $\rho_0$ ($U_{0ij}$). This amount of energy will be stored in the nucleus as Coulomb energy. Coulomb energy of the cell is,

$$U_{fij} = \frac{1}{4\pi\epsilon_0} \cdot \frac{3}{5} \cdot \frac{j^2 e^2}{R_{fij}},$$

and coulomb energy of the nucleus is

$$U_{0ij} = \frac{1}{4\pi\epsilon_0} \cdot \frac{3}{5} \cdot \frac{j^2 e^2}{R_{0ij}}.$$

Therefore, the work done,

$$\begin{aligned}
&= U_{0ij} - U_{fij} \\
&= \frac{1}{4\pi\epsilon_0} \cdot j^2 e^2 \left( \frac{1}{R_{0ij}} - \frac{1}{R_{fij}} \right) \\
&= \frac{1}{4\pi\epsilon_0} \cdot \frac{3}{5} \cdot \frac{j^2 e^2}{R_{0ij}} \left( 1 - \frac{R_{0ij}}{R_{fij}} \right),
\end{aligned}$$

which is the Coulomb energy of the fragment, modified by a factor within the first bracket. The total Coulomb energy of the system at freeze-out condition will be,

$$E_C = \frac{1}{4\pi\epsilon_0} \cdot \frac{3}{5} \cdot \frac{Z_0^2 e^2}{R_f} + \sum_{ij} \frac{1}{4\pi\epsilon_0} \cdot \frac{3}{5} \cdot \frac{j^2 e^2}{R_{0ij}} \left[ 1 - \left( \frac{R_{0ij}}{R_{fij}} \right)^{1/3} \right]. \tag{A.3}$$

Now,

$$\frac{V_{0ij}}{V_{fij}} = \frac{\frac{4}{3} \cdot \pi R_{0ij}^3}{\frac{4}{3} \cdot \pi R_{fij}}$$

$$\begin{aligned}
&\implies \frac{i/\rho_0^m}{i/\rho_f^m} = \frac{R_{0ij}^3}{R_{fij}^3} \\
&\implies \frac{\rho_f^m}{\rho_0^m} = \frac{R_{0ij}^3}{R_{fij}^3} \\
&\implies \frac{R_{0ij}}{R_{fij}} = \left( \frac{\rho_f}{\rho_0} \right)^{1/3},
\end{aligned} \tag{A.4}$$

and again,

$$\begin{aligned}
V_f &= \frac{4}{3}\pi R_f^3 \\
V_0 &= \frac{4}{3}\pi R_0^3 \\
A_0 &= V_f \,.\, \rho_f^m = V_0 \,.\, \rho_0^m \\
\Longrightarrow \frac{V_f}{V_0} &= \frac{\rho_0^m}{\rho_f^m} \\
\Longrightarrow \frac{R_f^3}{R_0^3} &= \frac{\rho_0^m}{\rho_f^m} \\
\Longrightarrow \frac{R_f^3}{R_0^3} &= \frac{R_{fij}^3}{R_{0ij}^3} \\
\Longrightarrow \frac{R_f}{R_0} &= \frac{R_{fij}}{R_{0ij}}. \qquad (A.5)
\end{aligned}$$

Therefore,

$$\begin{aligned}
E_C &= \frac{1}{4\pi\epsilon_0} \cdot \frac{3}{5} \cdot \frac{Z_0^2 e^2}{R_f} + \sum_{ij} \frac{1}{4\pi\epsilon_0} \cdot \frac{3}{5} \cdot \frac{j^2 e^2}{R_{0ij}} \left[1 - \left(\frac{R_0}{R_f}\right)^{1/3}\right] \qquad (A.6) \\
&= \frac{1}{4\pi\epsilon_0} \cdot \frac{3}{5} \cdot \frac{Z_0^2 e^2}{R_f} + \sum_{ij} \frac{1}{4\pi\epsilon_0} \cdot \frac{3}{5} \cdot \frac{j^2 e^2}{R_{0ij}} \left[1 - \left(\frac{\rho_f}{\rho_0}\right)^{1/3}\right]. \qquad (A.7)
\end{aligned}$$

We can easily see, this approximated expression for $E_C$ gives the correct result at the two extreme limits: i. For very large freeze-out volume, $R_f \to \infty$,

$$E_C = \sum_{ij} \frac{1}{4\pi\epsilon_0} \cdot \frac{3}{5} \cdot \frac{j^2 e^2}{R_{0ij}}. \qquad (A.8)$$

$E_C$ will be equal to the sum of the Coulomb energies of the individual fragments, as then, all the fragments will be at an infinite distance apart from each other, and so, all will become free. ii. If freeze-out volume = normal nuclear volume, $R = R_0$. This will represent a single nucleus of radius $R_0$, and $E_C = \frac{1}{4\pi\epsilon_0} \cdot \frac{3}{5} \cdot \frac{Z_0^2 e^2}{R_f}$ will give the Coulomb energy of that charged sphere (nucleus).

# Appendix B

# Secondary decay scheme

The disintegration of a hot nucleus yields the hot primary fragments and this is described by the statistical models of fragmentation. In laboratory, the primary fragments cannot be measured, because most of the excited primary fragments lose their excitation by secondary decay, and become stable isotopes in ground states when they reach the detectors. In order to compare results of fragmentation models with experimental data, one should incorporate this secondary decay part at the end of the statistical model simulation. The basic decay mechanism will be the sequential two body processes. Primary fragments are to be taken as excited compound nuclei, and input to the secondary decay simulations. Decay of the every fragment will be followed, and treated as a separate event [1].

For each primary fragment, the entire decay chain will be simulated, and followed until the end products lies in its stable ground state, thereby unable to decay further. Let us, now, consider an excited nucleus (primary fragment) of mass A, charge Z, temperature T. The possible de-excitation mechanism that the nucleus undergoes is assumed to be either the successive particle emission by evaporation or the fission of the hot nucleus. Light particle emissions e.g., nucleons, d, t, $He^3$, $\alpha$ are treated according to the Weisskopf evaporation theory [2]. Fission is taken into account according to simplified Bohr-Wheeler, although it does not contribute significantly for the nuclei of mass smaller than 100. $\gamma$-ray emissions are also taken into consideration for the particle stable excited states. The simulation of the entire decay chain is governed by the decay width of $\Gamma_\nu$ for each emitted particle. The partial decay width for emission of a particle of type $\nu$ is given by the Wiesskopf evaporation theory [2],

$$\Gamma_\nu = \frac{gm\sigma_0}{\pi^2\hbar^2}\frac{(E^* - E_0 - V_\nu)}{a_R} \exp\left(2\sqrt{a_R(E^* - E_0 - V_\nu)} - 2\sqrt{a_P E^*}\right) \tag{B.1}$$

where m is the mass of the emitted particle, g is the spin degeneracy of it, $E_0$ is the particle separation energy. The subscripts $\nu$, P, R refers to the type of the emitted particle, parent and residual daughter nucleus respectively and $a_P$, $a_R$ are the level density parameters of parent and daughter and given by, $a = A/16$ MeV$^{-1}$. Excitation energies of the parent and residual nuclei are given as,

$$\begin{aligned} E^* &= a_P T_P^2 \\ E^* - E_0 - V_\nu &= a_R T_R^2 \end{aligned} \tag{B.2}$$

where, $T_P$ and $T_R$ are the temperatures of the parent and residual nucleus respectively. The Coulomb barrier $V_\nu$ for charged particles is given by the touching sphere approximation [3],

$$\begin{aligned} V_\nu &= \frac{Z_\nu(Z_P - Z_\nu)e^2}{r_0'\left\{A_\nu^{1/3} + (A_P - A_\nu)^{1/3}\right\}} \qquad \text{for } \mathrm{A}_\nu \geq 2 \\ &= \frac{(Z_P - 1)e^2}{r_0' A_P^{1/3}} \qquad \text{for protons} \end{aligned} \tag{B.3}$$

where $r_0'$ is 1.44fm, and for neutral particle the $V_\nu$ will be zero.

$\sigma_0$ is the cross section for the reverse process i.e., formation cross section of the emitting compound nucleus from the residual nucleus and the emitted particle, and is given by, $\sigma_0 = \pi R^2$ where,

$$\begin{aligned} R &= r_0\left[(A_P - A_\nu)^{1/3} + A_\nu^{1/3}\right] \qquad \text{for } \mathrm{A}_\nu \geq 2 \\ &= r_0(A_P - 1)^{1/3} \qquad \text{for } \mathrm{A}_\nu = 1 \end{aligned} \tag{B.4}$$

where $r_0 = 1.2fm$. The width for $\Gamma$ emission [4],

$$\Gamma_\gamma = \frac{3}{\rho_P(E^*)}\int_0^{E^*} d\varepsilon \rho_R(E^* - \varepsilon) f(\varepsilon) \tag{B.5}$$

with,

$$f(\varepsilon) = \frac{4}{3\pi}\frac{1+\kappa}{m_n c^2}\frac{e^2}{\hbar c}\frac{N_P Z_P}{A_P}\frac{\Gamma_G \varepsilon^4}{(\Gamma_G \varepsilon)^2 + (\varepsilon^2 - E_G^2)^2} \tag{B.6}$$

where, $\kappa = 0.75$, $E_G$ is the position and $\Gamma_G$ is the width of the giant dipole resonance. Fission width is obtained from Bohr-Wheeler formula,

$$\Gamma_f = \frac{T_P}{2\pi} e^{-B_f/T_P}, \tag{B.7}$$

where the fission barrier of the compound nucleus $B_f$ is [5],

$$B_f(\mathrm{MeV}) = -1.40\mathrm{Z_P} + 0.22(\mathrm{A_P} - \mathrm{Z_P}) + 101.5. \tag{B.8}$$

So, the decay width of all the possible processes are known. Next job is to simulate the complete decay chain. One has to start by deciding which path the compound nucleus will follow, particle evaporation or fission, and that is decided by a Monte Carlo sampling [6]. If the Monte Carlo algorithm decides particle emission, then next step is to decide the type of the particle to be emitted and that will be decided by another Monte Carlo in accordance with the partial decay width $\Gamma_\nu/\Gamma_{tot}$. The energy of the emitted particle will be guided by the energy spectrum of the emitted particle running another Monte Carlo sampling. The mass, charge, energy of the residual are adjusted accordingly after each emission and the process is repeated until the residue loses all its excitation and becomes particle stable cold nucleus. The entire scheme is repeated over multiple events for decay of each fragment, and averaging is done over these events, following charge and mass conservations.

# Bibliography

[1] Gargi Cahudhuri, Swagata Mallik, Nucl. Phys. A **849** (2011) 190.

[2] V. Weisskopf, Phys. Rev. **52** (1937) 295.

[3] W.A. Friedman, W.G. Lynch, Phys. Rev. C **28** (1983) 16.

[4] J.E. Lynn, Theory of Neutron Resonance Reactions, Clarendon Press, Oxford, 1968, p. 325.

[5] C. Guaraldo, V. Lucherini, E.D. Sanctis, A.S. Iljinov, M.V. Mebel, S. Lo Nigro, Nuovo Cimento **103** A (1990) 4.

[6] G. Chaudhuri, PhD thesis, arXiv:nucl-th/0411005 (Chapter IV).

# Appendix C

# Second Largest Cluster

We consider an excited single component system of size $A_0$, goes through the process of fragmentation and produces several nuclear clusters. The average size of the largest cluster is denoted by $\langle A_{max} \rangle$, and the average size of the second largest fragment is $\langle A_{max-1} \rangle$. To calculate $\langle A_{max-1} \rangle$, we proceed in a similar way of $\langle A_{max} \rangle$ [1]. If $Pr_2(A_{max-1})$ is the probability for $A_{max-1}$ to be the second largest fragment size, then

$$\langle A_{max-1} \rangle = \sum A_{max-1} \, . \, Pr_2(A_{max-1}). \tag{C.1}$$

Now, we see that $A_{max-1}$ can be the size of the second largest cluster in two ways. (a) There is at least one fragment of size $A_{max-1}$, and just one fragment of size $A_{max} > A_{max-1}$. (b) There are more than one fragment of size $A_{max-1}$ but no fragment larger than it, i.e., $A_{max} = A_{max-1}$. The partition function for the case (a) is

$$Q_a = \sum \omega_{A_{max}} \, . \, \Delta Q_{A_0 - A_{max}}(A_{max-1}) \tag{C.2}$$

where the sum goes from $(A_{max-1} + 1)$ to its maximum possible value. For the case (b), the partition function is

$$Q_b = \Delta Q_{A_0}(A_{max-1}) - \omega_{A_{max-1}} \, . \, Q_{A_0 - A_{max-1}}(\omega_1, \omega_2, \, ..., \, \omega_{A_{max-1}-1}, 0, \, ...). \tag{C.3}$$

Here, $\Delta Q_{A_0}(B)$ is defined as,

$$\Delta Q_{A_0}(B) = Q_{A_0}(\omega_1,\, \omega_2,\, ...,\, \omega_B,\, 0,\, ...,\, 0) - Q_{A_0}(\omega_1,\, \omega_2,\, ...,\, \omega_{B-1},\, 0,\, ...,\, 0), \tag{C.4}$$

and represents the total partition function in fragmentation of the system of size $A_0$, considering only those events where the size of the largest fragment is exactly B.

Now the first term in $Q_b$ is the total partition function for the channels where the largest cluster size is $A_{max-1}$, but the number of such clusters can be one or more. The second term gives the total partition function for the channels, where the number of fragments of size $A_{max-1}$ (i.e., largest cluster) is just one. So the difference is the partition function for the case (b). Therefore, the second largest cluster probability will be,

$$Pr_2(A_{max-1}) = \frac{Q_a + Q_b}{Q_{A_0}}. \tag{C.5}$$

Once we get the probability, $\langle A_{max-1} \rangle$ can be calculated, using Eq. C.1.

# Bibliography

[1] G. Chaudhuri and S. Das Gupta and F. Gulminelli, Nucl. Phys. A **815** (2009) 89.